UNIVERSITÀ DEGLI STUDI DI SALERNO

UNIVERSITÀ DEGLI STUDI DI SALERNO

Dipartimento di Farmacia

PhD Program

in **Drug Discovery and Development**

XXXV Cycle — Academic Year 2022/2023

PhD Thesis

Targeted and untargeted proteomic approaches to disclose small molecules interactome

Candidate

Giusy Ferraro

Tutor

Prof. *Maria Chiara Monti*

PhD Program Coordinator: Prof. Dr. *Gianluca Sbardella*

Firmato digitalmente da:
GIANLUCASBARDELLA
Luogo: Fisciano
Data: 09/02/2023 15:48:07

Table of Contents

Abstract

The identification of natural products and synthetic compounds target proteins is pivotal to understand their mechanism of action for the development of molecular probes and/or potential drugs. Functional proteomics is a mass spectrometry-based discipline focused on the analysis of the interactome of *small molecules* and their targets discovery. Functional proteomics has become an invaluable tool in targets identification of *small molecules* since *Fishing for Partners* strategy, also named affinity purification mass spectrometry coupled approach (AP-MS), successfully disclosed a multitude of bioactive compounds interacting proteins in the past 15 years (Rix and Superti-Furga, 2009).

Unfortunately, this strategy is not universally applicable being limited by the need of a covalent modification of the molecular probe that should contain at least one reactive chemical group and, most importantly, the compound modification should not influence its original bioactivity. Thus, an alternative functional proteomics platform, based on a combination of untargeted Drug Affinity Responsive Target Stability (DARTS) with targeted Limited Proteolysis coupled to Multiple Reaction Monitoring (t-LiP-MRM), has been exploited during my PhD project to disclose and characterize the interacting proteins of bioactive compounds (Lomenick *et al.*, 2009; Feng *et al.*, 2014).

At first, DARTS has been exploited to identify *small molecules* most reliable cellular partners, then t-LiP-MRM has been carried out to investigate the molecules/target proteins interaction features. Moreover, the proteomics results were validated by Western Blotting to confirm *small molecules* interaction with their DARTS-identified targets and by *in silico* molecular docking to corroborate t-LiP-MRM information about the target region(s) involved in the binding. For an in-deep analysis of the binding between the investigated compounds and their protein counterparts and for moving through the activity of such compounds on their putative targets, proper *in vitro* and/or *in cell* biological assays were also employed.

In particular, during this PhD project, MS-based proteomics approaches have been exploited to profile the interactomes of two natural compounds (Artemetin and Tatridin A), abundant in the extracts from *Achillea millefolium* (De Souza *et al.*, 2011) and from *Anthemis melanolepis* (Saroglou *et al.,* 2010), respectively, and a synthetic benzodiazepine derivative, called 1g (Parenti *et.al*., 2016). The interactomes of Artemetin, 1g and Tatridin A in HeLa, U87MG and THP-1 cells proteome have been examined unveiling, respectively, the Filamin A and Filamin B (crucial role in the organization of the cytoskeleton interacting with F-actin) (Zhou *et al.*, 2021; Xu *et al.*, 2017), the Brain Glycogen Phosphorylase (crucial role in the degradation of the glycogen clusters in the brain and in the regulation of the cellular glucose concentrations) (Mathieu *et al.*, 2017) and the Phosphoglycerate Kinase 1 (crucial role in glycolysis) (Zieker *et al.*, 2010) as their principal cellular interactors.

Bibliography

De Souza, P. *et al.* (2011) 'Hypotensive mechanism of the extracts and artemetin isolated from Achillea millefolium L. (Asteraceae) in rats', *Phytomedicine : international journal of phytotherapy and phytopharmacology*, 18(10), pp. 819–825. doi:10.1016/J.PHYMED.2011.02.005.

Feng, Y. *et al.* (2014) 'Global analysis of protein structural changes in complex proteomes', *Nature biotechnology*, 32(10), pp. 1036–1044. doi:10.1038/NBT.2999.

Lomenick, B. *et al.* (2009) 'Target identification using drug affinity responsive target stability (DARTS)', *Proceedings of the National Academy of Sciences of the United States of America*, 106(51), pp. 21984–21989. doi:10.1073/PNAS.0910040106.

Mathieu, C., Dupret, J.M. and Rodrigues Lima, F. (2017) 'The structure of brain glycogen phosphorylase-from allosteric regulation mechanisms to clinical perspectives', *The FEBS journal*, 284(4), pp. 546–554. doi:10.1111/FEBS.13937.

Parenti, S. *et al.* (2016) 'A novel 2,3-benzodiazepine-4-one derivative AMPA antagonist inhibits G2/M transition and induces apoptosis in human leukemia Jurkat T cell line', *Life sciences*, 152, pp. 117–125. doi:10.1016/J.LFS.2016.03.051.

Rix, U. and Superti-Furga, G. (2009) 'Target profiling of small molecules by chemical proteomics', *Nature chemical biology*, 5(9), pp. 616–624.

doi:10.1038/NCHEMBIO.216.

Saroglou, V. *et al.* (2010) ‘Sesquiterpene lactones from Anthemis melanolepis and their antibacterial and cytotoxic activities. Prediction of their pharmacokinetic profile’, *Journal of natural products*, 73(2), pp. 242–246. doi:10.1021/NP9004129.

Xu, Q. *et al.* (2017) ‘Filamin B: The next hotspot in skeletal research?’, *Journal of genetics and genomics = Yi chuan xue bao*, 44(7), pp. 335–342. doi:10.1016/J.JGG.2017.04.007.

Zhou, J. *et al.* (2021) ‘The function and pathogenic mechanism of filamin A’, *Gene*, 784. doi:10.1016/J.GENE.2021.145575.

Zieker, D. *et al.* (2010) ‘Phosphoglycerate kinase 1 a promoting enzyme for peritoneal dissemination in gastric cancer’, *International journal of cancer*, 126(6), pp. 1513–1520. doi:10.1002/IJC.24835.

CHAPTER 1

Introduction

1.1 Bioactive *small molecules* in drug discovery

Bioactive *small molecules* are organic compounds affecting molecular pathways by targeting key role proteins. They can be isolated from natural sources or developed from leads derived from rational drug design.

Natural compounds (NPs) represent an advantageous and inspiring library of amenable scaffolds for drug-discovery and development. Employing NPs in drug-discovery is a crucial point because of their huge structural variability and their involvement in different cellular pathways influencing proteins structures, proteins interactomes, protein localization and so on (Atanasov *et al.*, 2021).

On the other side, the rapid development of biochemistry, molecular biology, pharmacology, and other related disciplines has provided the basis and means for the improved research, design and development of synthetic compounds targeting enzymes, receptors, ion channels and also nucleic acids (Li and Kang, 2020).

Therefore, the characterization of *small molecules interactome* has become decisive to understand their mechanism of action for the developing of new molecular probes

and/or potential therapeutic drugs. Because of its versatile characteristics, functional proteomics is considered pivotal in this process thanks to a new toolbox of established mass-spectrometry based techniques, useful for the targetome characterization of *small molecules*, as it will be discussed in my PhD thesis.

1.2 Natural compounds in drug discovery

Natural products are an invaluable source of compounds for drug discovery. Historically, natural products have been the font of virtually all medicinal preparations and, more recently, they have continued to enter in clinical trials or to provide leads for compounds that are entering in clinical trials, particularly as anticancer and antimicrobial agents (Dias *et al.*, 2012). Moreover, they could serve as tools to examine proteins involvement in physio-pathological processes and, thus, to contribute to the advancement in target-discovery and other fields of molecular biology, chemical biology and, more generally, life sciences.

Natural product collections exhibit a wide range of pharmacophores and a high degree of stereochemistry and these properties are expected to contribute to the ability of such collections to provide hits - even against the more difficult screening targets, such as protein– protein interactions (Drewry *et al.*, 2010). However, natural products may have the additional advantage over synthetic compounds of being natural metabolites: compounds that are successful as drugs have been suggested to have the property of 'metabolite-likeness'. This means that such compounds are not only biologically active but also likely to be substrates for one or more of the many transporter systems that can deliver the compounds to their intracellular site of action.

The crucial point in employing natural compounds in drug-discovery is their huge structural variability and their involvement in different cellular pathways influencing proteins structures (both their high-order arrangement and their co-/post-translational modifications), proteins interactomes and crosstalk, protein localization and so on (Wright and Sieber, 2016). These features represent both an impressive advantage and a dramatic limitation. The need for large-scale, high-throughput and extensive investigation of their bioactivities results in a limitation largely due to the challenging deconvolution of the effects exerted by natural compounds in their mode of action at the molecular level. This outstanding issue can be addressed by MS-based proteomics. Usually, *small molecules*, particularly natural compounds, have more than one cellular target affecting cells response from more than one point of the same pathway and/or from more than one level of different pathways. The old-fashioned rule of one-drug-one-target, based on the so-called "magic bullets", has been progressively replaced by the idea of the "magic shotguns", in which non-selective molecules are capable to act in the cell at multiple levels (Roth, Sheffer and Kroeze, 2004).

Indeed, the multiple bioactivity of a molecule should not be considered a priori as a negative feature and an unbiased approach could serve this kind of investigation. Because of their versatile characteristics, MS-based strategies are to date considered pivotal techniques in a multidisciplinary approach aiming to drug and target-discovery. In a physiological context, a molecule binding more than one protein might show desirable or undesirable consequences. Knowledge about the spectrum of proteins interacting with a small molecule could, in an early stage, inform about drug safety (i.e. by the identification of potential off-targets and their related toxicity effects), help in the decision making along the development process (e.g. which lead series to prioritize) and even lead to the repositioning of existing drugs (e.g. by the

identification of additional targets). In a later stage, knowing the drug multiple targets would enable a drug either to be therapeutically applied in several unrelated diseases or, as for the harmful side effects, to use adjunct therapies or dose adjustments. Therefore, in addition to carefully determining the molecule primary target(s), it is important to identify a drug target spectrum as thoroughly as possible, to exploit its full therapeutic potential and minimize the toxicity caused by the drug off-targets. The process aiming at the identification of the full spectrum of protein targets associated with a bioactive molecule and their induced cellular phenotype is called Drug-Target Deconvolution (Raida, 2011).

Despite these advantages, natural products have some drawbacks. Identifying the bioactive compounds of interest can be challenging and dereplication tools have to be applied to avoid rediscovery of known compounds. Accessing sufficient biological material to isolate and characterize a bioactive NP may also be difficult. Although the complexity of NP structures can be advantageous, the generation of structural analogues to explore structure–activity relationships and to optimize natural product leads can be challenging, particularly if synthetic routes are hard (Harvey *et al.*, 2015; Atanasov *et al.*, 2021).

1.3 Medicinal chemistry in drug discovery

Medicinal chemistry plays a key role in small-molecule drug discovery. In the early era of drug discovery (1950 to about 1980), medicinal chemists relied primarily on data from *in vivo* testing. Now, the role of medicinal chemists has changed because of the development of new technologies, such as high-throughput *in vitro* screening, large compound libraries, defined molecular targets and structure-based drug design.

Medicinal chemists prepare and/or select appropriate compounds for biological evaluation that, if found to be active, could serve as *lead compounds*. Then, they evaluate the structure-activity relationships (SARs) of analogous compounds with regard to their *in vitro* and *in vivo* efficacy and safety.

Although these new technologies, the multitude of new safety requirements that have arisen has also brought unanticipated hurdles for the task of translating *in vitro* to *in vivo* activity. Simultaneously, the knowledge base that supports drug research has expanded considerably, increasing the challenge for chemists to understand their fields of expertise. The demonstration of adequate clinical safety and efficacy in humans has also become more complex and ever-increasing amounts of data are now required by regulatory agencies. For this reason, inventing and developing a new medicine is a long, complex, costly and highly risky process (Freter, 1988; Soudijn, 1991).

The drug discovery process begins with the identification of a medical need, including a judgement on the adequacy of existing therapies (if there are any). From this analysis, together with an appraisal of the current knowledge about the target disease, the hypotheses on how to possibly improve therapy will come. Then, testing selected chemicals in appropriate biological tests start. Key subsequent steps in the process include detecting relevant biological activity (a 'hit') for a structurally novel compound *in vitro*, then finding a related compound with *in vivo* activity in an appropriate animal model, followed by maximizing this activity through the preparation of analogous structures and finally selecting one compound as the drug development candidate. This drug candidate then undergoes toxicological testing in animals, as required by law. If the compound passes all these tests, the accumulated research data are assembled and submitted as an Investigational New Drug Application (IND) to the Food and Drug Administration (FDA) in the United States (or comparable

agency in other countries) before clinical trials are initiated. In the clinic, there is a sequential evaluation in normal human volunteers of toleration (Phase I), efficacy and dose range in patients (Phase II), followed by widespread trials in thousands of appropriate patients to develop a broad database of efficacy and safety. For the few drug candidates that survive this series of development trials, a New Drug Application (NDA) that contains all the accumulated research data is filed for thorough review by the experts at the FDA. Only with their approval can the new drug be offered to doctors and their patients to treat the disease for which it was designed (Lombardino and Lowe, 2004).

Today, the rapidly expanding base-knowledge concerning diseases, their causes, symptoms and their effects on the human body holds great promise for the discovery of important new medicines.

Both NPs and synthetic *small molecules* will be the probe used in this PhD thesis to optimize a proteomic based platform aimed to disclose bioactive ligand targets.

1.4 Proteomics

The term proteome was first used by Marc Wilkins to describe the overall protein content of a cell with regard to protein localization, interactions, post-translational modifications (PTMs) and turnover at a particular time (Wilkins *et al.*, 1996). Proteins represent the majority of biochemically active components in biological systems and are the main targets of almost all drugs. Analytical methods are crucial to determine the activities and functions of proteins and to understand their connections with cellular activities and disease-related phenotypes. In particular, mass spectrometry has been developed as a powerful tool for a comprehensive characterization of a drug

interactome under physiological conditions. Moreover, this method enables the analysis of the drug mechanism of action in the context of a complex proteome accelerating the difficult process of target discovery and validation.

Protein characterization by mass spectrometry can be achieved following two main approaches, the bottom-up and top-down ones, as in Figure 1.1.

The top-down strategy is based on the fragmentation of intact proteins. The fragments are then analyzed giving a complete description of the protein primary structure and modifications.

However, top-down proteomics is not commonly employed because of issues in terms of sample handling, protein samples heterogeneity and transient or weak interactions of certain protein subunits in specific complexes (Heck, 2008).

The bottom-up approach recovers proteins structural information from the analysis of their peptides and represents the most popular approach in terms of identification and quantitation of proteins in a great variety of samples. In a representative bottom-up workflow, proteins are submitted to an enzymatic digestion, typically with trypsin, and the resulting peptides analyzed through tandem mass spectrometry. Peptides identification is achieved by comparing mass spectra derived from their fragmentations with the theoretical ones generated from *in silico* digestion of a protein database (Moradian *et al.*, 2014).

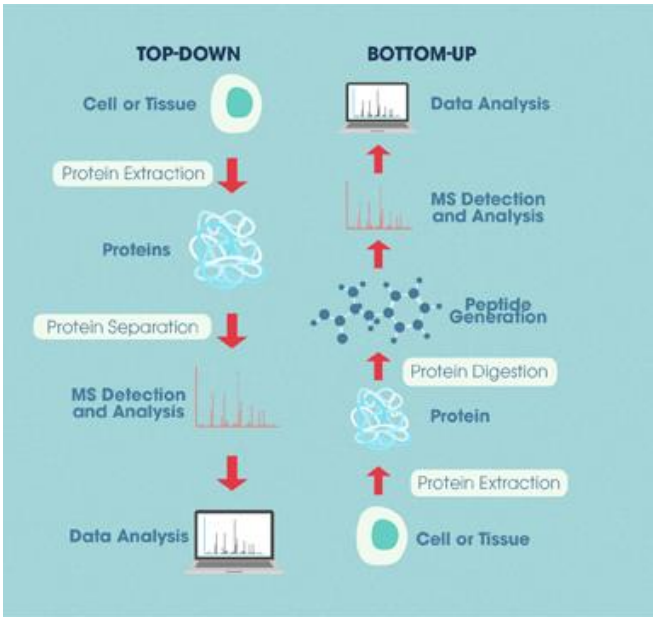

Figure 1.1 *Schematic view of "top-down" and "bottom-up" proteomics approaches.*

1.5 Functional proteomics

Functional proteomics is a mass spectrometry-based discipline focused on the analysis of the interactome of *small molecules* and their target discovery. Functional proteomics strategies can be divided into the following approaches: (1) activity-based protein profiling (ABPP), which investigates the enzymatic activity of a particular protein family using small-molecular probes and (2) compound-centric chemical proteomics (CCCP), devoted to the interactome characterization of an individual bioactive molecule. CCCP strategies include affinity chromatography coupled to mass spectrometry (AP-MS), which requires the compound to be covalently modified for being investigated and a pretty consistent number of relatively new label-free methods, which take the distance from the conventional ABPP and AP-MS approaches, since

they don’t require any chemical modification of the examined molecules (Rix and Superti-Furga, 2009).

Indeed, these methods use ligand-induced effects on biophysical properties of target proteins, by measuring changes in thermal stability or resistance to proteolysis. These techniques, comprising Drug Affinity Responsive Target Stability (DARTS), Limited Proteolysis (LiP), Pulse Proteolysis (PP), Stability of Proteins from Rates of Oxidation (SPROX), Cell Thermal Shift Assay (CETSA) and Thermal Proteome Profiling (TPP), will be discussed in the subsequent paragraphs.

Activity-based protein profiling (ABPP) is devoted to directly capturing, visualizing, identifying and quantifying active enzymes in complex biological systems, taking advantage of small active site-directed chemical probes (i.e. activity-based probes [ABPs]) designed to interact with active-site residues of target enzymes, forming stable covalent bonds (Sadaghiani, Verhelst and Bogyo, 2007; Nodwell and Sieber, 2012). An ABP consists of three fundamental building blocks: (1) a reactive group that covalently binds to the active-site of a given class of enzymes, (2) a linker that serves as the recognition element for the enzyme-binding pocket(s) and (3) a reporter tag for the detection and enrichment of the probe-labeled enzymes.

ABPP can be applied to any cell or tissue and can be combined with a range of analytical methods for data acquisition, including gel and mass spectrometry-based methods. ABPs are of great value for identifying deregulated enzymatic activities in various cancer models, although the specificity of these probes is not absolute and they can be toxic (Nomura *et al.,* 2010).

Among the CCCP strategies, the affinity purification mass spectrometry-based technique (AP-MS), also known as *Fishing for Partners*, successfully disclosed a multitude of natural compounds interacting proteins in the past 15 years, as in our Bio-

Organic Chemistry labs (Rix and Superti-Furga, 2009; Margarucci *et al.*, 2010; Capolupo *et al.*, 2017). Unfortunately, this strategy is not universally applicable, being limited by the need of a covalent modification of the molecule probe that should contain at least one reactive chemical group and, most importantly, by the fact that the molecule modification should influence its original bioactivity. This strategy can be carried out in either a heterogeneous or a homogeneous fashion as shown in Figure 1.2. The heterogeneous approach consists of three main steps: (1) a solid matrix covalently bounding the compound (e.g. agarose, sepharose or magnetic beads); (2) incubation with the matrix-compound complex with a cell lysate and (3) mass spectrometry-based identification of the compound interactome.

The homogeneous strategy takes advantage of the strong non-covalent interaction between biotin and streptavidin. Indeed, the small molecule is first modified with a biotin tag and then incubated with the cell lysate, to allow the interaction with its protein partner(s). In a last step, streptavidin bearing beads are added to bind the molecule and, consequently, to fish out the linked proteins, which are eluted and analyzed, as for the previous strategy.

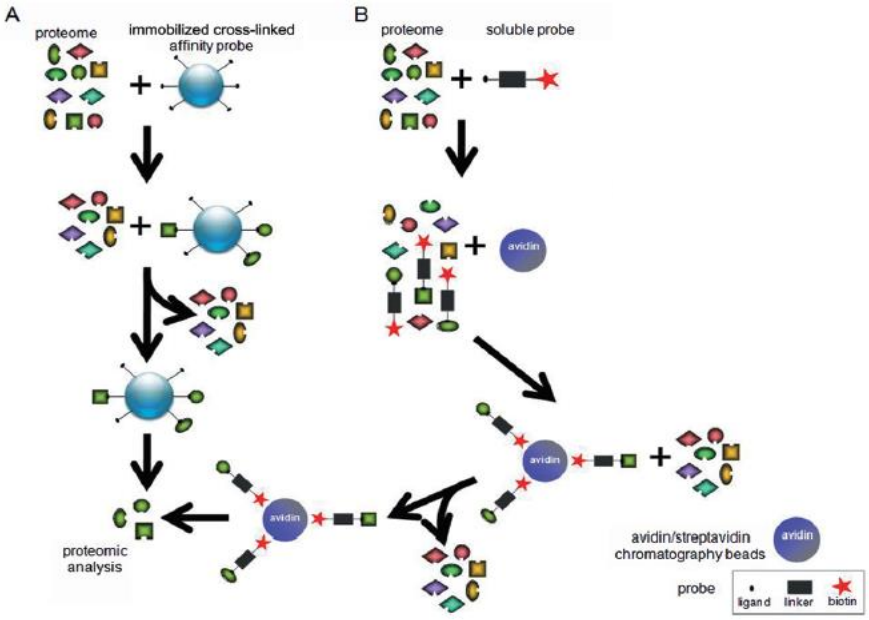

Figure 1.2 *Heterogeneous and homogeneous approach of Fishing for partners.*

In both approaches, a chemical derivatization step is required for the generation of a compound-bearing solid matrix. Furthermore, a covalent modification of the compound could affect its interactions with proteins (either in positive or negative behavior). Moreover, the attachment of a spacer arm between the small molecule and the solid matrix is mandatory to avoid matrix steric interference in the interaction with the proteins, thus guaranteeing this step is carried out under *solution-like* conditions. (Shiyama *et al.*, 2004).

For the incubation step, a cell extract is prepared, either from cells or tissues, under mild conditions and, subsequently, the lysate is incubated with the affinity matrix which, after a settling step, is extensively washed to reduce the amount of proteins un-specifically interacting with the linker or the matrix. In the last step, the small molecule interacting proteins are eluted from the matrix system (e.g. through high-salts

containing buffer or denaturing agents), separated and visualized, usually through 1D-SDS-PAGE and finally digested with trypsin (Bantscheff and Drewes, 2012).

The resulting peptides mixtures are, then, analyzed by nano-ESI LC-MS/MS and submitted to bioinformatics search using protein databases (e.g. SwissProt) and search engines (e.g. Mascot/Proteome Discoverer) to give protein identification. This approach identifies a small molecule interacting proteins in their natural state and environment, reflecting their endogenous abundance levels, PTMs and the presence of their natural binding partners. Furthermore, AP-MS could potentially be performed with any cell type, tissue or species, to investigate possible disease-relevant drugs. However, some drawbacks must be considered. First of all, the lysis method will not capture membrane proteins that require peculiar solubilization conditions. Another limit could be the elution step: when the molecule-linked beads are treated with denaturant agents or salts, only proteins interacting with the molecule in a non-covalent fashion will be released and this will prevent the identification of potential covalent interactors.

Another issue is represented by the false positive target(s): during the affinity purification step, highly abundant proteins with low affinity for the immobilized compound will often co-elute, as well as sticky proteins, prone to interact with either hydrophobic or charged surfaces of the matrix-compound complex.

In general, this approach does not give any clue on biological relevance of the interaction between the molecule and its target(s). Thus, further investigations (e.g. *in vitro* or *in vivo* biological assays) are needed to investigate the capability of the small molecule to modulate its partner(s) activity in a biological context.

1.6 Target deconvolution without chemical probes

A pretty consistent number of new label-free methods, which take the distance from the conventional AP-MS approach since they don't require any chemical modification of the examined molecule, have been developed over years (Saxena, 2016). Indeed, in these methods, the detection of the binding partner(s) of the label-free compound is carried out by evaluating proteins responses to a series of perturbations (e.g. thermal or proteolytic treatment) or chemical events. These strategies can be classified in two groups, as schematically reported in Figure 1.3, based on the readout nature of the LC−MS/MS approaches they rely on. In particular, DARTS, PP, CETSA and TPP are *protein-centered* strategies, meaning that the proteomics data produced in the LC−MS/MS analyses are used to generate quali/quantitative information about the interacting proteins of the sample compound, whereas LiP and SPROX are *peptide-centered* methods, because the differential behavior of the proteins exposed or not to a molecule is directly ascertained from the peptides identified (Jafari *et al.*, 2014; Mateus *et al.*, 2020; Iyer *et al.*, 2019; West *et al.*, 2010). Among these approaches, DARTS and LiP strategies have been the focus of this PhD project and will be discussed in the following paragraphs.

In the Cellular Thermal Shift Assay (CETSA) approach, the perturbation is represented by a thermal treatment to shock those proteins non-interacting with the small molecule by denaturation. Indeed, in principle, the interaction with a small molecule stabilizes protein targets from denaturation. To achieve this, cell samples are incubated with either vehicle or drug and heated at different temperatures. Subsequently, proteins that have unfolded can precipitate. Centrifugation is then used to separate the soluble

fraction from protein aggregates, and abundance of proteins is recorded and compared in supernatants using different techniques as immunoblotting if the targets of the small molecule are already known (Jafari *et al.*, 2014). If the approach is untargeted, CETSA can be coupled with multiplexed quantitative mass spectrometry-based proteomics in the so-called thermal proteome profiling (TPP) approach, which monitor changes in proteins thermal stability across the whole proteome and to identify direct and indirect drug targets. In a TPP experiment, CETSA workflow is followed until centrifugation which is performed after the heating step. Then, the relative soluble amounts of proteins, across the differentially heated and treated (i.e. compound exposed or not) samples, are submitted to tryptic digestion to obtain peptides mixtures that are individually labeled with different isobaric tags and combined, so that each temperature series is further processed as a single sample (Mateus *et al.*, 2020).
This approach is affected by some drawbacks as well, largely due to the optimization of the thermal gradient to emphasize the compound induced thermal stabilization of the interactors.

Pulse Proteolysis (PP) is a protein-centered limited proteolysis-based approach that exploits the chemical denaturant dependence of an unspecific proteolytic digestion to evaluate the thermodynamic properties of protein-ligand complexes, comparing relative stability of protein in the presence of urea and thermolysin. Folded and unfolded proteins have very different proteolytic susceptibilities: unfolded proteins are rapidly digested, whereas proteolysis of the folded ones is much slower (Iyer *et al.*, 2019). Therefore, a short incubation time (i.e. pulse proteolysis) will digest only unfolded proteins, leaving the folded intact: they can be determined after the pulse step by bottom-up proteomics. To obtain reliable results, the pulse proteolysis length must

be chosen properly, to ensure complete digestion of the unfolded proteins and a minimal digestion of the folded ones. While the lower limit of the pulse can be estimated by the intrinsic proteolytic kinetics of the enzyme, the upper limit depends on the protein targets, even if 1 min pulse is a reasonable choice.

PP is able to identify the protein target(s) of a bioactive compound in a simple and quantitative fashion, and of detecting the thermodynamic parameters associated with the interaction. If, anyway, a protein tends to unfold quite quickly or has an unstructured region in its native conformation, PP is not a good choice to study protein-ligand interactions, because of the extensive proteolysis of the folded protein that would occur within the pulse (Iyer *et al.*, 2019).

Stability of Proteins from Rates of Oxidation (SPROX) is a covalent labeling- and mass spectrometry-based method for evaluating the solution phase thermodynamic properties of protein-ligand complexes, using the denaturant dependence of the hydrogen peroxide-mediated oxidation of methionine side chains. A typical SPROX experiment starts with the incubation with a bioactive compound or just the vehicle and subsequently the equilibration of the protein samples in a series of buffers with increasing concentrations of a chemical denaturant (e.g. urea). The samples are then exposed to hydrogen peroxide to selectively oxidize the thioether group in the methionine side chain. Oxidation at other susceptible amino acid side chains (e.g., cysteine and tryptophan) is generally not observed, since their oxidation rates are much slower than the methionine one (West *et al.*, 2010).

Since methionines are oxidized when are solvent-exposed, and this condition is achieved during the protein unfolding in the denaturant-containing buffers, the interaction with a ligand should hamper their oxidation. The interacting proteins can

thus be identified because they need a significantly higher denaturant concentration for their methionine to be oxidized (e.g.> 1.0 M urea) (Strickland *et al.*, 2013).

Despite the huge advantage of identifying thermodynamic parameters associated with a small molecule/protein interaction, SPROX has a limitation when the sample compounds are unstable in presence of hydrogen peroxide and, furthermore, only methionine containing peptides are suitable for the readout, so that they often have to be enriched prior to the mass spectrometry analysis.

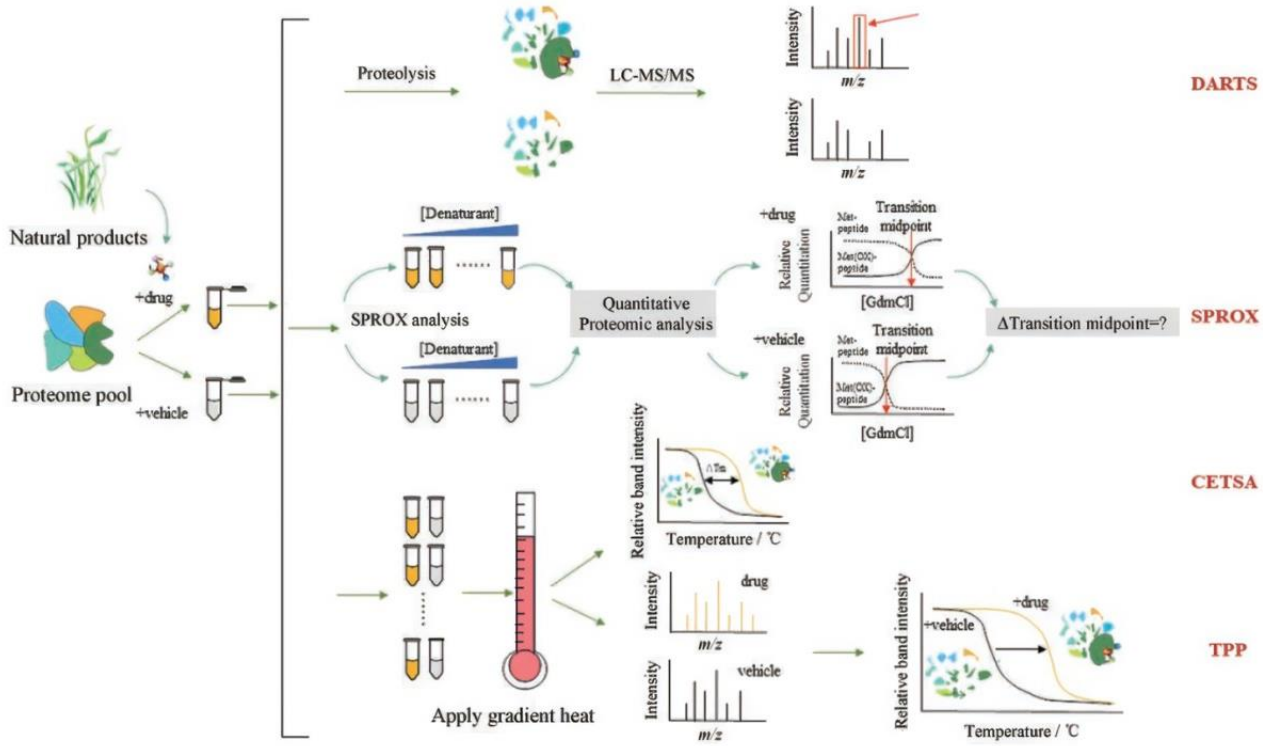

Figure 1.3 *General workflow of the following label-free proteomics approaches: DARTS, SPROX, CETSA and TPP.*

1.7 Drug Affinity Responsive Target Stability (DARTS)

DARTS exploits the thermodynamic stabilization conferred by a molecule to its protein target(s), whose conformational fluctuations (i.e. breathing) are dramatically decreased due to the interaction with the compound, as can be inferred by its altered proteolytic pattern when submitted to an unspecific protease exposure, by means of mass spectrometry and/or immunoblotting analysis.

Indeed, whereas under physiological conditions a protein is in a dynamic equilibrium with multiple alternative conformations, the interaction with a specific ligand will shift the equilibrium to highly favor the molecule-bound conformation, in a thermodynamically more stable state (Henzler-Wildman and Kern, 2007).

In a typical DARTS workflow as in Figure 1.4, cell lysates are incubated with the molecule to be studied at several concentrations, then the protein samples are submitted to limited proteolysis with an unspecific protease (e.g. thermolysin or subtilisin). The protease is quenched and the protein mixtures are separated through 1D-SDS–PAGE to give evidence, after staining the gel (e.g. with Coomassie Blue), of the proteins with altered proteolytic patterns in presence of the binding molecule. For this purpose, an on-eye inspection of the gel is carried out, in which the lanes corresponding to the differentially treated protein samples (with or without the small molecule) are compared, looking for bands that are more intense in the treated versus the untreated sample, evidence of a major abundance of the corresponding protein(s) because of the compound-exerted stabilization. Moreover, a densitometric analysis of the lanes of the gel is performed through the Image J software (Morretta *et al.*, 2021)

Each of these bands is then cut out and submitted to *in situ* tryptic digestion for the subsequent nano-ESI-LC-MS/MS analysis (Figure 1.4).

Then, the MS results are then searched against a database for the protein identification step and a label-free quantitation is carried out to evaluate their abundance level.

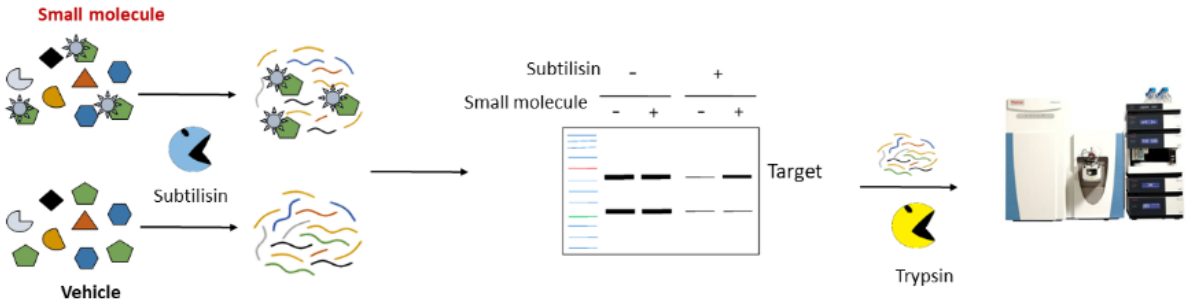

Figure 1.4 *Drug Affinity Responsive Target Stability (DARTS) workflow.*

DARTS is based on the in-solution interactions between the proteins of a cell lysate and the unmodified compound, thus eliminating the limitations due to its chemical features, as far as the molecule is soluble in the incubation buffer with possible addition of only small amounts of organic solvents, to preserve proteins in their native state (Lomenick *et al.*, 2009).

However, DARTS presents some tricky aspects that need to be established prior to perform the experimental procedure. The choice of the protease is an important parameter to be optimized since different proteases target specific protein residues and also show preferences for folding or location of the recognition site within a polypeptide. These aspects make the proteome-wide susceptibility to proteolysis strongly dependent on both proteins and proteases.

In the very first DARTS experiments, as reported in literature (Lomenick *et al.*, 2011), the unspecific metallo-endopeptidase thermolysin, very efficient only on unfolded proteins, has been used. In non-denaturing conditions, this protease can only digest unfolded proteins or proteins presenting unstructured regions. Thus, thermolysin was replaced with other proteases, such as subtilisin, able to give a broad response to the digestion of differentially folded proteins for a less biased drug target identification.

Another important parameter to be optimized is the protease to proteins ratio. Indeed, in order to point out the different intensities of the gel bands, a high digestion level of the non-target proteins beside a low digestion level of the protected target proteins should be maximized. This ideal situation is, however, unlikely to be reached and a fine tuning of the protease amount to be used must be performed, depending on both the chosen enzyme and the molecule behavior.

DARTS has some drawbacks regarding the poor dynamic range of its 1D-SDS-PAGE readout. The target proteins need to be highly abundant and not extremely sensitive or resistant to the protease. Indeed, if a protein is not sufficiently abundant or is highly sensitive to proteolysis, it could be hardly visible after gel staining.

Furthermore, in case of co-migration between proteins of the same or similar molecular weight, a highly abundant protein will hide the target one, while the presence of several low or moderately abundant proteins could just mask the differential abundance of the targets. This is common for binders whose molecular weight is below 30 kDa: thus, the identification of low-molecular weight targets is particularly daunting by an on-eye visualization of the gel bands. Even if this issue could be partially circumvented by exploiting high poly-acrylamide percentage gels, for a better resolution of the low molecular weight regions, the peptide mixtures

coming from digestion of a gel slice would anyway be highly complex, partially hampering the mass spectrometric analysis.

For this reason, alternative DARTS approaches have been proposed, coupling DARTS with 2D-SDS-PAGE or DIGE, or pursuing gel-free DARTS. In the latter case, differences in proteins abundances due to a compound-exerted protection can be accomplished after separation of the limited proteolysis products from the remaining intact proteins by dialysis or filtration (e.g. through molecular weight filters), prior to submit the samples to in-solution digestion and 2D-LC-MS/MS (Lomenick, Olsen and Huang, 2011).

1.8 Bioinformatics

Several bioinformatics strategies have been settled for the interpretation of the mass spectrometric data exploiting identification and/or identification algorithms, or a combination of them, based on search in protein data banks, such as SwissProt, to compare the theoretical information with the experimental ones. Among these, Mascot Daemon by Matrix Science and Proteome Discoverer by Thermo Scientific are the most commonly used.

Mascot Daemon is an automatized software exploiting spectral information both from MS and MS/MS spectra and from the combination of mass data with amino acids sequence data. When an experimental peptide peak has a value in the narrow mass range of the theoretical value, Mascot recognizes this so-called “match” and correlates it to a casual event probability (P)- related “score” corresponding to the coLog(P). The higher is the “score”, the higher is the reliability of the “match”. The protein-associated score is calculated by means of the MS- and MS/MS- associated scores of the peptides

and their fragments relating with that protein. Moreover, the output table from Mascot Daemon elaboration reports both the total number and the significative number of the matches recognized for the peptides and their fragments. Additionally, the Exponentially Modified Protein Abundance Index (emPAI) is conveyed in the table for each of the identified proteins referring to the number of the experimentally observed peptides normalised on the theoretically observable peptides for each specific protein digested in a peculiar way, thus roughly expressing the protein coverages (Koenig *et al.*, 2008).

The raw files (.raw) are converted into Mascot Generic Format data files (.mgf) through MSConvert and loaded onto the Mascot Daemon graphical user interface (MatrixScience, London, UK) to achieve proteins identification. The SwissProt database (release January 2017, 553474 sequences, 198069095 residues) is employed to retrieve *in silico* proteins digestion and the following settings were exploited: trypsin as the enzyme, two missed cleavages allowed; carbamidomethyl (C) as fixed modification; oxidation (M) and phosphorylation (ST) as variable modifications; 30 ppm as peptide tolerance; 0.8 Da as MS/MS tolerance. The obtained data were filtered by molecular weight ranges accordingly with the gel cutting patterns and a semi-quantitative analysis was then performed comparing MASCOT matches among the analyzed compounds. Protection percentages were thus calculated as follows:

Protection (%) = [(MatchesSamples - MatchesControl)/MatchesLysate]*100.

Proteome Discoverer is a comprehensive and expandable software platform allowing the quali-/quantitative analysis of mass spectrometric data from a wide range of proteomics workflows. A point of strength of this software by Thermo Scientific, besides the possibility to expandable nodes for peculiar investigations, is the versatility

of the search algorithms (several database search algorithms can be used such as Mascot, SEQUEST and Z-Core) and the possibility to combine outputs obtaining from all of them for a cross-validation of the data.

The raw files (.raw) were elaborated into Proteome Discoverer™ (version 2.4.1.15). To conduct the spectral library search, MSPepSearch was used, and the NIST Human Orbitrap HCD Library was selected with a mass tolerance of 10 ppm for MS1 and 0.02 Da for MS2. The false discovery rate (FDR) was set at 1% (corresponding to a high confidence in the identification) and 5% (corresponding to a medium confidence in the identification).

The MS/MS spectra were also processed by Sequest by making a comparison with a database of Homo Sapiens (SwissProt, November 2020) using the following parameters: tryptic digestion, maximum of two missed cleavages, carboxyamido-methylation of cysteines (Cys) as a permanent modification, oxidation of methionines (Met), acetylation at the N-terminus of proteins, and/or de-methylation as variable modifications. A label-free quantification was performed exploiting both unique and razor peptides to calculate protein abundance (Orsburn, 2021).

1.9 Limited Proteolysis coupled to Multiple Reaction Monitoring Mass Spectrometry (LiP-MRM)

LiP-MRM is based on the same principle exploited by DARTS, which is the thermodynamic stabilization of a target protein interacting with a small molecule when it comes to limited proteolysis. LiP-MRM one is peptide-centered, indeed the molecule induced proteolytic resistance is perceived through changes in abundance of its tryptic peptides (Feng *et al.*, 2014).

As for DARTS, a LiP experiment starts with the incubation of cell lysate samples obtained in non-denaturing conditions with the molecule to be investigated or just with the vehicle for negative controls (Figure 1.5). The protein mixtures are then submitted to limited proteolysis with a broad-specificity protease (e.g., thermolysin, subtilisin) at a low enzyme to substrate ratio and for a short time, such that the initial cleavage sites are dependent on the structural features of the proteins, generating on average large protein fragments. After quenching the protease, instead of visualizing the molecule exerted protection(s) on gel, samples are shifted to denaturing conditions to carry out a complete *in-solution* tryptic digestion to generate peptides suitable for bottom-up MS analysis. As a positive control, an aliquot of the same cell lysate is subjected to trypsinization only. The obtained peptides are, then, submitted to a desalting step (e.g. through C18 packed cartridges) and analyzed, exploiting the sensitivity and high background filtering capabilities of multiple reaction monitoring (MRM) MS to probe different proteolytic patterns in complex matrices (Figure 1.5) (Picotti *et al.*, 2009).

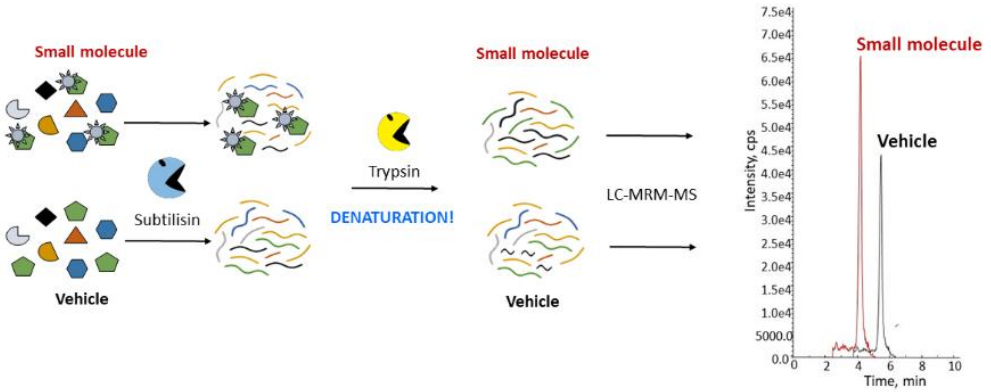

Figure 1.5 *Limited proteolysis (LiP) coupled to Multiple Reaction Monitoring (MRM) mass-spectrometry.*

MRM is a mass spectrometry acquiring mode that takes advantage of the unique capability of triple quadrupole (QQQ and Q-TRAP) mass spectrometers to act as mass filter, for the selective monitoring of specific molecular ions and one or several of their daughter ions. Thus, multiple species with known fragmentation pathways can be detected and quantified even in complex backgrounds. In this technique, precursor/fragment ion pairs are termed transitions. When applied to LiP, MRM measures peptides produced by the tryptic digestion of the differentially treated protein samples: peptide ions of a designated protein are selected in the first mass analyzer (Q1), fragmented by CID in Q2 and then one or several fragment ions (uniquely derived from the Q1 selected peptides) are analyzed by the Q3 quadrupole (for QQQ instruments) or by the Linear Ion Trap (for Q-TRAP instruments). Integration of the chromatographic peaks for each transition allows the relative quantification of the targeted peptides. The development of a robust MRM assay needs the selection of peptides unique to the target protein(s) and easily detectable by mass spectrometry.

In order to choose the correct peptides to measure, information from prior experiments stored in repositories like PeptideAtlas can be exploited. PeptideAtlas is an on-line collection of observed peptides and their related annotations, retrieved by a large number of data sets that have been deposited and reprocessed through the trans-proteomic pipeline. (Deutsch *et al.*, 2008).

More in details, raw files from MS/MS experiments are collected and converted into mzXMl files for the sequence searching step, performed with Sequest (MS/MS data analysis program). The top hits are then validated and the results combined to retrieve protein-level probability matches. The spectral library-building tool SpectraSt is then used to create a consensus spectrum library comprising all of the observed high-scoring peptide ions. All the raw data are then subjected to a second round of searching

and validation, and all of the identified high-scoring peptides are finally assigned to a single reference Ensembl build and mapped to the genome. All these data are then loaded into the PeptideAtlas database for browsing or downloading purposes. (https://db.systemsbiology.net/sbeams/cgi/PeptideAtlas). For a given protein, tryptic peptides having a high-probability to be produced and detected by MS are presented and ranked on the basis of different criteria and proteotypic peptides can thus be picked as the best choice for a targeted proteomics experiment. Once chosen the peptides, a selection of the proper transitions should be made: for each precursor-ion charge state, fragment ions providing the highest intensity and lowest level of interfering signals should be preferred. Such selection can be guided by SRMAtlas, a public available resource of SRM assays generated for entire proteomes by the analysis of known synthetic peptides (and to lesser extent natural peptides) on different mass spectrometers, mainly having a quadrupole as detector. (https://db.systemsbiology.net/sbeams/cgi/PeptideAtlas/GetTransitions) (Deutsch *et al.*, 2008). SRMAtlas allows the user to retrieve high probability fragmentations for a given peptide, searching into one of the available SRM builds (i.e. Complete Human SRMAtlas, M. tuberculosis SRMAtlas, Yeast SRMAtlas). More in details, it is possible to either query the peptides transitions of a given protein or to retrieve them by searching the proteotypic peptides of interest, previously selected through PeptideAtlas. Furthermore, it is possible to specify the number of fragment ions to be reported from each peptide (i.e. Number of highest Intensity Fragment Ions to Keep), to select the mass spectrometer to be used to run the retrieved MRM assays (i.e. Target Instrument), to select the MS instrument that should be considered to build the MRM assays (i.e. Transition Source), to search for labeled peptides if necessary, to select the fragment ions types included in the assays (i.e. Allowed ions types, usually b and y

ions) and to select the peptide modifications to return the query results (i.e. Allowed peptide modifications). Once specified these search parameters, the interface will return a query result table in which m/z ratios of both precursors and their fragments are reported, as well as their charge state, ion type and predicted retention time. With appropriate MRM assays in hand, samples treated or not with a bioactive compound and submitted or not to the double-digestion procedure are analyzed by LC-MRM-MS to quantify as many fully tryptic peptides as possible for a given protein. Interaction with a drug stabilizes a protein, inducing structural changes that may render the regions directly or distally involved in this event less exposed to the un-specific protease action, as opposed to the un-treated sample where the limited proteolysis trend is only dictated by the conformational features of the protein itself. When trypsin is added to the partially digested samples, cleavages can either occur on the unspecific protease products or in protein regions not being already processed: the former case will produce semi-tryptic peptides, whereas in the latter circumstance fully-tryptic peptides are generated. Thus, in comparison to the sample un-treated by NP in which no stabilization event takes place, the treated sample should present more tryptic peptides or, much more realistically, the intensity of tryptic peptides mapping for those protein regions directly interacting with the molecule or distally affected by the interaction should be significantly higher, whereas no significant change should be detectable for peptides mapping for other protein regions (Picotti *et al.*, 2009).

Targeted LiP-MRM (t-LiP-MRM) offers the undeniable advantage of both confirming the interaction a compound engages with its target protein(s) and, most importantly, of pinpointing the specific target(s) region(s) locally or distally affected by the compound binding, such as direct binding sites or allosteric paths (Morretta *et al.*, 2021).

Nevertheless, LiP requires extraction and handling of a proteome under non-denaturing conditions, which restricts its use to soluble proteins and hampers the characterization of membrane proteins, requiring peculiar extraction and solubilization strategies. Moreover, targeted LiP requires a priori known data about the protein to be analyzed, thus the target protein of a bioactive compound must have already been discovered (Feng *et al.*, 2014).

1.10 Aim of the PhD project

Functional proteomics is a mass spectrometry-based discipline, focused on the analysis of the interactome of *small molecules* and their target discovery. The identification of NPs and synthetic compounds target proteins is pivotal to understand their mechanism of action for the development of molecular probes and/or potential drugs.

In this scenario, my PhD project has been devoted to the development of a functional proteomics platform based on two complementary label-free strategies, DARTS and t-LiP-MRM. This platform has the advantage of being universally applicable to any molecule, regardless of its chemical features, not requiring any chemical modification of the compound to be studied for both the identification of its interacting protein partner(s) and the characterization of their interaction features. Indeed, at first DARTS is exploited to identify *small molecules* most reliable cellular partners, then t-LiP-MRM is carried out to investigate the molecules/target proteins interaction features.

In particular, during the three-years project, the interactome analysis of three *small molecules* has been evaluated. Moreover, the proteomics results were validated by Western Blotting, to confirm *small molecules* interaction with their DARTS-identified target and by *in silico* molecular docking, to corroborate t-LiP-MRM information about the target region(s) involved in the binding. The direct effects of the disclosed interactions were also assessed through proper in vitro and/or in cell biological assays.

CHAPTER 2

Functional proteomics on Artemetin discloses Filamins as the main cellular targets

Adapted from

Ferraro, G., Belvedere, R., Petrella, A., Tosco, A., Stork, B., Salamone, S., Minassi, A., Pollastro, F., Morretta, E., Monti, M.C. Drug Affinity Responsive Target Stability unveils Filamins as biological targets for Artemetin, an anti-cancer flavonoid 2022, Frontiers in Molecular BioSciences, 9:964295. doi: 10.3389/fmolb.2022.964295.

CHAPTER 2

PART 1

Results

2.1 Background

NPs from plants have been studied since the earliest times due to their therapeutic usefulness against various diseases, having weighty influences on pharmacological science. Mostly, secondary metabolites of plants such as terpenoids, flavonoids, and alkaloids are well documented to hold anti-cancer properties (Choudhari *et al.*, 2020). Indeed, they may positively or negatively control metabolic pathways altered in cancer cells such as proliferation, migration and apoptosis through a multitude of action mechanisms. Therefore, an in-depth investigation of the interactome of NPs is a key step in the drug and target discovery course. Proteins represent the majority of targets of almost all drugs, and they are regulated at multiple levels, mainly by non-covalent or covalent interactions with other ligands varying in their activity and conformation. Specifically, chemo-functional proteomics empowers biochemical or biophysical procedures to detect direct interactions of a bioactive metabolite with its partners, mainly using thermal stability-based approaches or enlarged resistance to proteolysis (Lomenick *et al.*, 2009; Feng *et al.*, 2014). Indeed, NPs binding to targets affects protein conformation and alters their susceptibility to

proteolytic action by stabilization of the folded state: DARTS monitors the reduction in protease exposure of the target protein(s) upon direct binding of the molecule of interest. Similarly, LiP-MS measures proteolytic peptides that play as reporters to determine which protein regions are hugely affected by the NP interaction (Morretta *et al.*, 2021; Schopper *et al.*, 2017; Del Gaudio *et al.*, 2018; Hwang *et al.*, 2020).

2.2 The molecule: Artemetin

Artemetin (Art) is a valuable 5-hydroxy-3,6,7,3′,4′-pentamethoxyflavone (Figure 2.1) present in many different medicinal plants such as *Achillea millefolium L., Artemisia absinthium, Artemisia gorgonum, Cordia verbenacea, Vitex trifolia* and *Vitex negundo* (Ortet *et al.*, 2011; De Souza *et al.*, 2011; De Almeida *et al.*, 2016; Wee *et al.*, 2020; Martim *et al.*, 2021; Sichaem *et al.*, 2021) with very good oral bioavailability and drug-likeness values (Lee *et al.*, 2018) owing bioactivities, such as anti-inflammatory (Sertie *et al.*, 1990; Sertié *et al.*, 1991; Grossini *et al.*, 2015 al., Wee *et al.*, 2020) and anti-cancer (Li *et al.*, 2005; Kim *et al*., 2013; Martins *et al.*, 2014; Sinha *et al.*, 2015; Rosa *et al.*, 2022).

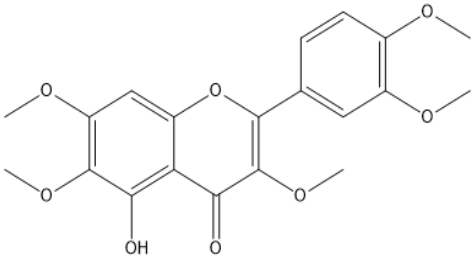

Artemetin

Figure 2.1 *5-hydroxy-3,6,7,3',4'-pentamethoxyflavone (Artemetin, Art) chemical structure.*

Art anti-inflammatory activity has been studied both at a cellular level and *in vivo*. Mainly, Art enlarged eNOS-dependent NO production by mechanisms linking muscarinic receptors, β2-adrenoreceptors, and kinases and upgraded cell viability in porcine aortic endothelial cells by counteracting apoptosis and through the modulation of mitochondria, acting as an antioxidant agent (Grossini *et al.*, 2015). Vice versa, the anti-cancer activity of this molecule has been disclosed in less detail: Art has been found to have a good anti-proliferative effect on many cancer cells, inducing apoptosis of human myeloid leukemia K562 cells and tsFT210 cells through weak inhibition of the cell cycle at the G2/M phase (Li *et al.*, 2005). Moreover, it has been found that Art showed significant cytotoxic activity against human breast cancer cells (MCF-7 and T47D), modulating microtubule depolymerization by activating the mitotic spindle checkpoint and leading to cell apoptosis. However, Art targets in cancer cells have not been truly recognized and thus we moved to investigate its complete interactome in HeLa cell lysates. It has been recently reported that eupatilin, a chemical analog of

Art, showed a cytotoxic effect on cancer HeLa cells (Rosa *et al.*, 2020) and the effect of Art and 8-prenylated-artemetin (8-p-Art, Figure 2.2) has been investigated on this cell line (Salamone *et al.*, 2021). As reported by Salamone et al. (2021), Art and 8-p-Art were able to affect HeLa cell viability at concentrations higher than 25 µM after 72 h of incubation. Moreover, both compounds changed the cell lipid composition, thus affecting the lipid metabolism which is recognized as a novel anti-cancer target. Besides, phase-contrast images of HeLa cells after 72-h treatment with both molecules showed some changes in the cell morphology compared to control cells, mainly in terms of cell elongation (Salamone *et al.*, 2021). Thus, since it was demonstrated that the prenylation hardly enlarges the cytotoxic effect in cancer HeLa cells and also increases the alteration of cell phospholipid and fatty acid composition. The 8-p-Art isomer has also been tested here in comparison with Art in cell assays.

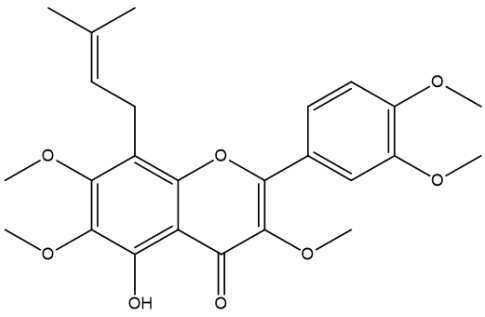

8-prenyl-Artemetin

Figure 2.2 *8-prenyl-Artemetin chemical structure.*

2.3 Identification of Artemetin cellular targets through DARTS

To identify Art cellular interacting proteins, DARTS experiments were performed. This approach is based on a controlled proteolysis of a cellular lysate, pre-treated or not with the small molecule with the low-specificity protease subtilisin under native conditions. A SDS-PAGE of the samples allows monitoring of proteins resistance to the enzymatic cleavage: the band intensity corresponding to the putative protein target(s) will raise in the samples pre-treated with the small molecule, due to its protective effect, in a concentration dependent manner. Thus, the target protein(s) can be identified through *in situ* digestion, nano-UPLC-MS/MS and bioinformatics tools.

Thus, HeLa cell samples lysed in mild non-denaturing conditions, were incubated with increasing Art concentrations and then subjected to subtilisin-mediated limited proteolysis. Only one sample was treated with the vehicle and represented the negative control. An undigested lysate sample without Art was kept as a positive control. All the samples were submitted to SDS-PAGE separation and revealed by Coomassie blue staining. The gel lanes were carefully excised and digested, principally those bands whose intensity raised at increasing Art concentrations (Figure 2.3 Panels A and B). The nano-UPLC-MS/MS analysis of the digested peptide samples, followed by Mascot database search, gave proteins identification. All the experiments were carried out in triplicate: proteins identified in all DARTS were considered (Figure 2.3 Panel C) to recognize Art interacting ones by comparing the Mascot Score outputs with both the positive and negative control samples. Indeed, Mascot scores are related to the protein identification confidence: higher scores reflect a better match of experimental spectra to *in silico* MS and MS/MS ones due to a higher abundance of the intact protein

in the gel lane. Thus, Art protection levels (reported as percentages) were evaluated for each identified protein. Among them, Filamin A (FLNA) and B (FLNB) have been selected as the main partners since they were better protected from proteolysis in all DARTS replicates (Figure 2.3 Panel D).

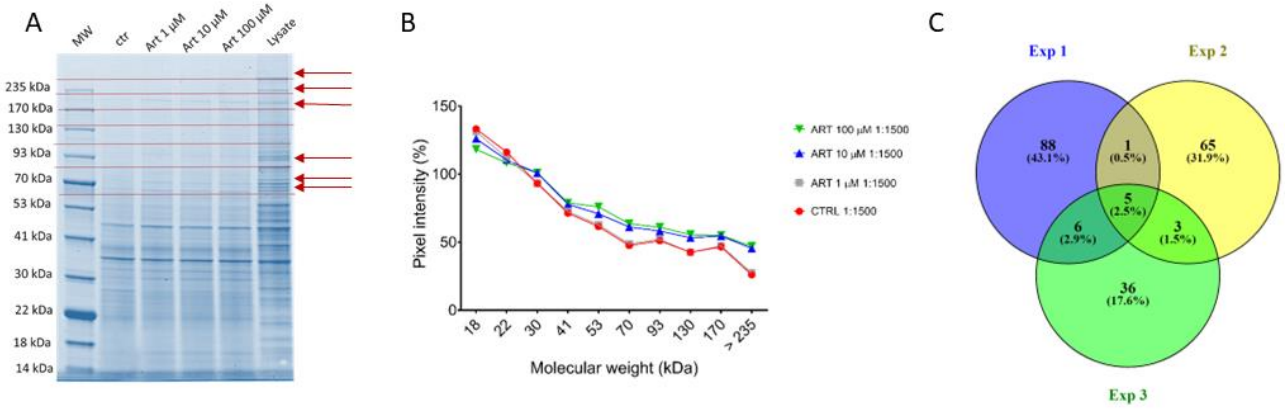

D

			Protection Level (%)		
Accession	Mass (Da)	Description	1 µM	10 µM	100 µM
P21333	283301	Filamin-A	13.2	53.6	61.0
O75369	280157	Filamin-B	11.1	22.4	26.8
P55060	111145	Exportin-2	0.0	18.2	28.3
P43246	105418	DNA mismatch repair protein Msh2	0.0	25.6	30.8
P13639	96246	Elongation factor 2	3.0	37.0	42.6

Figure 2.3 ***(A)*** *Coomassie-stained gel showing protection of proteins (red arrows) to protease upon Art interaction. Red lines indicate gel cutting patterns.* ***(B)*** *SDS-PAGE densitometric analysis.* ***(C)*** *Venn diagram showing shared Art protected proteins among three DARTS experiments.* ***(D)*** *Mascot retrieved protection percentages of the five proteins shared among all the DARTS experiments.*

Since both FLNA and FLNB were the most protected targets at the low Art concentration, accordingly to MS, a bio-orthogonal validation has been planned using a more quantitative technique such as immunoblotting. Thus, the direct interaction

between these two putative partners and the small molecule was unequivocally confirmed by western blotting analysis, submitting all DARTS samples to an anti-FLNA and FLNB antibodies reaction (Figure 2.4). Actually, comparing immunoblotting signals corresponding to undigested FLNA and FLNB, it is clear that the intact proteins signals increase their intensity accordingly to Art concentration (MW~280-260 kDa).

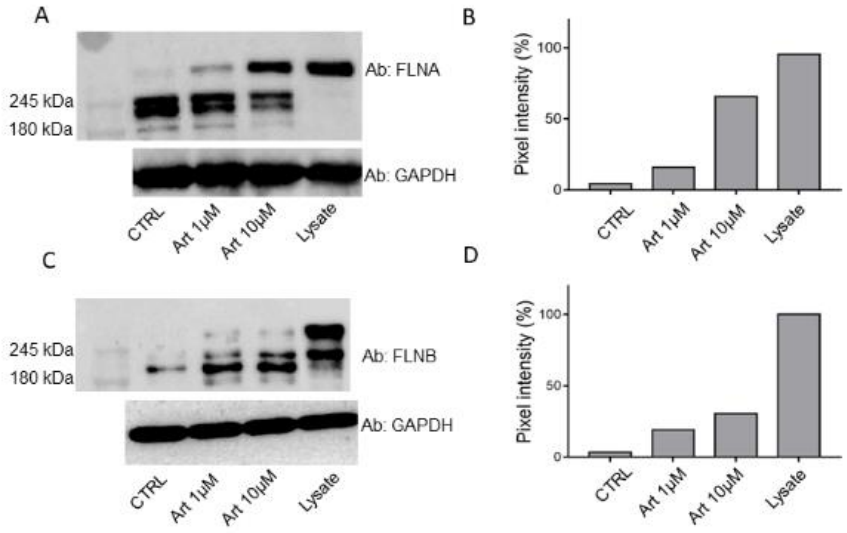

Figure 2.4 *Immunoblotting analysis of one of the DARTS experiments revealing FLNA (panel A) and FLNB (panel C), together with their densitometric analysis (panels B and D, respectively). GAPDH is resistant to subtilisin under these experimental conditions and is used as a loading control.*

2.3.1 Analysis of the interaction features of FLNA and FLNB binding to Artemetin by targeted limited proteolysis approach

To further explore Art interaction profile with both its targets, a t-LiP-MRM strategy has been carried out. T-LiP MRM allows the recognition of the target/ligand interface region(s) in a whole-cell lysate, looking at the protein conformational alterations due to a ligand bond.

The HeLa cells native proteins were treated or not with Art and then a double-protease digestion was performed: first, a subtilisin limited proteolysis was achieved under native conditions and then, a full tryptic digestion was settled in denaturing settings. This sequential treatment generates a combination of semi-tryptic and fully tryptic peptides, the latter suitable for targeted MRM-MS quantification analysis. Indeed, the area of fully tryptic peptides can be considered indicative of the local target structural changes due to ligand binding: it will be higher when subtilisin limited proteolysis is less effective due to Art masking proteolytic protein regions. An initial *in silico* search using the bio-informatics device *PeptideAtlas* and *SRMAtlas* is performed to set the more likely MRM transitions of FLNA-FLNB theoretical fully tryptic peptides to map the proteins. Then, a cell lysate sample was denatured and extensively proteolyzed by trypsin to unequivocally recognize the most reliable peptide signals and their most intense daughter ions by LC-MRM-MS. Next, native protein mixtures were incubated with Art (10 μM and 100 μM) or vehicle (negative control) and treated with subtilisin in restricted conditions of time, temperature and at the enzyme to proteins ratios of 1:500 and/or 1:1500 (w/w). Subtilisin was then quenched, the samples were denatured and fully digested by trypsin and the mixtures were run on the LC-MRM-MS system to quantify the area of each FLNA and FLNB tryptic peptides. Then, peptides mapping

for FLNA and FLNB regions putatively interacting with Art were analyzed by comparing the controls and the treated samples: peptides with increased intensity in the samples exposed to the small molecule were considered symptomatic of Art protection on specific FLNA and FLNB regions.

As shown in Figure 2.5 A and B, Art interacts differently with FLNA and FLNB; in particular, the main FLNA protected regions were the N-terminal and the C-terminal, which are the actin-binding domain and the self-association site tail interacting with FLNB, respectively. Differently, more peptides have been protected by Art along the entire sequence of FLNB: five of them fall in the C-terminal region, deputed to the interaction with FLNA. The C-terminal is also the region involved in the dimerization of filamins allowing the formation of a V-shaped flexible structure that is essential for their function.

More in deep, FLNA can combine with a variety of proteins through direct or indirect interaction to effect downstream target proteins. FLNA changes lead to cytoskeleton reconstruction, vesicles transport disorders and signal transduction changes. So, FLNA plays an important role in the occurrence of genetic diseases, the development of tumors and the infection of pathogenic microorganism. The role is different in different tumors. High expression of FLNA may promote metastasis of some tumors but it can have also an inhibitory effect in other tumors. Mainly, it depends from the activation form and cellular localization of FLNA. Post-translational modification such as phosphorylation is an important form of its function. PKA can induce phosphorylation of FLNA Ser2152, which could resist calpain cleavage the hinge. Then, phosphorylated FLNA regulates cytoskeleton reconstruction, migration and invasion of cancer cells, formation of membrane ruffling (Zhou *et al.*, 2021). Furthermore, when it localizes in the cytoplasm, it promotes tumor progression through cell

migration, adhesion and growth signals. However, when it is hydrolyzed, the C-terminal will locate in the nucleus, which can inhibit tumor growth and metastasis by interacting with transcription factors (Zhou *et al.*, 2021).

FLNB crosslinks actin cytoskeleton filaments into a dynamic structure. Up to present, pathogenic mutations in FLNB are solely found to cause skeletal deformities, indicating the important role of FLNB in skeletal development. FLNB-related disorders are classified as spondylocarpotarsal synostosis (SCT), Larsen syndrome (LS), atelosteogenesis (AO) and boomerang dysplasia (BD). The mechanisms of FLNB mutations causing skeletal malformations remain obscure, though several hypotheses have been proposed (Xu *et al.*, 2017).

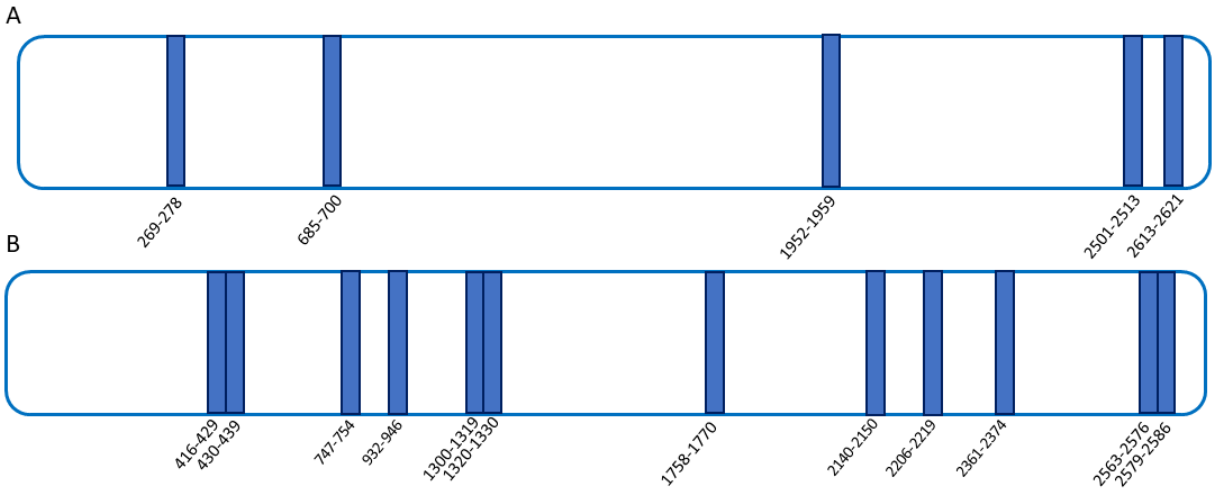

Figure 2.5 *t-LiP-MRM experimental results: Art protected peptides are reported as blue bars in both FLNA (panel A) and FLNB (panel B) schematic representations.*

2.4 8-prenyl-Artemetin targets Filamin A and Filamin B

Since during my experimental work on Art, it was demonstrated that the prenylation hardly enlarges the cytotoxic effect in cancer HeLa cells and also increases the alteration of cell phospholipid and fatty acid composition (Salamone *et al.*, 2021), we moved to prove that this chemical modification didn't alter the interaction with FLNA and B.

A DARTS-based experiment was performed using 8-p-Art in the same experimental conditions used for Art and above-described, followed by nano-UPLC-MSMS analysis and Mascot identification. As expected, 8-p-Art is able to well protect both FLNA and FLNB already at the lowest tested amount, even if without a concentration dependent fashion (Figure 2.6). This is full in line with the next results showing a higher effect of the 8-p-Art.

8p-Art			Protection Level (%)		
Accession	**Mass (Da)**	**Description**	**1 µM**	**10 µM**	**100 µM**
P21333	283301	Filamin-A	53.2	42.7	55.1
O75369	280157	Filamin-B	53	39.3	47.1

Figure 2.6 *Mascot retrieved protection percentages of Filamin A and B in a DARTS experiment carried out on HeLa cell lysates incubated with 8-p-Art at the reported concentrations.*

2.5 Artemetin and 8-prenyl-Artemetin permeation of artificial membranes

Before moving to assays in live cells, we tested Art and its supposed more permeable 8-p-Art derivative in the parallel artificial membrane permeability assay (PAMPA) to measure their effective permeability (expressed as a -Log Pe) through an artificial lipid membrane (Le Roux *et al.*, 2020). Propranolol and furosemide at 250 µM were used as positive and negative control molecules giving a -Log Pe of 5.30 for propranolol and 6.90 for furosemide (-Log Pe < 6 is considered good permeability and -Log Pe > 6.5 as impermeable). In this assay, as shown in Figure 2.7, Art displayed a good propensity to cross the membrane *in vitro*, with a - Log Pe of 5.87 ±0.01; as expected, 8-p-Art showed an even better permeability profile with a -Log Pe of 5.57 ±0.01.

	Propranolol 250 µM	Furosemide 250 µM	Art 50 µM	8p-Art 50 µM
logPe	-5.30	-6.90	-5.87	-5.57
dev.st.	0.02	0.01	0.01	0.01

Figure 2.7 *Results of Parallel Artificial Membrane Permeability Assay (PAMPA) assay.*

2.6 Effects of Artemetin and 8-prenylated Artemetin on Filamin A and B and F-actin in HeLa cells

To monitor the interaction of Art and its prenylated form with FLNA and FLNB in living HeLa cells, a confocal microscopy has been performed, thanks to a collaboration with Prof. Antonello Petrella group (University of Salerno, Department of Pharmacy) and Prof. Björn Stork group (University of Düsseldorf, Department of Molecular Medicine I). The immunofluorescence staining of FLNA showed that, in presence of Art and 8-p-Art, this protein appeared disassembled in pointed structures starting from 24 hours of treatments (Figure 2.8, upper panels b-e). This effect has been more evident in the case of 48 hours of treatments with both substances (Figure 2.8, upper panels f-i) to remain constant at 72 hours (Figure 2.8, upper panels j-m). There are no significant differences between Art and its relative prenylated form and the highest concentration (25 µM) of both compounds showed the strongest activity. The same tendency has been highlighted on FLNB (Fig. 2.8, lower panels). In particular, after 48 hours from the addition of Art and 8-p-Art, this protein began to form fragmented structures, mainly at 25 µM of both molecules (Figure 2.8, lower panels f-m) indicating a cytoskeletal disassembling.

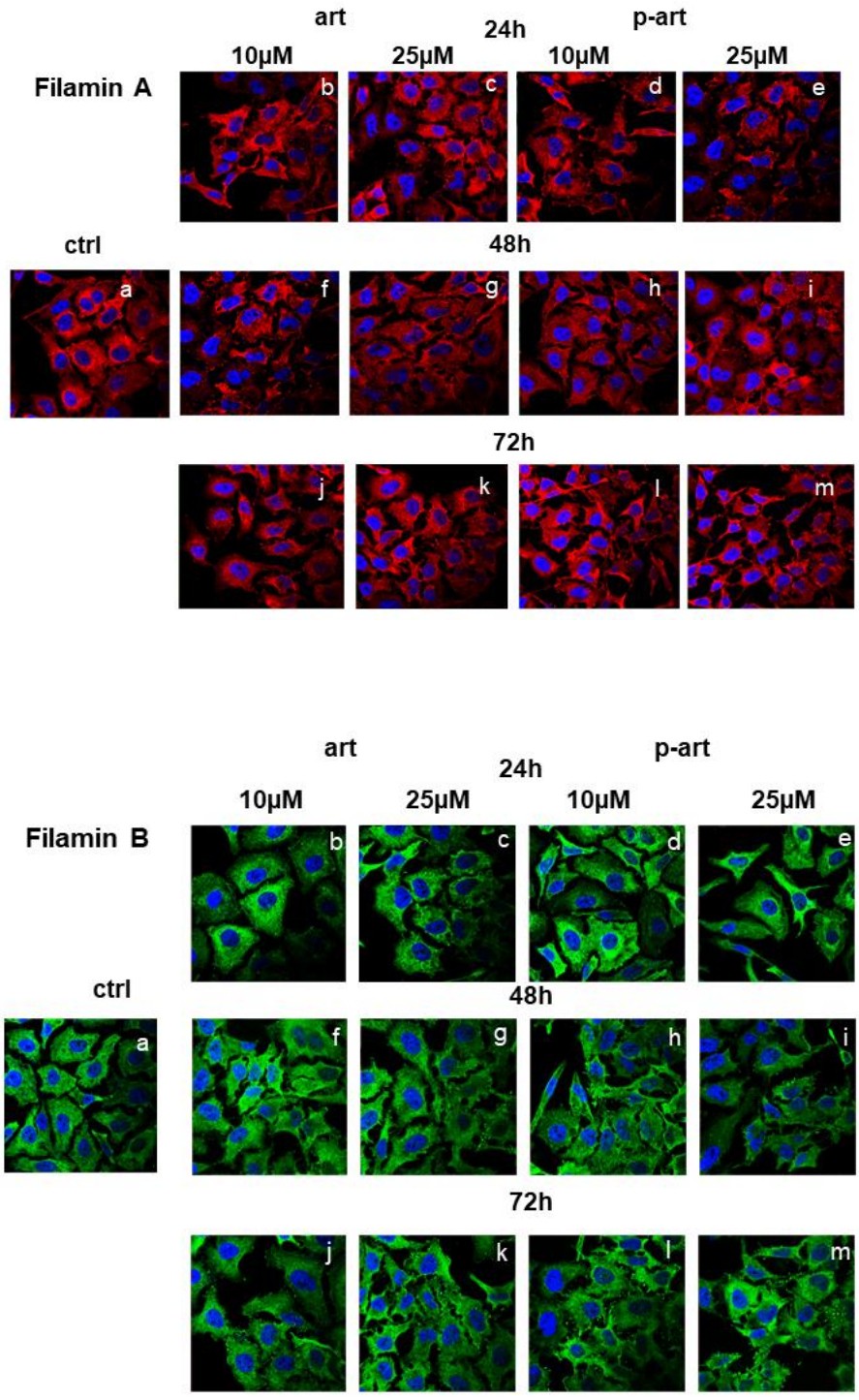

Figure 2.8 *Immunofluorescence analysis of Art and 8-p-Art-treated (10 and 25 μM; from 24 up to 72 hours) HeLa cells. These ones were fixed and labeled with an antibody against FLNA (red) and FLNB (green). Magnification 63 × 1.4 NA. Bar =*

100 μm. All images are representative fields of n = 3 experiments with similar results.

One of the main roles of FLNA and B is the connection with F-actin by which these proteins can coordinate biomechanical responses to force extracellular matrix stiffness and/or adhesive properties, with intracellular consequences (Sutherland-Smith, 2011). The administration of Art and the 8-p-Art to HeLa cells induced substantial disorganization of the F-actin filaments in a definitive manner compared to not treated cells. Interestingly, these effects appeared from 24 hours until 72 hours of treatments. There are no differences between the two compounds and their concentrations (Figure 2.9, panels a-m). Actin filaments cross-link into bundles to form the dynamic actin cytoskeletal network, which is finely tuned by multiple families of cytoskeletal proteins belonging to the microfilaments class, among which filamins represent one of the essential elements. Together with microfilaments, intermediate filaments and microtubules constitute the cytoskeleton (Yue *et al.*, 2013). To prove the selectivity of Art and 8-p-Art on microfilaments, we performed further confocal analyses on tubulin and vimentin (Figure 2.10) as representative proteins of intermediate filaments and microtubules, respectively. They are not affected neither by Art neither by 8-p-Art.

Taken together, these results have highlighted that the tested compounds have shown a notable selectivity for FLNA and FLNB whose disorganization could be the cause of the following disassembling of F-actin filaments. Additionally, these filaments appeared to be affected by Art and its prenylated counterpart more rapidly than filamin ones as they are characterized by a dynamic steady state conferring a high degree of plasticity to cytoskeleton networks (Plastino *et al.*, 2018).

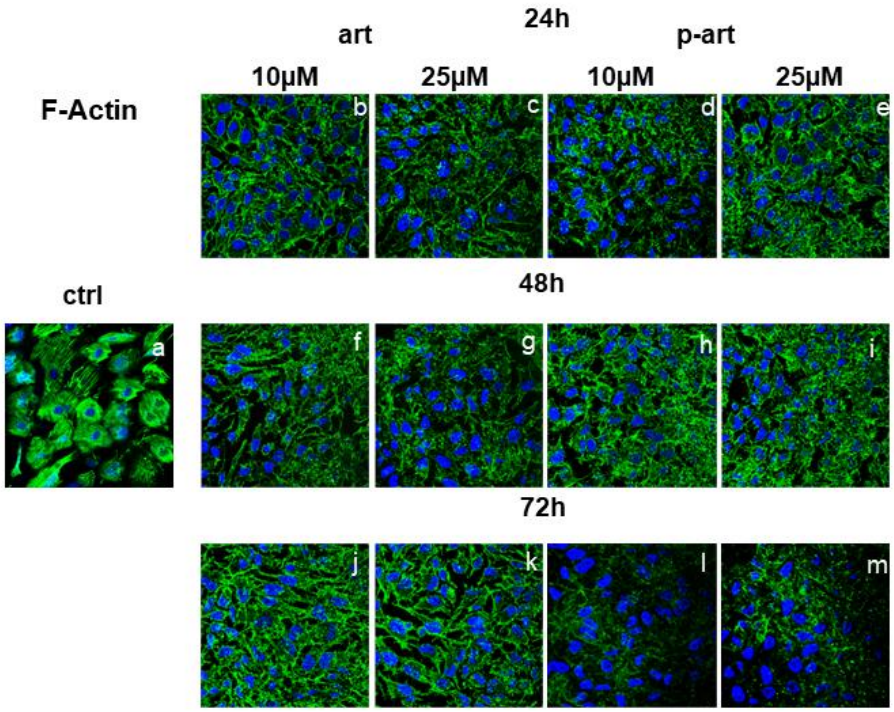

Figure 2.9 *Immunofluorescence analysis of Art and 8-p-Art-treated (10 and 25 μM; from 24 up to 72 hours) HeLa cells. These ones were fixed and labeled with phalloidin-FITC to detect F-actin. Magnification 63 × 1.4 NA. Bar = 100 μm. All images are representative fields of n = 3 experiments with similar results.*

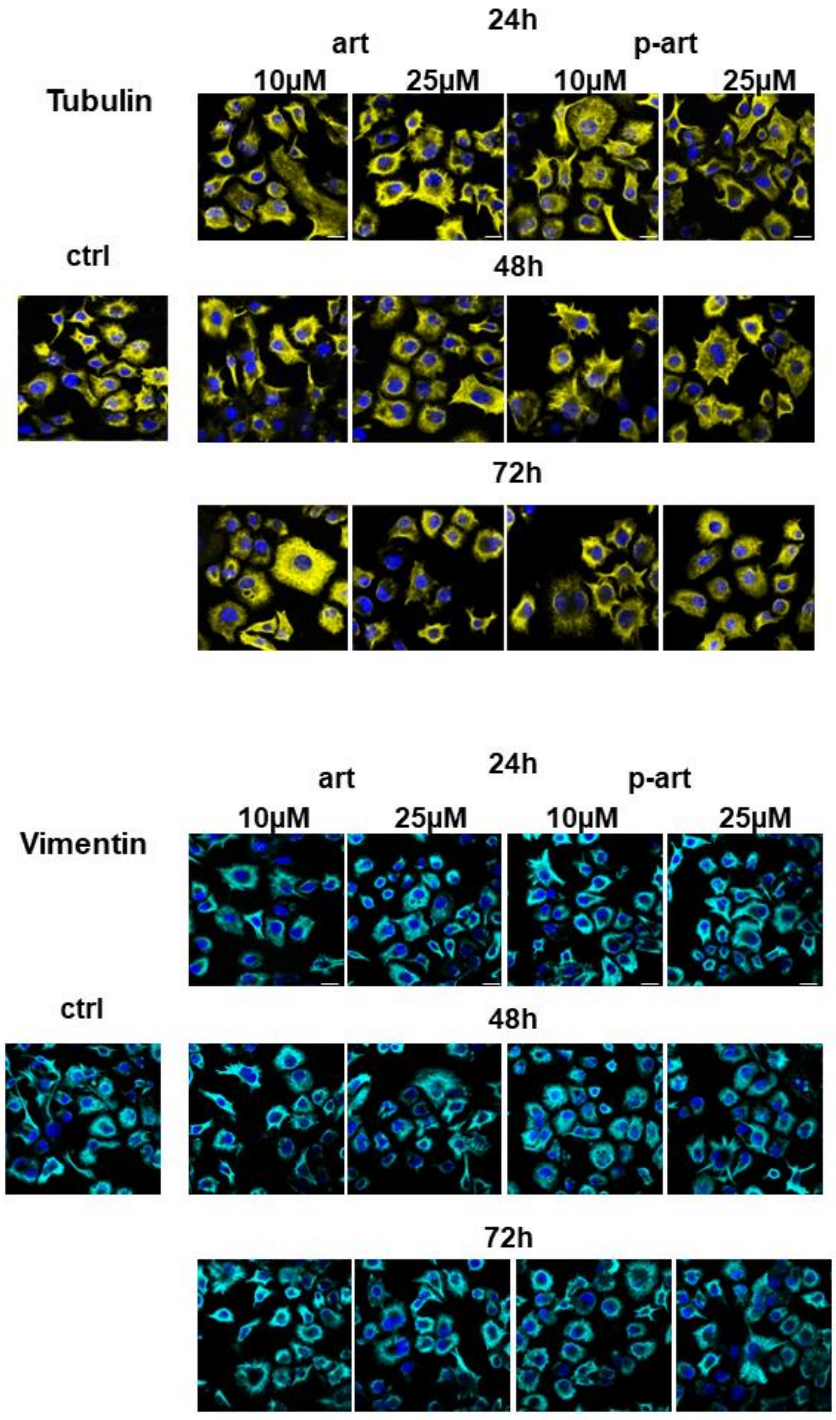

Figure 2.10 *Confocal microscopy analysis of HeLa cells tubulin and vimentin in presence of Art and of 8-p-Art. Treatments with both compounds were performed at 10 and 25 μM from 24 to 72 hours.*

2.7 Effects of Artemetin and 8-prenylated Artemetin on HeLa cell migration

Since the compounds have shown a strong induction of actin disorganization, we focused on cell migratory ability, which is well related to cancer progression (Schaks *et al*., 2019), thanks to a collaboration with Prof. Antonello Petrella group (University of Salerno, Department of Pharmacy). By the wound-healing assay, we assessed that in presence of Art and 8-p-Art, the migration of HeLa cells appeared notably affected. In particular, as shown by the histogram and the bright field representative images (Figure 2.11 A and B, respectively), the prenylated compound showed a more potent inhibitory activity in replacing destroyed or damaged tissue.

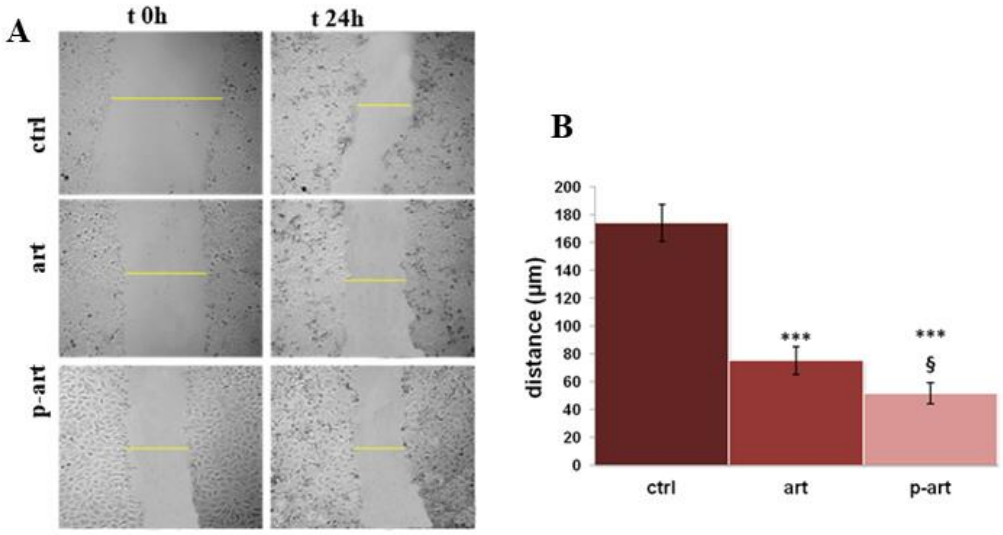

Figure 2.11 *Results from the scratch wound healing assay on HeLa cells treated or not with Art and 8-p-Art at 25µM. (A) Representative bright-field images of cells captured by Time Lapse microscope (Leica AF-6000 LX; Leica Microsystems). Magnification ×10. ***p < 0.001 versus untreated controls; p < 0.05 for 8-p-Art versus Art. (B) Analysis of the migration rate determined by measuring the distances*

covered by individual cells from the initial time to the selected time points (bar of distance tool; Leica ASF software). The data are representative of n = 3 independent experiments ± SD.

CHAPTER 2

PART 2

Discussion

2.8 Conclusive remarks

The aim of the first part of my PhD was to investigate the interactome of Art in HeLa cancer cells to go in deep into the anti-tumoral profile of this bioactive compound and its more permeable 8-p-Art. In this study, a multidisciplinary approach has been adopted to study the cellular targets in the unbiased contest of the full proteome from HeLa cells. Firstly, a proteomic-based DARTS has been exploited and the Art and 8-p-Art interactors have been identified by a bioinformatic analysis of the mass spectrometric results.

FLNA and B were disclosed as the most protected proteins by Art and the same effect has been validated for 8-p-Art.

To further explore Art interaction profile with both its targets, a t-LiP MRM strategy has been carried out. T-LiP MRM allows the recognition of the target/ligand interface region(s) in a whole-cell lysate, looking at the protein conformational alterations due to a ligand bond. Filamin isoforms seem to interact with the small molecule by different features, both mainly in the N-terminal and C-terminal regions deputed to actin binding and their homo and hetero-oligomerization. In particular, the main FLNA

protected regions were the N-terminal and the C-terminal, which are the actin-binding domain and the self-association site tail interacting with FLNB, respectively. Differently, more peptides have been protected by Art along the entire sequence of FLNB: five of them fall in the C-terminal region, deputed to the interaction with FLNA. The C-terminal is also the region involved in the dimerization of filamins allowing the formation of a V-shaped flexible structure that is essential for their function.

Filamins are actin-binding proteins, which participate in the formation of the cytoskeleton, anchor a variety of proteins in the cytoskeleton and regulate cell adhesion and migration. Moreover, they are members of the focal adhesion protein machinery and therefore act as a linker between the extracellular matrix (ECM) and the actin cytoskeleton. Indeed, by binding several partner proteins such as integrins, filamins regulate cell functions such as migration, proliferation, apoptosis and mechano-protection. Thus, the biological effect of Art and its prenylated form has been studied in detail, revealing an impact on cytoskeleton disassembly and on F-actin filaments disorganization mediated by filamins dissociation, stronger induced by 8-p-Art. Indeed, it is already reported in the literature that the microtubule dynamics interference is an effective tool to kill tumor cells (Wordeman *et al.*, 2021): the so-called microtubule-targeting agents (MTAs) represent one of the most successful first-line therapies prescribed for cancer treatment and they are believed to kill cells via apoptosis by blocking cell migration. Since F-actin and filamin disorders are critical elements for different fundamental cellular functions, including cell migration, this phenomenon has been investigated in HeLa cells treated or not with both compounds of interest, revealing that Art and 8-p-Art are potent inhibitors of cellular migration.

In conclusion, since the downregulation of cell adhesion and migration in the tumor microenvironment is a crucial step to block tumor metastasis' occurrence and development, the discovery of the Art interactome by our functional proteomic platform and the insights on the interaction between the *small molecules* with filamins paves the way for consideration of these compounds as leads in the treatment of cancer.

CHAPTER 2

PART 3

Materials and Methods

2.9 Identification of Artemetin cellular targets

2.9.1 Cell Culture

HeLa cells (ATCC® CCL-2™; Manassas, VA USA) were grown in Dulbecco's Modified Eagle Medium (DMEM) with 10% fetal bovine serum (FBS) and 1% penicillin and streptomycin (Euroclone, Milan, Italy). Cells were grown at 37 °C in air humidified 5% CO_2.

2.9.2 Drug Affinity Responsive Target Stability

HeLa cells were lysed in PBS 0.1% v/v Igepal supplied with a protease inhibitor mixture (final concentration 1x, Sigma Aldrich). The lysate was centrifuged at 10,000 g for 10 min (4°C) and the protein concentration of the obtained supernatant was determined by Bradford assay. Then, DARTS experiments were carried out: different amounts of Art or 8-p-Art (1 μM, 10 μM and 100 μM) were incubated with 300 μg of HeLa cell lysate for 1 hour at room temperature under rotary shaking. The samples were then submitted to limited proteolysis, for 30 minutes at 25°C, at a ratio

of 1:1500 w/w of subtilisin (Sigma Aldrich) in respect of proteins amount. Two samples of cell lysates were treated with dimethyl sulfoxide (DMSO) and one of them with subtilisin, as control experiments. Then, the protease was quenched by adding PMSF (phenylmethylsulfonyl fluoride, Sigma-Aldrich, 1 mM final concentration) to each sample. Then, all samples were boiled in Laemmli buffer (60 mM Tris-HCl pH 6.8, 2% SDS, 0.001% bromophenol blue, 1% glycerol, 2% β-mercaptoethanol) and 20 µg were loaded on a 4-12% Bis-Tris Criterion™ XT Precast Gel (Bio-Rad Laboratories S.r.l.) which was then stained with a Coomassie solution and submitted to a densitometric analysis through ImageJ. This experiment was carried out in triplicate for Art, and it was repeated incubating with 8-p-Art at the same concentrations. Protein bands were cut out from the gels and submitted to an *in situ* tryptic digestion protocol (Shevchenko *et al.,* 2006). Briefly, gel slices were reduced with DTT (1,4-dithiothreitol), alkylated with IAA (iodoacetamide), washed and rehydrated on ice for 1 h in a 12 ng/µl trypsin solution. Then, the enzyme excess was removed and replaced with ammonium bicarbonate (AmBic, 50 mM, pH 8.5), allowing protein digestion to proceed overnight at 37 °C. Subsequently, supernatants were collected and peptides were extracted from each gel slice, shrinking them in 100% ACN (acetonitrile). The obtained peptides mixtures were dried under vacuum and dissolved in formic acid (FA, 10%) for the LC-MSMS analysis.

2.9.3 nanoLC-MS-MS analysis

1 µl of each peptide sample was injected into a nano-UPLC system (ThermoFisher Scientific, Bremen) separating peptides on an EASY-Spray PepMAP™ RSLC C18 column (3µm, 100Å, 75 µm x 50 cm, ThermoFisher Scientific,

Bremen) at a flow rate of 0.3 ml/min. Peptides elution was achieved at a flow rate of 300 nL/min with the following gradient: 1 min at 3% B, 1 min to 40 min to 28% B, 40 min to 41 min to 70% B, 41 min to 49 min at 70% B and 50 min to 60 min back to 3% B (A: 95% H_2O, 5% ACN, 0.1% AcOH; B: 95% ACN, 5% H_2O, 0.1% AcOH). The mass spectrometer was operated in data-dependent acquisition mode (DDA). Full scan MS spectra were acquired with the following settings: scan range 400–2000 m/z, full-scan automatic gain control (AGC) target 1e6 at 70000 resolution, maximum injection time 100 ms. MS/MS spectra were generated for up to 10 precursors (normalized collision energy of 30%) and the fragment ions acquired at a resolution of 17500 with an AGC target of 1e5 and a maximum injection time of 50 ms.

2.9.4 Bioinformatic Analysis of targets

Subsequently, database searches were carried out on Mascot Deamon, employing the SwissProt database and the following settings: two missed cleavages; carbamidomethyl (C) as fixed modification; oxidation (M) and phosphorylation (ST) as variable modifications; peptide tolerance 30 ppm; MS/MS tolerance 0.8 Da.

2.10 Immunoblotting analysis

The DARTS samples of Art were submitted to western blotting analysis. First, 20 µg of each sample were loaded on an 8% SDS-PAGE and transferred onto a nitrocellulose membrane; then, they were incubated for 1 h in a blocking solution (5% w/v milk in TBS-t: 31 mM Tris pH 8, 170 mM NaCl, 3.35 mM KCl, 0.05% Tween

20) and left for 16 h at 4°C with monoclonal antibodies against FLNA and FLNB (1:1000 v/v, RayBiotech). Then, a rabbit peroxidase-conjugated secondary antibody (1:1000 v/v, Thermo Fisher Scientific) was added, and the signal was detected using an enhanced chemiluminescent substrate and LAS 4000 digital imaging system. Finally, an antibody against glyceraldehyde 3-phosphate dehydrogenase (GAPDH, 1:2000 v/v, Invitrogen) in 5% milk has been used as a loading normalizer.

2.11 Filamins A and B LiP-MRM method building

Filamin A (FLNA) and B (FLNB) tryptic peptides previously detected by MS were selected through the proteomics data resource *Peptide Atlas* on its Human build and queried into *complete Human SRM Atlas* to obtain their best daughter ions. Thus, comprehensive methods listing filamins peptides and their three best transitions were obtained and subsequently tested onto a HeLa lysate tryptic digest. HeLa cell lysate, obtained as described before, was submitted to an *in-solution* digestion protocol: proteins were denatured with 8 M urea/50 mM AmBic (4 M final urea concentration), disulfide bonds were reduced with 10 mM DTT for 1 h at 25°C and 800 rpm and then alkylated with 20 mM iodoacetamide for 30 minutes, at 25°C and 800 rpm, in the dark. Iodoacetamide was quenched with 10 mM DTT (10 minutes, 25°C, 800 rpm) and urea was diluted to 1 M with 50 mM AmBic before adding the trypsin/LysC solution (Promega, Madison, Wisconsin) at the enzyme to proteins ratio of 1:100 w/w. Digestion proceeded overnight at 37°C under continuous shaking and was then quenched by adding FA to lower the pH to 3. The peptides mixture was then dried under vacuum, dissolved in 1 mL 5% FA and desalted through a Sep-Pak C18 1 cc (50 mg) cartridge (Waters, Milford, MA, USA). The cartridge was activated by flushing 3

mL of 100% ACN and then conditioned with 3 mL of 0.1% FA. The sample was then loaded, desalted by flushing the cartridge with 3 mL of 0.1% FA and finally eluted by flushing two times 500 μL of 80% ACN, 20% H2O, 0,1% FA. For the subsequent MS analysis, the peptides mixture was dried under vacuum and re-dissolved in 10% FA. UPLC–ESI-MRM-MS analyses were performed on a 6500 Q-TRAP from AB Sciex equipped with Shimadzu LC-20A and Auto Sampler systems. UPLC separation was performed on a Kinetex PS C18 column (50 × 2.1 mm, 2.6 μm, 100 Å, Phenomenex, Torrance, USA), using 0.1% FA in H_2O (A) and 0.1% FA in ACN (B) as mobile phases, and a linear gradient from 5 to 95% of B over 20 min (flow rate: 300 μL/min). Q-TRAP 6500 was operated in positive MRM scanning mode, with declustering potential (DP) set at 80 V, entrance potential (EP) at 10 V and cell exit potential (CXP) at 22 V. Collision energy (CE) was calculated for each precursor as follows: CE = 0.044 × (Q1 m/z) + 5.5 (precursor charge 2+) and CE = 0.051 × (Q1 m/z) + 0.5 (precursor charge >2+).

2.12 Artemetin/Filamins interaction features evaluation through t-LiP-MRM

HeLa cells were incubated with DMSO or Art (10 μM and 100 μM final concentrations), for 1 h at room temperature. The samples were then submitted to limited proteolysis with 1:500 and 1:1500 (w/w) ratio of subtilisin in respect to protein amount, leaving an aliquot of the DMSO treated one undigested to be kept as a positive control. Subtilisin was then quenched with PMSF (1 mM final concentration) and the mixtures shifted to denaturing conditions adding urea (4 M final concentration) to perform *in-solution* digestion and desalting, as previously reported. The samples were then injected into the previously reported UPLC-ESI-MS system and analyzed through

the optimized filamins MRM methods. Each protein tryptic peptide peak area was then measured using the Analyst Software from AB Sciex. Each sample was analyzed in duplicate.

2.13 Artemetin and 8-prenyl-Artemetin PAMPA assays

Donor solution (50 μM) was prepared by diluting 5 mM Art or 8-p-Art stock solutions using phosphate saline buffer (PBS: 137 mM NaCl, 2.7 mM KCl, 10 mM Na_2HPO_4, 2 mM KH_2PO_4, pH 7.4). The filter membrane was coated with 5 μL of specific lipid solution prepared as a 1% w/v phosphatidylcholine solution in n-dodecane. Donor solution (150 μL) was added to each well of the filter plate. To each well of the acceptor plate, 300 μL of solution (5% DMSO in PBS) were added. Donor and Acceptor plates were assembled to obtain a sandwich and incubated for 24 h at room temperature under gentle shaking. Then, the sandwich plates were separated and 250 μL of the solution from the acceptor plate and 100 μL of the solution from the donor one were transferred to a new multi-well plate and the absorbance was measured by UV spectroscopy using a Multiscan GO microplate spectrophotometer (Thermo Scientific) at 250−500 nm (5 nm steps). The permeability value Log Pe has been determined. The membranes' integrity was checked using propanolol and furosemide as control molecules.

2.14 Confocal Microscopy

HeLa cells were seeded in glass bottom multiwell plate at 8.0 x 10^4. After treatments with either Art or 8-p-Art, cells were fixed in p-formaldehyde at 4% v/v in PBS (Lonza; Basilea, Swiss), permeabilized with Triton X-100 at 0.5% v/v in PBS (Lonza; Basilea, Swiss) and then blocked with goat serum at 20% v/v in PBS (Lonza; Basilea, Swiss). Incubation with the respective antibodies against FLNA and B was performed O/N at 4°C. F-actin detection was evaluated by Phalloidin-FITC (5 μg/mL, Sigma-Aldrich; Saint Louis, MO, USA) for 30 minutes at RT in the dark. The staining with conjugated secondary antibodies (1:500, anti-mouse), the nuclei with DAPI (1:1000) and the subsequent confocal microscope analysis were performed as described in (Belvedere *et al.*, 2017; Belvedere *et al.*, 2018).

2.15 Wound-Healing Assay

The confluent monolayer of HeLa was scraped with a pipette tip to produce a wound. Next, cells were treated for 24 h with 25 μM Art or 8-p-Art following a previous administration of mitomycin C (10 μg/mL, Sigma-Aldrich; Saint Louis, MO, USA) to ensure the block of mitosis. The wounds were photographed and analyzed as previously reported (Belvedere *et al.*, 2017; Franco *et al.*, 2020). Briefly, the wounded cells were incubated at 37°C in a humidified and equilibrated (5% v/v CO_2) incubation chamber of an Integrated Live Cell Workstation Leica AF-6000 LX. A 10× phase contrast objective was used to record cell movements with a frequency of acquisition of 10 min for each experimental condition. The migration rate of individual cells was determined by measuring the wound closure from the initial time (0 h) to the selected

time-points (over 24 h) (bar of distance tool, ASF software, Leica, Wetzlar, Germany). For each wound, five different positions were registered, and for each position, ten different cells were randomly selected. Carrying on with the images taken every 10 min, the made distance was recorded each 2 h.

2.16 Statistical Analysis

All the biological assays data and statistical analyses were made with Microsoft Excel. We reported the number of independent repetitions and p values in the legends of the figures for each experiment. All results are the mean ± standard deviation of at least 3 experiments performed in triplicate. The statistical data analysis was performed thanks to the two-tailed t-test comparing two variables and the differences were considered significant if $p < 0.05$, $p < 0.01$ and $p < 0.001$.

CHAPTER 3

Disclosing brain glycogen phosphorylase as the main target of 1g

Adapted from

Ferraro, G., Mozzicafreddo, M.; Ettari, R.; Corsi, L.; Monti, MC.; A proteomic platform unveils the brain glycogen phosphorylase as a potential therapeutic target for glioblastoma multiforme. 2022, Int. J. Mol. Sci. 2022, 23, 8200. https://doi.org/10.3390/ ijms23158200.

CHAPTER 3

PART 1

Results

3.1 Background

Glioblastoma multiforme (GBM) is the most common and aggressive malignant tumor of the Central Nervous System (SNC). In the last few years, several efforts have been ended to identify original strategies against glioblastoma multiforme (GBM): this requires a more detailed investigation of the molecular mechanism of GBM so that novel targets can be identified for new possible therapeutic agents. In this context, a very interesting and BBB-permeable compound endowed with multiple biological activities, the (1-(4-amino-3,5-dimethylphenyl)-3,5-dihydro-7,8-ethylenedioxy-4h-2,3-benzodiazepin-4-one) called 1g (Figure 3.1) has been investigated (Grasso *et al.*, 1999).

3.2 Benzodiazepines

Benzodiazepines (BZDs) are a class of drugs known for their depressant effect on the central nervous system (SNC). They quickly diffuse through the blood-brain barrier and act as positive allosteric modulators on the gamma amino butyric acid

(GABA) receptor. The GABA receptor is a ligand-gated chloride-selective ion channel, it is the most common neurotransmitter in the central nervous system and it has an inhibitory nature and thus reduces the excitability of neurons, producing a calming effect on the brain (Olsen *et al.*, 1984).

BZDs are classified in terms of their elimination half-life. Short-acting BZDs have a median elimination half-life of 1-12 hours, intermediate-acting BZDs have an average elimination half-life of 12-40 hours and long-acting BZDs have an average elimination half-life of 40-250 hours. Another way to characterize BZDs is by relative potency. They were classified in low, medium and high potency. The high-potency BZDs showed improved therapeutic effects as well as faster onset of action. However, with increased potency comes an increase in the risk of undesired effects. Therefore, clinicians must consider individual properties such as absorption, distribution, elimination half-life, and lipid solubility (Griffin *et al.*, 2013).

Common side effects include drowsiness, lethargy and fatigue and higher dosage can impair motor coordination, vertigo, slurred speech, blurry vision and mood swings. BZDs are eliminated slowly from the body, so repeated doses over a prolonged period can result in significant accumulation in fatty tissues. Drug interaction is another issue with BZDs. They are metabolized in the liver via the cytochrome p450 and then renally excreted. Drugs that either attenuate or potentiate cytochrome p450 enzymes will either increase or decrease the elimination half-life of BZDs, respectively (Kienitz *et al.*, 2022).

Due to their rapid onset, they are used for sleep, anxiety, spasticity due to SNC pathology, muscle relaxation and epilepsy. Their sedative effect aids in sleep and insomnia disorders. Their SNC depressant effects potently reduce anxiety and abort acute-onset panic and anxiety attacks. Benzodiazepines are also incredibly effective at

aborting convulsant activity in those with epilepsy or other seizure disorders. Furthermore, chronic use has been linked to a decline in cognitive function, increased risk of dementia and dementia-like illnesses, and impaired sensory and motor function in the elderly, as well as aggressive behavior in consumers (Griffin *et al.*, 2013; Edinoff *et al.*, 2021).

3.3 The molecule: 1g

It has been shown that the antagonism of glutamate receptors activity was able to inhibit proliferation and induce apoptosis in several cancer cells lines. Glutamate might facilitate the spread and growth of leukemia T cells through interactions with AMPA receptors.

In literature, it has been reported that a 2,3-benzodiazepine-4-one non-competitive AMPA antagonist derivative, called 1 g, exerted a significant growth inhibition of leukemia Jurkat T cells in a time and dose dependent manner, arresting the transition of G2/M phase through activation of Myt-1. The molecule also induced apoptosis through the enhanced expression of the pro-apoptotic p53, and the inhibition of Bcl-2, and Bcl-xl, followed by the activation of caspase-3. The results suggested that compound 1 g might act mostly as a cytostatic rather than cytotoxic compound and it might be a good molecule for future development in the cancer research (Parenti *et al.*, 2016).

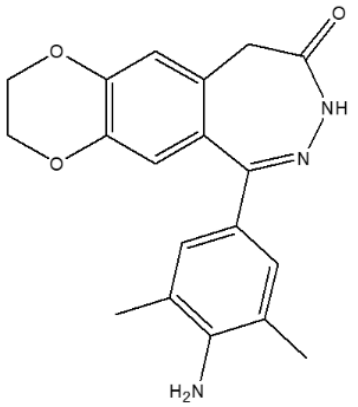

Figure 3.1 *Structure of 1-(4-amino-3,5-dimethylphenyl)-3,5-dihydro-7,8-ethylenedioxy-4h-2,3-benzodiazepin-4-one, called 1g*

3.4 Effects of 1g on Cell Growth in U87MG, Neuronal Differentiated SHSY5Y and Primary Neuronal Culture

To determine a possible specific activity of 1g derivative on glioblastoma cell line, it has been evaluated its growth inhibition effect on different cell cultures, such as primary neuronal cerebellar granule cells, astrocyte primary cells and the differentiated neuroblastoma cell line SHSY5Y (dSHSY5Y), thanks to a collaboration with Prof. Lorenzo Corsi (University of Modena & Reggio Emilia, Department of Life Sciences). 1g was able to significantly inhibit the cell growth in a dose and time-dependent manner in U87MG cell line (Figure 3.2A) in comparison to the cells treated with the vehicle alone (0.1% DMSO). Indeed, the GI_{50} ranged from 30 ± 3 µM, 17 ± 3 µM to 4 ± 2 µM at 24, 48 and 72 h, respectively. Noteworthy, 1g produced a greater inhibition at 48 h of treatment when compared to the temozolomide (TMZ) and

Talampanel (TMP) used as a reference drug. In particular, the GI_{50} of 1g was about five times less than that measured with TMZ (89 ± 5 µM) and TMP (99 ± 12 µM), as indicated in Figure 3.2B.

Differently, 1g was unable to modulate the cell proliferation of granule neurons, astrocytes and dSHSY5Y at all the concentrations tested after 48 h of incubation (Figure 3.2C), suggesting that the compound did not affect well differentiated neurons and low proliferating cells.

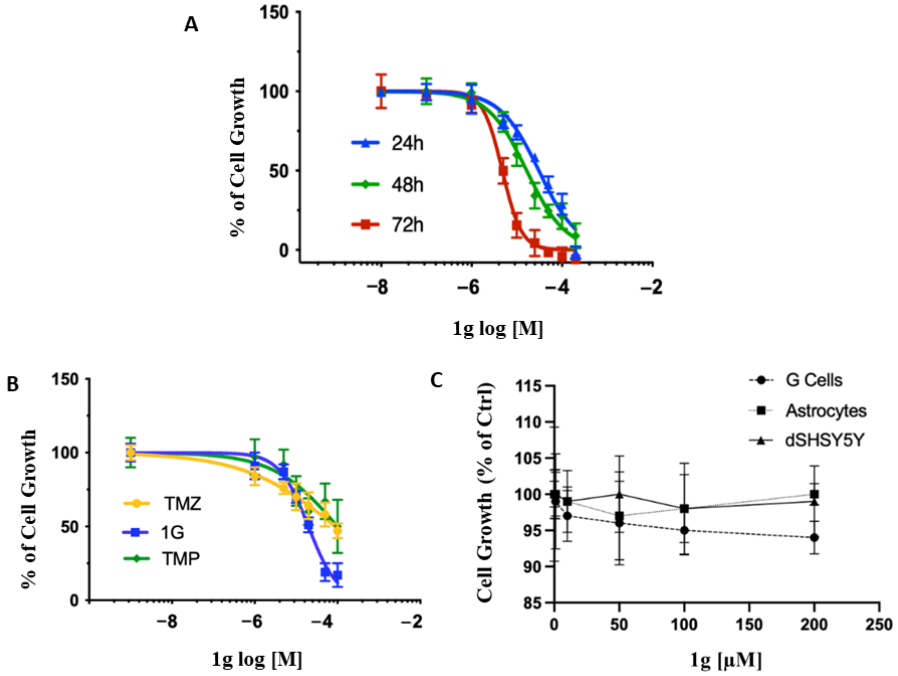

Figure 3.2 *Cell viability of U87MG, dSHSY5Y, primary cerebellar granule neurons and primary astrocytes after pharmacological treatments. (**A**) Dose-response curves of 1g at different time points on U87MG; (**B**) Comparison of the inhibitory effect of 1g, TMZ and TMP on U87MG cell viability at 48 h; (**C**) Effects of 1g on primary cerebellar granule neurons and primary astrocytes after 48 h of incubation times at different concentrations. The values are expressed as % of control ± standard deviation (SD). GI_{50} is reported in the text.*

3.5 Cell Cycle Analysis

Then, the cell cycle distribution of U87MG cells was evaluated at different time points (8, 12, 24, 48h) using a concentration of 1g corresponding to the GI_{50} obtained after 24 h of incubation time, thanks to a collaboration with Prof. Lorenzo Corsi (University of Modena & Reggio Emilia, Department of Life Sciences). Flow cytometry analysis showed that 1g was able to induce a cells accumulation in G2/M phase in a time-dependent fashion (Figure 3.3A), reaching a maximum response after 24 and 48 h of incubation time. In particular, 1g produced a significant increase of percentage of G2/M arrest already after 8 h of incubation, from 6.7 ± 3.7% in the control cells to 27 ± 3 %, increasing over time and reaching 34 ± 4% at 12 h and 66 ± 5% of G2/M arrest at both 24 and 48 h. (Figure 3.3B). In parallel, we assisted to a progressive decrease in the percentage of cells in the G0/G1 phase from 63 ± 4 % to 54 ± 3% at 8 h of treatment and to 16 ± 5% and 14 ± 5% after 24 h and 48 h of incubation time, respectively (Figure 3.3B). Interestingly, the cell line change morphology after the first 8 h of 1g treatment, becoming rounded and they maintain that structural conformation over time (Figure 3.3C).

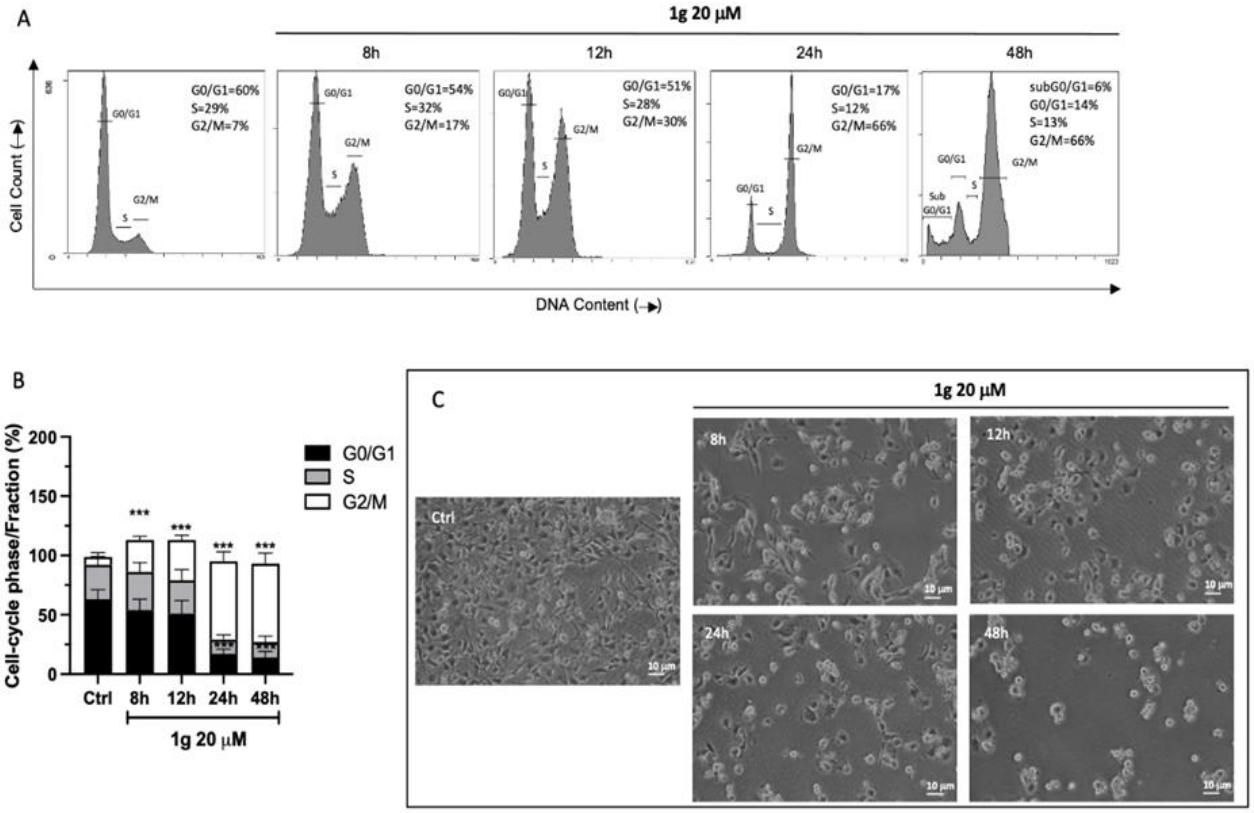

Figure 3.3 *Effect of 1g on U87MG cell cycle. (**A**) Representative cell cycle distributions assessed by propidium iodide staining and 5'-bromo-2'-deoxyuridine BrdU incorporation in enzymatically disaggregate U87MG cells treated with 20 µM of 1g at the indicated time points. (**B**) The percentages of cells in G0/G1, S and G2/M phases are presented in the histograms. Data are expressed as the mean ± SD obtained from three independent experiments performed in duplicate. The values are expressed as the mean ± SD of three independent experiments (n = 4 per group). *** p < 0.001 vs. untreated cells (Ctrl), using a one-way ANOVA with Dunnett's as post-test. (**C**) Light microscopic micrographs at 20× magnification of U87MG treated or not with 1g 20 µM at different time points.*

3.6 Protein Expression Evaluation

In order to get more inside in the 1g induced G2/M arrest, several cell-cycle determinants directly involved in the G2/M phase transition, such as cyclin B1, phospho-Cdc2 (Tyr15), phospho-Wee-1 (Ser642), and p21 were evaluated by immunoblot analysis. Figure 3.4A shows a decrease of protein levels of phospho-Wee-1 and phospho-Cdc-2 after 12 h, reaching significant values after 24 h in cell treated with 1g at 20 μM compared to the control (Figure 3.4B). Cyclin B1 immunoreactivity, instead, did not change significantly at all the time points tested. Interestingly, the level of the endogenous p21 protein increased significantly already after 8 h of treatment, reaching a maximal induction between 12 and 24 h, confirming the block of the mitotic activity. Similarly, the data of Akt protein expression showed that the 1g was able to modulate the phosphorylation of this protein. Indeed, the incubation with 20 μM of 1g decreased significantly the intensity of the p-Akt (Ser473) after 12 h of incubation time, while the expression of non-phosphorylated Akt did not show any variation (Figure 3.4 C,D). After 1 and 5 h of incubation, no change in immunoreactivity for all tested protein has been detected. Interestingly, 1g was unable to modulate the expression of p-Akt (Thr308) (Figure 3.4 C,D), indicating a specific interaction towards the phosphorylation at Ser473.

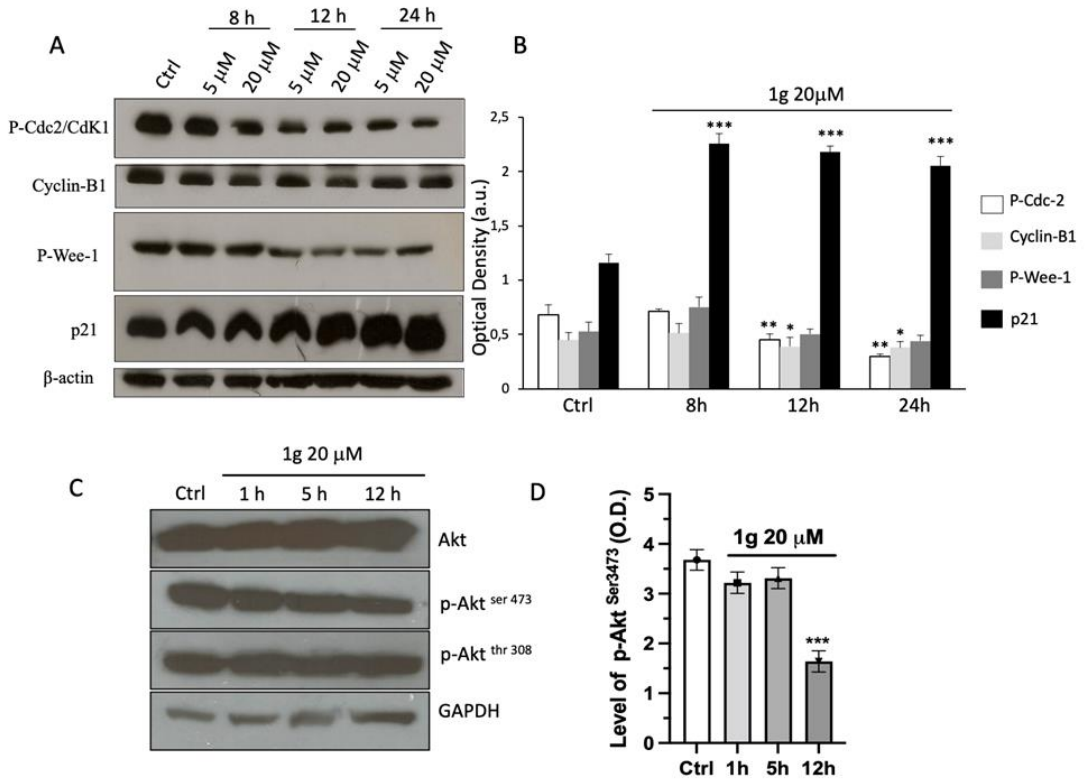

Figure 3.4 *Effect of 1g on P-Cdc2, cyclin-B1, P-Wee-1, p21, Akt, p-Akt (Ser473) and p-Akt (Thr308) protein expression in U87MG cells. (**A**) Representative Western blots of P-Cdc2, cyclin-B1, P-Wee-1 and p21 at different times and concentrations and (**B**) Densitometric analyses of protein levels of P-Cdc2, cyclin-B1, P-Wee-1 and p21. (**C**) Representative Western blots at different time points of Akt, p-Akt (Ser473) and p-Akt (Thr308) of U87MG cell lysate after incubation with 20 µM of 1g for 1, 5 and 12 h. (**D**) Densitometric analyses of protein levels of Akt, p-Akt (Ser473) of U87MG cell lysate after incubation with 20 µM of 1g for 1, 5 and 12 h. Densitometry values were normalized to the protein loading control, beta-actin or Glyceraldehyde 3-phosphate dehydrogenase (GAPDH). The values are expressed as the mean ± SD of three independent experiments (n = 4 per group). * p < 0.01, ** p < 0.005, *** p < 0.001 vs. untreated cells (Ctrl), using a one-way ANOVA with Dunnett's as post-test.*

3.7 Target Identification of 1g by a Proteomic Platform

In order to investigate the molecular mechanism of action of 1g on U87MG cells, we moved to apply our novel proteomic platform on this interesting system: in particular, our combined multidisciplinary approach can be summarized in the following steps: (a) identification of 1g interactome by DARTS coupled to high resolution mass spectrometry, bioinformatics and Western blotting analysis to validate the results; (b) t-LiP MRM analysis to look over at the interaction features between 1g and its main target and (c) molecular docking of the complex between 1g and its most reliable protein partner.

3.7.1 Identification of 1g Cellular Partner(s) through DARTS

A typical DARTS experiment initiates with the controlled proteolysis of a cellular lysate, pre-treated or not with the small molecule, with the low-specificity protease subtilisin under native conditions. The following SDS-PAGE of the samples allows to monitor proteins resistance to the enzymatic hydrolysis: the lane intensity corresponding to the putative protein target(s) will raise in the samples pre-treated with the small molecule, due to its protective effect, in a concentration dependent fashion. Thus, the target protein(s) can be identified through classical proteomic approaches by *in situ* digestion, nano-UPLC-MS/MS experiments and the use of bioinformatics tools. In our experiments, U87MG cell samples lysed in mild non-denaturing conditions were incubated with increasing 1g concentrations, except one treated with the vehicle and representing the negative control, and then subjected to subtilisin-

mediated limited proteolysis. An undigested lysate sample without 1g was kept as a positive control. Then, all samples were submitted to SDS-PAGE separation and revealed by Coomassie blue and the gel lanes were carefully excised and digested, principally those bands whose intensity raised up at increasing 1g concentrations (Figures 3.5 A,B). The nano-UPLC-MS/MS analysis of the digested peptide samples, followed by a Mascot database search, gave proteins identification. All the experiments were carried out in triplicate: proteins identified in all DARTS were considered (Figures 3.5 C,D) to identify 1g interacting ones by comparing the Mascot Score outputs with both the positive and negative control samples. Thus, 1g protection levels (reported as percentages) were evaluated for each identified protein: among them, Glycogen Phosphorylase, brain form (PYGB) has been selected as the main and most reliable 1g partner, since it was better protected from proteolysis in all DARTS replicates (Figure 3.5D). The direct interaction between the protein and the small molecule was then unequivocally determined by Western blotting analysis, submitting all DARTS samples to an anti-PYGB antibody reaction (Figure 3.5E). In fact, from the comparison of the immunoblotting signals corresponding to undigested PYGB (97 kDa bands), it emerges that the intact protein signal increases its intensity accordingly to 1g concentration. An accurate densitometric analysis was carried out on the full-length PYGB signal, using GAPDH as loading normalizer (Figure 3.5E).

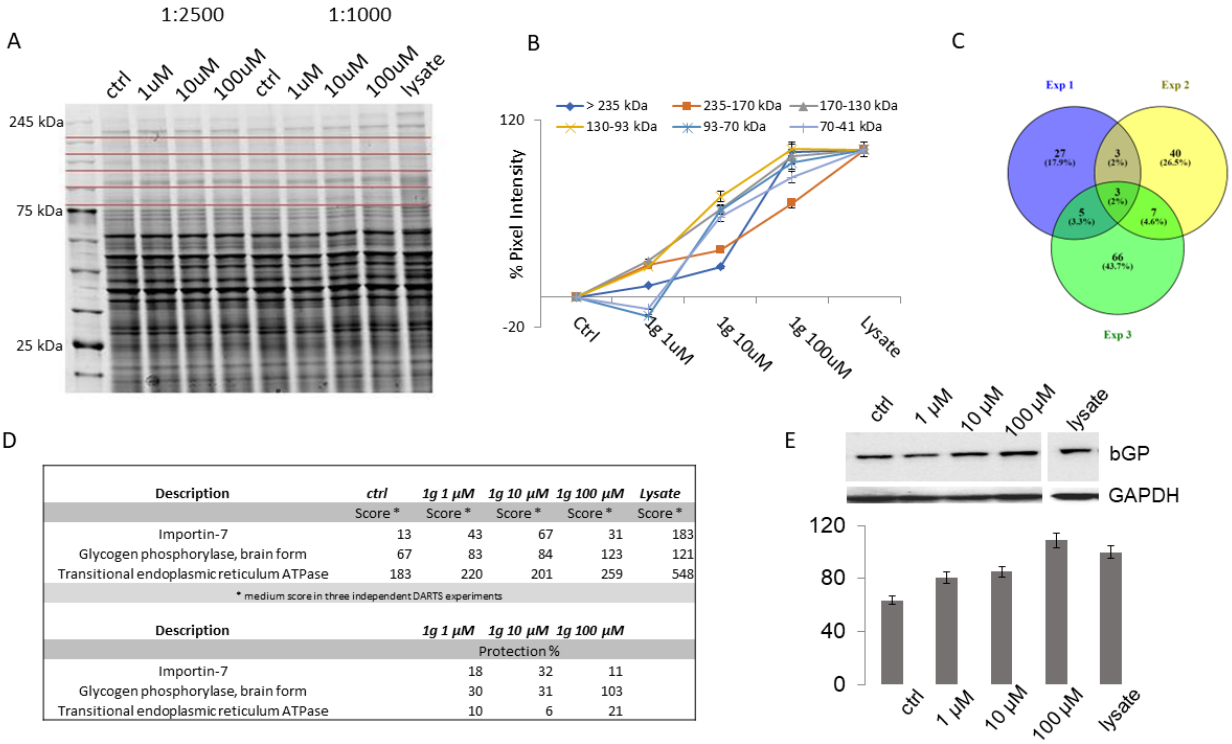

Description	*ctrl*	*1g 1 µM*	*1g 10 µM*	*1g 100 µM*	*Lysate*
	Score *	Score *	Score *	Score *	Score *
Importin-7	13	43	67	31	183
Glycogen phosphorylase, brain form	67	83	84	123	121
Transitional endoplasmic reticulum ATPase	183	220	201	259	548

* medium score in three independent DARTS experiments

Description	*1g 1 µM*	*1g 10 µM*	*1g 100 µM*
	Protection %		
Importin-7	18	32	11
Glycogen phosphorylase, brain form	30	31	103
Transitional endoplasmic reticulum ATPase	10	6	21

Figure 3.5 ***(A)*** *Coomassie stained SDS-PAGE of a DARTS experiment performed with increasing 1g amounts. Red lines indicate the gel cutting pattern.* ***(B)*** *Densitometric analysis of the SDS-PAGE as the pixel intensity of each gel region versus molecular weight. The major variation of pixel intensity of 1g-treated samples can be observed at molecular weights (MW) higher between 130 and 93 kDa.* ***(C)*** *Venn diagram of 1g protected proteins identified in three independent DARTS experiments. Three of them were protected in all performed assays.* ***(D)*** *Filtered list of 1g putative partners, reported with their protection (%) from proteolysis in DARTS biological replicates.* ***(E)*** *Western blotting and densitometric analysis of one DARTS experiment showing increasing 1g amounts shelter PYGB from proteolysis (95 kDa signals). GAPDH has been used as a loading normalizer.*

3.7.2 Analysis of the Interaction Features at the Basis of 1g-PYGB Binding by t-LiP MRM

To further explore the interaction profile of 1g, our optimized t-LiP MRM strategy has been carried out. t-LiP MRM lets the recognition of the target/ligand interface region(s) in a crude cell lysate, looking at the protein conformational alterations due to a ligand binding. The native proteins from U87MG cells were treated or not with 1g and a double-protease digestion was performed: first, a subtilisin limited proteolysis step was achieved under native controlled conditions and, then, a full tryptic digestion was finalized in a denaturing setting. This sequential treatment generates a combination of semi-tryptic and fully tryptic peptides, the latter suitable for targeted MRM-MS quantification analysis. Indeed, the area of fully tryptic peptides peaks can be considered indicative of the local target structural changes due to ligand binding: it will be higher when subtilisin limited proteolysis is less effective due to small molecule covering attackable protein regions. Initially, an *in-silico* search using the bio-informatics device PeptideAtlas and SRMAtlas set the more likely MRM transitions of PYGB theoretical fully tryptic peptides to map the protein, then a cell lysate sample was denatured and extensively proteolyzed by trypsin to unequivocally recognize the most reliable peptide signals and their most intense daughter ions by LC-MRM-MS. Next, native protein mixtures were incubated with 1g (1 and 10 μM) or vehicle (negative control) and treated with subtilisin in restricted conditions of time, temperature and at an enzyme-to- protein ratio of 1:1500 (w/w). Subtilisin was then quenched and all of the samples were denatured and fully digested by trypsin and the mixtures were run on the LC-MRM-MS system to quantify the area of each PYGB

tryptic peptide. Then, peptides mapping for PYGB regions sensitive to subtilisin (also called LiP peptides) were selected as the ones whose area was significantly inferior in the doubly digested sample (negative control) compared to the trypsin-only digested sample (positive control). Next, these peptides were examined in the controls and 1g treated samples: LiP peptides with an increased intensity in the samples exposed to the small molecule were considered symptomatic of 1g protection on specific PYGB region(s). In particular, PYGB conformational changes were identified on the peptide 71–78, in the region from 193 to 290, on the peptide 610–618 and from 459 to 479 and from 741 to 823, as shown in Figure 3.6 A,B. The fold changes reported in Figure 3.6B represent the grade of protection due to 1g interaction: they have been calculated as the ratio between the area of the tryptic peptide in the 1g-treated sample and in the untreated sample. The same t-LIP experiments have been repeated three times and the fold changes were calculated over the means of the peptides area. As reported by the group of Prof. Fernando Rodrigues-Lima (Mathieu *et al.*, 2017), PYGB monomer is composed of two domains: the N-terminal domain from residues 22 to 484 and the C-terminal domain from residues 485 to 822 bearing the catalytic site at their interface. PYGB is found as an equilibrium between a monomeric and dimeric form, which is shift toward the dimeric state upon activation. The association of two PYGB monomers into the functional dimer involves helix 2 (residues 49–77), the β4/β5 loop (residues 180–198), the cap loop (residues 41–48) and the tower helices (residues 259–278). The helices are connected to the gate loop (residues 279–289). The gate loop adopts either an open or a closed configuration depending the activation state of the enzyme (active or inactive). Moreover, the side chain of Tyr196 from the β4/β5 loop is involved in the binding with the phosphate of AMP as well as the nucleotide moiety of AMP interacts weakly with helix 2, forming co-planar stacking with the side chain

of Tyr75. The conformation of Tyr75 in PYGB is stabilized by the formation of a hydrogen bond between the phosphate group of AMP and Tyr196, which contributes to the geometry of AMP in PYGB by favoring the co-planar stacking between Tyr75 and the nucleotide part of AMP. Thus, looking at t-LIP-MRM data, 1g seems to affect the interface between PYGB monomers and the so-called 'gate loop', since both peptides 71–78 and 279–290 are protected, thus altering the dimerization process. Moreover, since Tyr75 and Tyr196 are in t-LIP protected peptides, namely at amino acids 71–78 and 193–206, it is plausible that 1g also affects the binding of AMP, a known PYGB positive modulator.

3.7.3 Molecular Docking Analysis of PYGB/1g Complex

In order to provide information on the molecular basis of PYGB/1g interaction, a docking simulation has been carried out. Figure 3.6 C reports the best docking geometry of 1g into the AMP binding site of PYGB which is at the basis of the minimum predicted equilibrium dissociation constant (K_{Dpred}) of 1.65 μM, obtained from $\Delta G = -7.884$ kcal mol−1; this value is at least one order of magnitude lower than the dissociation constant for the first AMP ligand bound to enzyme dimer (Crerar *et al.*, 1995). In detail, this geometry contemplates the formation of two H-bonds of 1g with Arg81 and Asp227 and a hydrophobic contact with Tyr75, fully fitting with t-LIP-MS data.

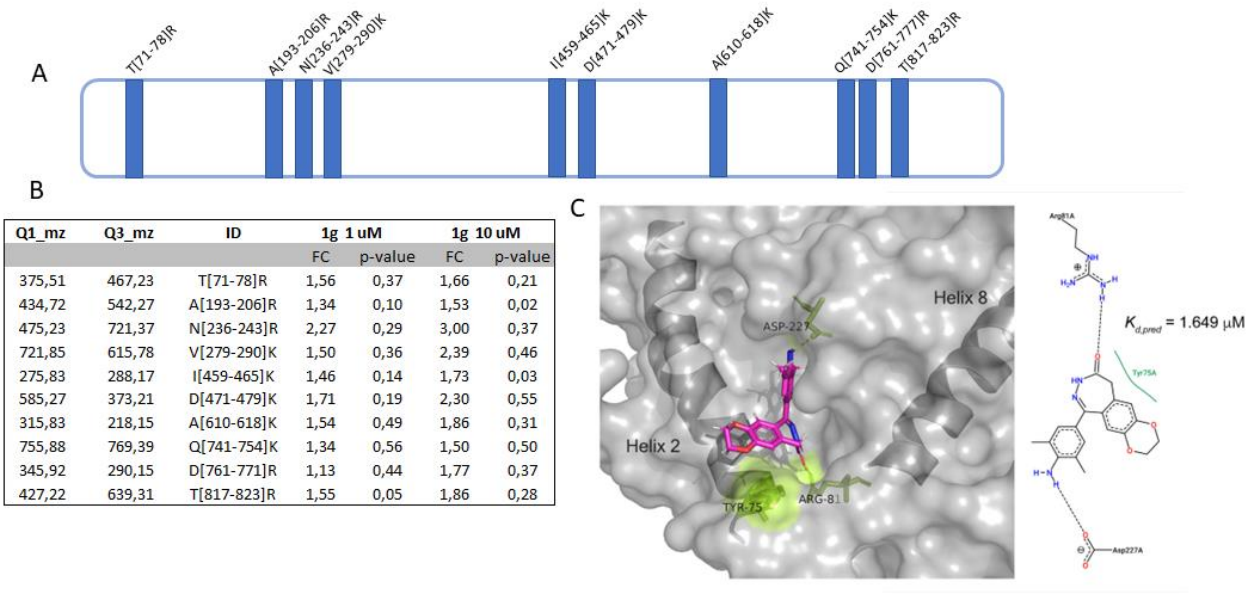

Q1_mz	Q3_mz	ID	1g 1 uM		1g 10 uM	
			FC	p-value	FC	p-value
375,51	467,23	T[71-78]R	1,56	0,37	1,66	0,21
434,72	542,27	A[193-206]R	1,34	0,10	1,53	0,02
475,23	721,37	N[236-243]R	2,27	0,29	3,00	0,37
721,85	615,78	V[279-290]K	1,50	0,36	2,39	0,46
275,83	288,17	I[459-465]K	1,46	0,14	1,73	0,03
585,27	373,21	D[471-479]K	1,71	0,19	2,30	0,55
315,83	218,15	A[610-618]K	1,54	0,49	1,86	0,31
755,88	769,39	Q[741-754]K	1,34	0,56	1,50	0,50
345,92	290,15	D[761-771]R	1,13	0,44	1,77	0,37
427,22	639,31	T[817-823]R	1,55	0,05	1,86	0,28

Figure 3.6 ***(A)*** *Schematic PYGB cartoon is depicted in azure, with the 1g-protected peptides highlighted in blue.* ***(B)*** *Selected PYGB peptides reported with their parent and daughter m/z values, their length and the calculated fold changes (FC) due to 1g protection. p-values have been calculated and only tryptic peptides with a* $p \leq 0.5$ *are reported.* ***(C)*** *Best predicted docking pose of 1g (in violet sticks) on PYGB. The amino acids involved in the interaction are reported in the 2D representation and as yellow sticks in the 3D model. The AMP binding site containing 1g is delimited by the two helices in the cartoon representation.*

3.8 1g Permeation by PAMPA Assay

The behavior of 1g in the parallel artificial membrane permeability assay (PAMPA) has been tested to measure its effective permeability (expressed as -Log Pe) through an artificial lipid membrane (Le Roux *et al.*, 2020). Propranolol and furosemide at 250 µM were used as positive and negative control molecules giving a

-Log Pe of 5.30 for propranolol and 6.64 for furosemide (-Log Pe < 6 is considered good permeability and -Log Pe > 6.5 as impermeable). In this assay, as shown in Figure 3.7, 1g displayed a good propensity to cross the membrane *in vitro*, with a - Log Pe of 5.22 ± 0.04.

	Propranolol 250 µM	Furosemide 250 µM	1g 50 µM
logPe	-5.30	-6.64	-5.22
dev.st.	0.02	0.03	0.04

Figure 3.7 *Results of Parallel Artificial Membrane Permeability Assay (PAMPA) assay.*

3.9 1g Negatively Affected PYGB Expression and Activity

Then, an *in vitro* activity assay has been equipped aiming to explore the effect of 1g on PYGB by measuring the glycogenolytic activity of this enzyme in presence or not of different concentrations of 1g and/or AMP, the endogenous PYGB positive effector. To simplify the detection of variations in the PYGB-dependent glycogenolysis, this reaction has been coupled with the phosphoglucomutase-mediated conversion of its product, the glucose-1-phosphate into glucose-6-phosphate, which is converted by glucose-6- phosphate dehydrogenase into the corresponding lactone. The last reaction of this enzymatic chain is a Nicotinamide Adenine Dinucleotide Phosphate ($NADP^+$)-dependent transformation also generating NADPH as product. Thus, the PYGB activity has been monitored by measuring the Optical Density (OD)

at 340 nm and corresponding to the amount of the produced NADPH. The spectrophotometric assay has been performed in a kinetic mode and the histogram in Figure 3.8A has been obtained by calculating the variation of Absorbance (Abs) with respect to an opportune blank for each experimental condition. The trend of this activity assay means that 1g modulates in a negative mode the activity of PYGB. Finally, the analysis of protein expression of PYGB on U87MG cell line revealed that 1g treatment was able to reduce the band intensity in a time-dependent manner. Indeed, as shown in Figure 3.8 B,C, the protein level of cells treated with 20 μM of 1 g decreases significantly after 24 h of incubation time, whereas after 5 and 12 h, the reduction of immunoreactivity was not present.

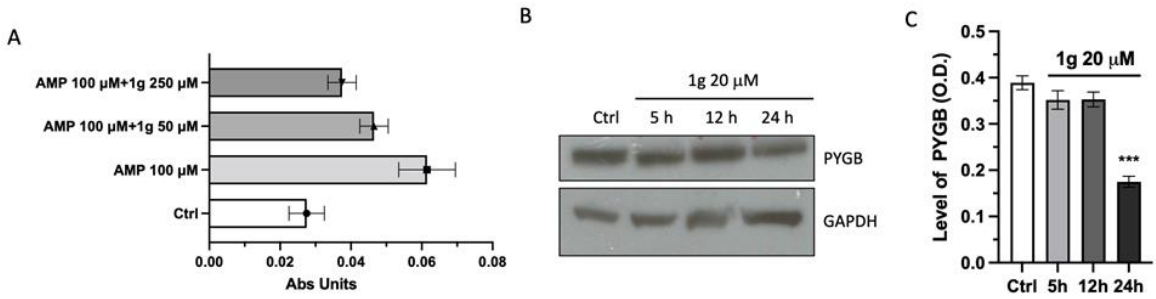

Figure 3.8 *Effect of 1g and AMP on the PYGB activity and expression in U87MG cell lysates.* ***(A)*** *The Abs Units Increment is the variation in the absorbance of the sample after 30 min of reaction. S.D. was calculated on three independent measurements.* ***(B)*** *Representative Western blots of PYGB at different time points.* ***(C)*** *Densitometric analyses of protein levels of PYGB, of U87MG cell lysate after incubation with 20 μM of 1g for 5–12 and 24 h. *** $p < 0.001$ vs. untreated cells (Ctrl), using a one-way ANOVA with Dunnett's as post-test.*

CHAPTER 3

PART 2

Discussion

3.10 Conclusive remarks

The aim of the second year of my PhD was to investigate the interactome of 1g and to evaluate the ability of the synthetic compound to interfere with the activity and the protein expression of the brain glycogen phosphorylase (PYGB) on U87MG cell line in parallel with the capability of the compound to inhibit the cell growth. The data obtained on cell viability inhibition clearly showed that the efficacy 1g is more potent than TMP and TMZ. This result acquires even greater significance considering the no-effect of 1g on differentiated dSHSY5Y, suggesting a possible specific action on hyper-proliferating cells. In particular, 1g was able to arrest the cell cycle in the G2/M phase, confirming our previous data. Then, it was performed a proteomic analysis to find out a range of possible protein targets interacting with 1g. In detail, DARTS experiments disclosed PYGB as the best protected at all 1 g tested concentrations, as also detected by immunoblotting. Moreover, thanks to limited proteolysis and molecular docking analysis, it has been revealed that 1g interacts well inside the AMP recognition hole, establishing favorable contacts with the amino acids into the AMP binding site.

Furthermore, an *in vitro* activity assay has been planned by exploiting the effect of 1g on glycogenolytic activity of the enzyme. The results have been suggested that 1g modulates in a negative mode the activity of PYGB.

Glycogen metabolism plays an important role in the cancer progression. Several lines of evidence suggest that the different isoforms of PYGs are over-expressed and involved in the progression and invasiveness (Altemus *et al.*, 2019) of different cancer cells. In particular, PYGB has been reported to implicated both in tumor progression of gastric cancer through the modulation of Wnt/β-catenin pathway (Xia *et al.*, 2020)and in the invasion of breast cancer cells (Altemus *et al.*, 2019). In addition, Zhan at al. showed that PYGB activates the PI3k/Akt signaling pathway and, therefore, the tumorigenesis of non-small cell lung cancer (Zhan *et al.*, 2021).

The inhibition of PYGB activity and protein expression by 1g measured in the biochemical assays is well related to a reduction of U87MG cell proliferation both due to a decrease of cancer cell fuel and the modulation of the PI3k/Akt pathway. Indeed, the inhibition of PI3k/Akt signal with the specific inhibitors (LY 294002 or genistein) also arrests the cell cycle in G2/M phase by increasing p21 expression. 1g decreased the expression of p-Akt (Ser473), not altering the non-phosphorylated Akt and the p-Akt (Thr308). This result is interesting since the phosphorylation site at Ser473 has been identified as mammalian target of rapamycin (mTOR) (Sarbassov *et al.*, 2005; Jacinto *et al.*, 2006) and it is over activated in cancer cells.

In this context, our results support the hypothesis that the phosphorylation at Ser473 could be an upstream site-specific regulation of Akt pathway. The downregulation of p-Akt (Ser473) might be attributable to the modulation of PYGB activity elicited by

1g rather than a consequence of the inhibition of PYGB protein expression, which occurs only after long time.

This study has been mostly focused on the investigation of the interaction and action mechanism of 1g towards PYGB and its related pathways: a deeper analysis is necessary to better characterize the pharmacological profile of 1g, mainly in terms of pharmacokinetic and pharmacodynamic profile. In conclusions, our research highlights PYGB as a potential therapeutic target in Glioblastoma Multiforme proposing 1g as a lead compound for developing a new class of simplified analogs active as anticancer drugs for glioblastoma, keeping unchanged its ability to cross the blood–brain barrier.

CHAPTER 3

PART 3

Materials and Methods

3.11 Cell Culture

Primary cultures of rat cerebellar granule neurons and astrocytes were prepared from 8-day-old Sprague-Dawley rat cerebella as previously described (Novelli *et al.*, 1988). Briefly, both primary granule cells and astrocytes were dispersed with trypsin (0.25 mg/mL; Sigma, Milan, Italy) and plated at a density of 100–105 cells/cm^2 on 96 multi wells plate coated with poly-L-lysine (10 mg/mL; Merck Life Science, Milan, Italy). Cells were cultured in DMEM (Euroclone, Pero, Milan, Italy) supplemented with 10% FBS, 2 mM glutamine, and 100 mg/mL of gentamycin (Euroclone, Pero, Milan, Italy). In the cerebellar granule cells, 1 mM of cytosine arabinofuranoside (Ara-C; Merck Life Science, Milan, Italy) was added 18–24 h after plated to inhibit glial proliferation. Culture medium was replaced at days in vitro (DIV) 7 and 10, and the confluent cultures used at DIV 11.

Human cell line U87MG (ATCC), were cultured at 10–105 cells/cm^2 on 96 multiwell plates in EMEM supplemented with 4 mM L-glutamine, 100 U/mL penicillin, 100 mg/mL streptomycin, 1% sodium pyruvate, 1% non-essential amino acids, and 10%

FBS. Human neuroblastoma SH-SY5Y cells (ATCC) were grown at 10–105 cells/cm^2 on 96 multiwell plates, in a mixture of 1:1 of Ham's F12 and DMEM supplemented with 10% FBS, 2 mM L-glutamine, 100 U/mL penicillin and 100 µg/mL streptomycin. The cells were then differentiated into neuron-like population by adding retinoic acid (10 µM) for 10 days and used at DIV 12. The cells were all maintained at 37 °C in 5% CO_2. Cells were visualized with Nikon Inverted Microscope Eclipse Ti-E equipped with a Digital Sight camera DS-Qi2 (Nikon Instruments, Tokyo, Japan) and images were acquired with NIS-Elements (Nikon Instruments, Tokyo, Japan) software.

3.12 Determination of Cell Growth Inhibition

1g, TMP and TMZ (Sigma) were initially dissolved in DMSO at concentration of 100 mM, and serial dilutions were then prepared in culture medium, so that the final concentration of DMSO was <0.1%. Cell proliferation was assessed after 24–48–72 h of continuous exposure with different concentrations of the compounds (0.1–200 µM) using CCK-8 assay (Dojindo Laboratories, Kumamoto, Japan). Briefly, the different cell lines were plated on 96-well plates (Euroclone) at concentrations described above. After exposure to desired concentrations of the different compounds, 10 µL CCK-8 was added to each well and incubated for of 2.5 h at 37 °C. The absorption was measured at 450 nm using a multiplate reader multiscan FC (Thermo Scientific). The percentage growth was calculated using the following calculation: % growth = 100 × [(T − T0)/(C − T0)] where (T) was the growth of the cells in presence of the compound at different concentrations and at a specific time point, (T0) represents the number of

cells at the time 0 of the experiment and (C) the growth of the control at a specific time point. The inhibition that reduces the cell population by 50% (GI_{50}) was calculated using GraphPad Prism 6 (Graph-Pad 9 Software Inc., San Diego, CA, USA).

3.13 Cell Cycle Analysis

U87MG were seeded at a density of approximately 90,000 cells/cm^2 into 6-well plates, cultured overnight and treated with 20 µM of 1g or 0.1% DMSO (control). Following 8–12–24-48 h of incubation, cells were harvested, washed with saline phosphate buffer (PBS) and the different phases of cell cycle was analyzed by BrdU/PI staining. Evaluation of the different phases of cell cycle was analyzed by BrdU/PI staining performed as described by Manfredini et al. (Manfredini *et al.*, 1997). Briefly, cells were pre-incubated with 10 µM BrdU (Sigma Aldrich) and stained with a purified mouse primary monoclonal antibody directed against BrdU (BD Biosciences, Allschwil, UK) followed by a rabbit anti-mouse immunoglobulin IgG secondary antibody conjugated with fluorescein isothiocyanate (FITC) (Dako A⁄S, Hilden, Germany). Samples were then resuspended in a 50 µg/mL PI water solution. Both the assays were analyzed by Coulter Epics XL flow cytometer (Coulter Electronics Inc., Miami, FL, USA).

3.14 Western Blot Analysis

Immunoblot was performed as already described by (Gemelli *et al.*, 2014). Briefly, proteins from U87MG treated or not with different concentrations of 1g at different time points were extracted by lysing and homogenized (in ice) the samples in RIPA buffer (50 mM Tris-HCl pH 7.4, 150 mM NaCl, 1% Na deoxycolate, 1% Triton X-100, 2 mM PMSF, Merck Life Science S.r.l). The protein concentrations were quantified using Bradford colorimetric method (Pierce, Rockford, IL, USA) according to the manufacturer's instruction. An equal amount of protein, 0.5 µg/µL for each sample, was loaded onto a pre-cast 12% SDS-PAGE (Thermofisher Invitrogen, Waltham, MA, USA) and transferred to nitrocellulose membrane (Thermofisher Invitrogen). Membrane was blocked in TBST buffer (20 mM Tris-HCl, 0.5 M NaCl and 0.05% Tween 20) containing 5% non-fat dried or 5% BSA and incubated with primary anti-cyclin B1 (1:1000), anti-cdc-2 (1:1000), anti-phospho-cdc2(Tyr15) (1:1000), anti-p21 Waf/Cip1 (1:1000), anti-pospho-Wee-1(Ser642) (1:1000), anti-PYGB (1:1000), Anti-Akt (1:1000), Anti-phospho-Akt(Ser473) (1:2000) and Anti-phospho-Akt(Thr308) (1:1000) (I Thermofisher Invitrogen), at 5 °C overnight under agitation. Membrane was then washed 3 times in TBST, incubated for 1.5 h with HRP-conjugated anti-mouse or anti-rabbit antibody (Cell Signaling, Danvers, MA, USA) and visualized using chemiluminescence method (GE Healthcare, Amersham, UK). The determination of relative immunocomplexes was performed using densitometric analysis using a BioRad GS 690 Imaging densitometer with molecular analysis software (Version 8.1, Life science, Milan, Italy). B-actin or GAPDH was used a loading control.

3.15 Identification of 1g Cellular Targets

U87MG cells were lysed in PBS 0.1% Igepal in presence of a protease inhibitor mixture (Sigma Aldrich). Lysate was centrifuged at 10,000× *g* for 10 min and the protein concentration of the supernatant was determined by Bradford assay. DARTS experiments were performed as reported: different amounts of unmodified 1g (1 μM, 10 μM and 100 μM) were incubated with 300 μg of U87MG cell lysate for 1 h at room temperature. The obtained samples were then submitted to limited proteolysis, for 30 min at 25 °C, with subtilisin (Sigma Aldrich) at different concentrations. The best subtilisin defect has been evaluated as 1/1000 *w/w* in respect of proteins amount. Two samples of cell lysate were solely treated with DMSO and one of them with subtilisin, as control experiments. Then, the protease was quenched by adding phenylmethylsulfonyl fluoride (PMSF, Sigma-Aldrich, St. Louis, MO, USA, 1 mM final concentration) to each sample. Subsequently, all samples were boiled in SDS-PAGE loading buffer and 20 μg were loaded on a 4–12% Bis-Tris Criterion TM XT Precast Gel (Bio-Rad Laboratories S.r.l., Hercules, CA, USA), which was then stained with a Comassie solution and submitted to a densitometric analysis through ImageJ. This experiment was carried out in triplicate. Protein bands were excised from the gels and submitted to an in situ tryptic digestion protocol (Shevchenko *et al.*, 2006). Briefly, gel slices were reduced with DTT (1,4-dithiothreitol), alkylated with IAA (iodoacetamide), washed, and rehydrated on ice for 1 h in a 12 ng/μL trypsin solution. Then, the enzyme excess was removed and replaced with ammonium bicarbonate (AmBic, 50 mM, pH 8.5), allowing protein digestion to proceed overnight at 37 °C. Subsequently, supernatants were collected and peptides were extracted from each gel

slice, shrinking them in 100% ACN (acetonitrile). The obtained peptides mixtures were dried and dissolved in 10% FA for the subsequent nano-UPLC-MS/MS analysis on a Q-Exactive Classic Mass Spectrometer coupled to an UltiMate 3000 Ultra-High-Pressure Liquid Chromatography (nano-UPLC) system, equipped with an EASY-Spray PepMAP^{TM} RSLC C18 column (3 µm, 100 Å, 75 µm × 50 cm, ThermoFisher Scientific). Peptides elution was achieved at a flow rate of 300 nL/min with the following gradient: 1 min at 3% B, 1–50 min at 45% B, 50 min–51 min at 80% B, 51–54 min at 80% B, 55 min back at 3% B, until 61 min (A: 0.1% AcOH, 95% H_2O, 5% ACN; B: 0.1% AcOH, 95% ACN, 5% H_2O). The mass spectrometer was operated in data-dependent acquisition mode. Full scan MS spectra were acquired with the following settings: scan range 375–1500 *m/z*, full-scan automatic gain control (AGC) target 3×10^6 at 70,000 resolution, and maximum injection time 50 ms. MS2 spectra were generated for up to 10 precursors (normalized collision energy of 28%); fragment ions were acquired at a 17,500 resolution with an AGC target of 1×10^5 and a maximum injection time of 50 ms. Subsequently, database searches were carried out on Mascot Deamon, employing the SwissProt database and the following settings: two missed cleavages; carbamidomethyl (C) as fixed modification; oxidation (M) and phosphorylation (ST) as variable modifications; peptide tolerance 30 ppm; MS/MS tolerance 0.8 Da.

3.15.1 Validation of DARTS Results via Immunoblotting

The samples obtained from the previously described experiments were submitted to Western blotting analysis. First, 7 µg of each sample were loaded on an

8% SDS-PAGE and transferred onto a nitrocellulose membrane; then, they were incubated for 1 h in a blocking solution (5% milk) and left for 16 h at 4 °C with monoclonal antibodies against PYGB (1:1000, Thermofisher, Invitrogen). Then, a mouse peroxidase-conjugated secondary antibody (1:1000) was added, and the signal was detected using an enhanced chemiluminescent substrate and LAS 4000 digital imaging system. Finally, an antibody against GAPDH (1:2500) in 5% milk has been tested as a loading normalizer.

3.15.2 t-LiP-MRM Analysis

An in-silico search for investigating PYGB tryptic peptides using the bio-informatics tool Peptide Atlas has been optimized to write appropriate MRM methods, setting the best MRM transitions of the theoretical PYGB fully tryptic peptides to map the protein sequences. Then, samples treated or not with 1g and submitted or not to the double-digestion procedure were analyzed by LC-MRM-MS to quantify as many fully tryptic peptides as possible for these proteins.

3.15.3 Molecular Docking Analysis

The molecular docking procedure was performed, in order to identify the most probable binding complex between the human PYGB (pdbID: 5ikp) (Mathieu *et al.*, 2016) and the 1g molecule, following the method previously reported by (Del Gaudio *et al.*, 2018) and using the online docking web server SwissDock (Grosdidier *et al.*, 2011) as the docking algorithm. All parameters were set as default. The final complex

geometry was rendered by PyMol software (The PyMOL Molecular Graphics System, Version 2.0, Schrödinger, LLC., Cambridge, MA, USA), whereas the 2D representation was created using the PoseView server (Stierand *et al.*, 2006).

3.16 1g PAMPA Assay

Donor solution (50 μM) was prepared by diluting 5 mM 1g stock solution using phosphate saline buffer (PBS: 137 mM NaCl, 2.7 mM KCl, 10 mM Na_2HPO_4, 2 mM KH_2PO_4, pH 7.4). The filter membrane was coated with 5 μL of specific lipid solution prepared as a 1% w/v phosphatidylcholine solution in n-dodecane. Donor solution (150 μL) was added to each well of the filter plate. To each well of the acceptor plate, 300 μL of solution (5% DMSO in PBS) were added. Donor and Acceptor plates were assembled to obtain a sandwich and incubated for 24 h at room temperature under gentle shaking. Then, the sandwich plates were separated and 250 μL of the solution from the acceptor plate and 100 μL of the solution from the donor one were transferred to a new multi-well plate and the absorbance was measured by UV spectroscopy using a Multiscan GO microplate spectrophotometer (Thermo Scientific) at 250−500 nm (5 nm steps). The permeability value Log Pe has been determined. The membranes' integrity was checked using propanolol and furosemide as control molecules.

3.17 Activity Assay

U87MG was suspended in the lysis buffer (PBS pH 6.9, 0.1% Igepal, 1x Protease Inhibitors Cocktail) and then lysed carrying out three cycles of

homogenization (1′on/1′off; on ice). The obtained proteome (10,000 rpm; 4 °C; 5′ in Eppendorf Centrifuge 5424-R) was quantified by Bradford spectrophotometric assay and diluted with PBS pH 6.9 containing glycerol to reach 10% of the disaggregating agent in the protein mixtures. A reaction mix, containing all the enzymes and the substrates (50% glycogen, 16 mM NADP, 500 µM glucose-1,6-diphosphate, 0.02 U/µL glucose-6-phosphate dehydrogenase, 0.02 U/µL phosphoglucomutase) involved in the combined reactions to follow the PYGB-dependent glycogenolysis, was prepared in PBS pH 6.9, 200 mM EDTA, 1M Magnesium acetate Mg (OAc).

U87MG cells lysate and the reaction mix have been blended with and without AMP. The mixture has been divided into three aliquots: two of them have been treated with 1g (50 µM and 250 µM), while the last one served as control without 1g. All the samples have been incubated for 15′ (37 °C; 300 rpm) and then transferred onto a 384-multiwell plate (in duplicate; 30 µL for each replicate). The absorbance of the produced NADPH has been monitored in a kinetic mode for 200' using the MultiskanGO spectrophotometer by Thermo Scientific (37 °C, orbital shaking: medium intensity, 10″ on/10″ off; $\lambda = 340$ nm; 1 scan/5′).

3.18 Statistical Analysis

All data are presented as the mean ± SD of at least three different experiments done in triplicate or quadruplicate. Differences between the treated cells versus control cells were analyzed using one-way analysis of variance ANOVA with Dunnett's post-test, as indicated in the figures (Graph-Pad 9 Software Inc.). p values < 0.05 were considered significant.

CHAPTER 4

Targeting PhosphoGlycerate Kinase-1 by a natural sesquiterpenoid endowed with anti-cancer activity by a DARTS-based proteomic platform

Adapted from

Ferraro, G., Voli, A., Mozzicafreddo. M., Pollastro, F., Tosco, A., Monti, MC.;

Submitted Manuscript

CHAPTER 4

PART 1

Results

4.1 Background

Sesquiterpene lactones (SLs) are a bulky and widespread group of bioactive plant secondary metabolites: the scientific interest on this class of compounds has emerged due to their vast biological activity beneficial for human health. They can inhibit numerous transcription factors responsible for downstream effects such as the release of several pro-inflammatory mediators, including cytokines (IL-1β, TNF-α, IL-6, IL-8, etc.) and enzymes (iNOS, COX-2, kinases, proteases, etc.). Besides these effects at the level of gene expression, SLs can also directly affect the release or activity of these mediators. Chemically, they are characterized by a 15-carbon backbone containing α-β-unsaturated carbonyl moiety and a conserved α-methylene-γ-lactone. Some of the numerous acknowledged activities for sesquiterpene lactones comprise anti-microbial, anti-fungal, anti-viral, anti-tumor, anti-malarial and anti-inflammatory activities (Matos *et al*., 2021).

Among them, Tatridin A (Tat A, Figure 4.1), isolated for the first time from the aerial parts of *Anthemis melanolepis* (Saroglou *et al.*, 2010), showed an *in vitro* antimicrobial potential against Gram-positive bacteria as *B. cereus, M. luteus* and *Staph. aureus* and a certain *in vitro* cytotoxic activity against a panel of human tumor cell lines. In

particular, Tat A resulted cytotoxic on the myeloid leukemia cell lines HL-60 and U937 (Rivero *et al.*, 2003).

With the aim of deepen Tat A anti-cancer mechanism of action, a combination of drug affinity responsive target stability (DARTS) and targeted limited proteolysis assisted by multiple reaction monitoring mass spec (t-LIP-MRM) has been applied on a human leukemia monocytic cell line (THP-1), chosen as a model system.

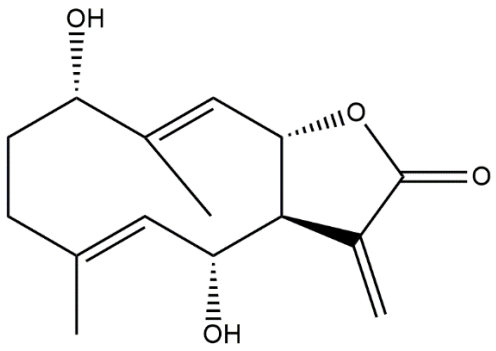

Figure 4.1 *Tatridin A chemical structure*

4.2 Identification of Tatridin A cellular targets through DARTS

Commonly, the interaction between a small molecule and its specific protein target produces a more compacted tridimensional structure of the target itself, with a resultant lower sensitivity to enzymatic proteolysis. A typical DARTS experiment initiates with the controlled proteolysis of a cellular lysate, pre-treated or not with the small molecule, with the low-specificity protease subtilisin under native conditions. The following SDS-PAGE of the samples allows to monitor proteins resistance to the enzymatic hydrolysis: the lane intensity corresponding to the putative protein target(s)

will raise in the samples pre-treated with the small molecule, due to its protective effect, in a concentration dependent fashion. Thus, the target protein(s) can be identified through classical proteomic approaches by *in situ* digestion, nano-UPLC-MS/MS experiments and the use of bioinformatics tools.

In our experiments, THP-1 cell samples lysed in mild non-denaturing conditions were incubated with increasing Tat A concentrations, except one treated with the vehicle and representing the negative control and then subjected to subtilisin-mediated limited proteolysis. An undigested lysate sample without Tat A was kept as a positive control. Then, all of the samples were submitted to SDS-PAGE separation and revealed by Coomassie blue and the gel lanes were carefully excised and digested, principally those bands whose intensity raised up at increasing Tat A concentrations (Figure 4.2A). The nano-UPLC-MS/MS analysis of the digested peptide samples, followed by Proteome Discoverer search, gave proteins identification (Figure 4.2B). Among the putative identified targets, PGK1 and PGK2 have been selected as the main and most reliable Tat A partners since they were better protected from proteolysis in all DARTS replicates. The direct interaction between the proteins and the small molecule was then unequivocally determined by Western blotting analysis, submitting all DARTS samples to an anti-PGK1 and PGK2 antibody reaction (Figure 4.2C). In fact, from the comparison of the immunoblotting signals corresponding to undigested PGK1 and PGK2 (47 kDa bands), it emerges that the intact protein signal increases its intensity accordingly with Tat A concentration. An accurate densitometric analysis was carried out on the full-length PGK1 and PGK2 signals, using GAPDH (Glyceraldehyde 3-phosphate dehydrogenase) as loading normalizer (Figure 4.2C).

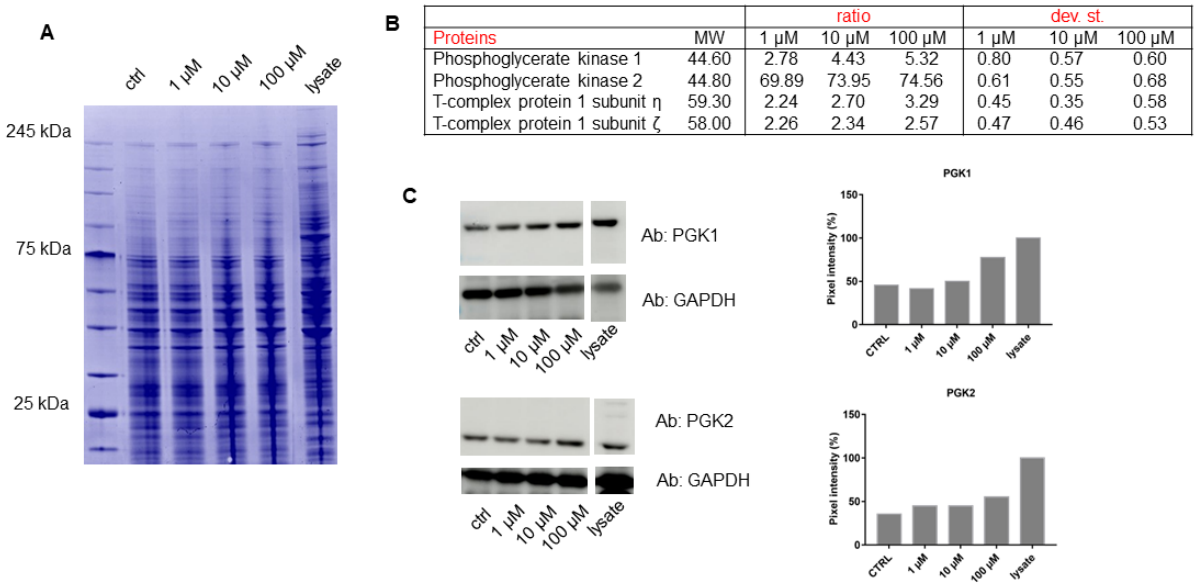

		ratio			dev. st.		
Proteins	MW	1 µM	10 µM	100 µM	1 µM	10 µM	100 µM
Phosphoglycerate kinase 1	44.60	2.78	4.43	5.32	0.80	0.57	0.60
Phosphoglycerate kinase 2	44.80	69.89	73.95	74.56	0.61	0.55	0.68
T-complex protein 1 subunit η	59.30	2.24	2.70	3.29	0.45	0.35	0.58
T-complex protein 1 subunit ζ	58.00	2.26	2.34	2.57	0.47	0.46	0.53

Figure 4.2 ***(A)*** *Coomassie stained SDS-PAGE of a DARTS experiment performed with increasing Tat A amounts.* ***(B)*** *Filtered list of Tat A putative partners, reported with their ratios form proteolysis for DARTS biological replicates.* ***(C)*** *Western blotting analysis of a DARTS experiment showing increasing Tat A amounts shelter PGK1 form proteolysis accordingly (47 kDa signals). GAPDH has been used as a loading normalizer. Densitometric analysis of the Western Blotting.*

4.2.1 Analysis of the interaction features of PGK1 binding to Tatridin A by targeted limited proteolysis approach

To explore Tat A interaction profile with PGK1 target, our optimized t-LiP MRM strategy has been applied (Feng *et al.*, 2014).

T-LiP MRM allows the identification of the target/ligand crossing region(s) in a complex cell lysate, observing the protein conformational variations due to the ligand

interaction. THP-1 cells native proteins were treated or not with Tat A and then a double-protease digestion was allowed: first, a subtilisin mediated limited proteolysis was achieved under native conditions and, then, a full tryptic digestion was established in denaturing settings. This consecutive sample handling generates a combination of semi-tryptic and fully tryptic peptides, which can be easily quantified by targeted MRM-MS. Indeed, the area of fully tryptic peptides is symptomatic of the target structural changes induced by ligand: it will be higher when subtilisin proteolysis is less operative due to Tat A. On the contrary, if the area of fully tryptic peptides is lower after subtilisin action in presence of Tat A, it can be suggested a long range effect on protein structure by the ligand with a favourable exposure of subtilisin proteolytic aminoacids.

A preliminary *in-silico* quest using the bio-informatics tools PeptideAtlas and SRMAtlas was performed to establish the more probable MRM transitions of PGK1 theoretical fully tryptic peptides to map the proteins. Then, a cell lysate sample was denatured and extensively proteolyzed by trypsin to recognize the occurring peptide signals and their most intense daughter ions by LC-MRM-MS. Next, THP-1 native proteins mixture was incubated with Tat A (1 μM and 10 μM) or vehicle (negative control) and treated with subtilisin in controlled conditions of time, temperature and at the enzyme to proteins ratios 1:500 (w/w). Subtilisin was then quenched, the samples were denatured and fully digested by trypsin and the mixtures were run on the LC-MRM-MS system to quantify the area of each PGK1 fully tryptic peptides. Then, peptides mapping for PGK1 regions were analyzed by comparing the controls and the treated samples to disclose the direct or long-term conformational changes induced by Tat A. As reported in Figure 4.3, the Fc term represents the ratio of the area of the fully tryptic peptides in a certain experiment en respect of the control without Tat A.

Interestingly, the peptide 193-199 showed an increased intensity in the samples exposed to the small molecule in a Tat A concentration dependent fashion and it can be considered symptomatic of Tat A interaction and protection. This peptide covers a large part of the central helix (aa from 187 to 201) which is fundamental for PGK1 activity allowing the two domains of the enzyme to approach each other during the catalytic cycle.

Q1_mz	Q3_mz	ID	Tat A 1 µM		Tat A 10 µM		Lysate	
			Fc	p-value	Fc	p-value	Fc	p-value
442.73	365.22	E [193-199] K	1.73	0.04	2.97	0.01	22.79	0.01

Figure 4.3 *Selected PGK 1 peptides reported with its parent and daughter m/z values, its length and the calculated fold changes (FC) due to Tat A protection. p-values have been calculated and only tryptic peptides with a p value* ≤ 0.1 *are reported.*

4.2.2 Molecular Docking Analysis of PGK1/Tat A Complex

Molecular docking analysis of the complex Tat A/PGK1 revealed an interaction strength, expressed as equilibrium dissociation constant, in the order of the micromolar ($K_{D,pred}$ = 5.52 µM). This value is comparable with that of the affinity of Terazosin (TZN), the alpha-adrenergic blocker drug, for the PGK1 (K_D = 2.78 µM). Structurally, as show in Figure 4.4, Tat A is able to form non-covalent interactions with Tyr75 and Asp374 (H-bonds), and with Arg65 and Lys215 (Salt Bridges). In

particular, this site is placed in proximity of the 3-phosphoglyceric acid (3PG) binding site, most likely, hindering its access.

Following both these data set, it seems that Tat A interacts with PGK1 in a key region near to the active site and that this binding is able to hardly alter the exposition of the hinge region, probably interfering with the enzyme activity.

Moreover, PGK1 was incubated with Tat A at 50X molar excess both for 3 h and for 16 h and LCMS analysis were carried out to evaluate a possible covalent binding between the counterparts. As shown in Figure 4.5, no increment of PGK1 molecular weight was measured after the incubation and, thus, no covalent adducts were disclosed by our analysis.

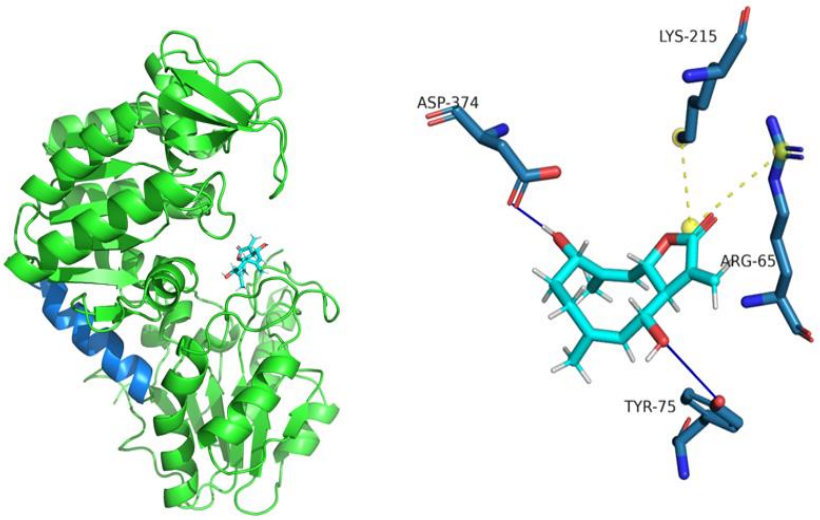

Figure 4.4 *Molecular docking of Tat A on PGK1.*

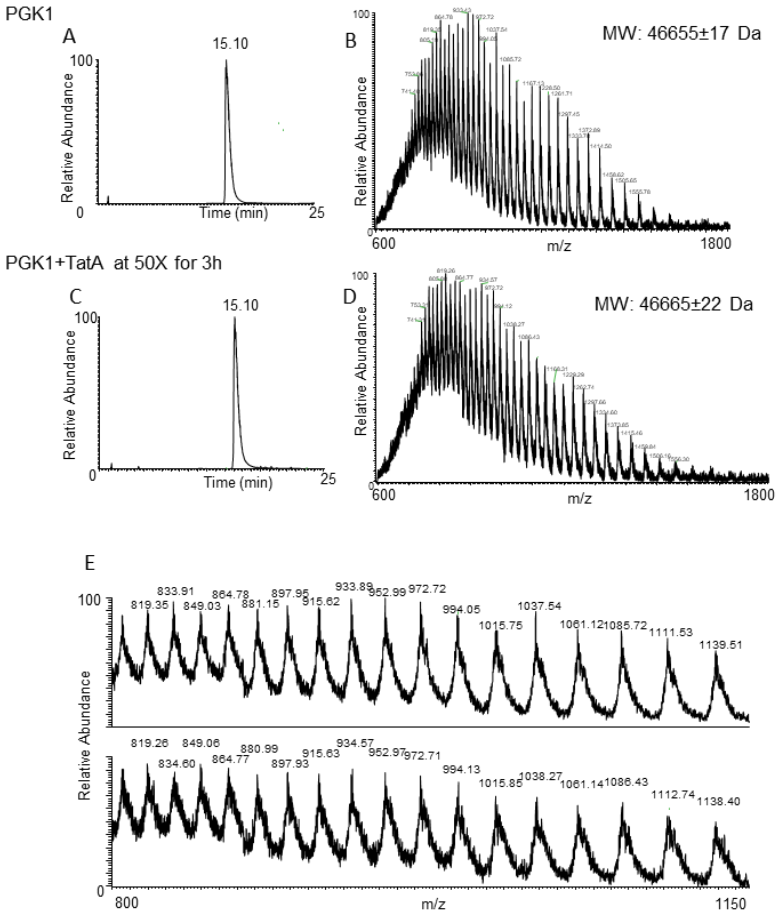

Figure 4.5 *In Panel A and B, the LC trace and MS spectrum of PGK1 at 5 µM are reported, together with the deconvoluted MW as obtaine dusing the software ESIProt online. In Panel C and D, the LC trace and MS spectrum of PGK1 at 5 µM incubated for 3 h with TatA at 250 µM at room temperature in PBS buffer are reported, together with the deconvoluted MW as obtained using the software ESIProt online. In panel E, a zoom-in of both spectra are compared: the upper one is relative to PGK1 alone, the lower one to PGK1 incubated with TatA as described.*

4.3 Tatridin A permeation by PAMPA assays

Then, the behavior of Tat A in the parallel artificial membrane permeability assay (PAMPA) has been tested to measure its effective permeability (expressed as -log Pe) through an artificial lipid membrane (Le Roux *et al.*, 2020). Propranolol and furosemide at 250 µM were used as positive and negative control molecules giving a -log Pe of 5.19 and 6.63, respectively (−log Pe < 6 is considered good permeability and −log Pe > 6.5 as impermeable). In this assay, Tat A displayed a very good propensity to cross the membrane *in vitro* with a -log Pe of 4.87 ±0.01, as shown in Figure 4.6.

	Propranolol 250 µM	Furosemide 250 µM	Tat A 50 µM
logPe	-5.19	-6.63	-4.87
dev.st.	0.03	0.00	0.01

Figure 4.6 *Results of Parallel Artificial Membrane Permeability Assay (PAMPA).*

4.4 Tatridin A negatively affected PGK1 activity

An *in vitro* activity assay has been equipped aiming to explore the effect of Tat A on PGK1 by measuring the activity of this enzyme in presence or not of different concentrations of Tat A. In the first step of this enzymatic assay, PGK converts 3-PG and ATP to 1,3-BPG and ADP. The nascent intermediate is detected via a series of

enzymatic reactions and the last one is the oxidation of NADH to NAD+, which can be easily detected (OD= 340 nm).

Initially, the human recombinant PGK1 activity has been monitored performing the spectrophotometric assay in a kinetic mode in presence or not of Tat A at different amounts. As shown in Figure 4.7A, Tat A modulates in a negative mode the activity of PGK1, showing an IC_{50} of 3760 ± 870 nM.

Then, the same expriment has been carried out using THP-1 and KATO III native cellular lysates as a source of PGK in order to investigate if, even in presence of pseudo-physiologically conditions, Tat A was able to modulate PGK bioactivity. As expected and as reported in Figure 4.7 B,C Tat A inhibits the enzymatic activity also in these more complex systems with a good potency profile and IC_{50} of 372 ± 112 nM and 397 ± 250 nM, respectively.

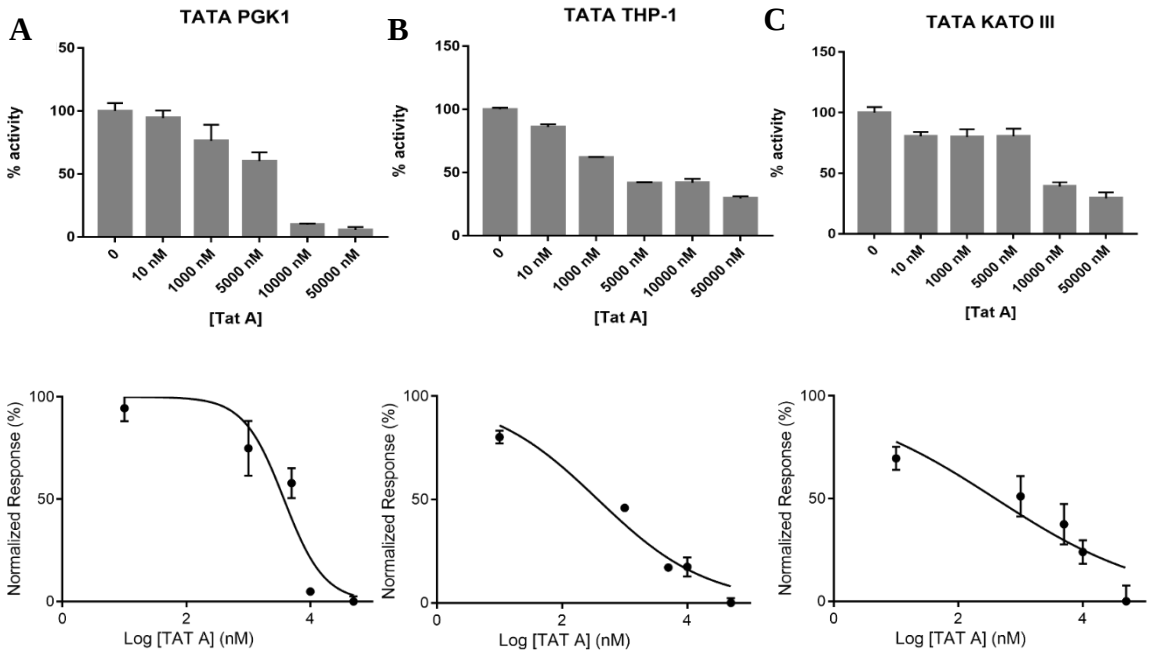

Figure 4.7 ***(A)*** *The effect of Tat A on PGK1.* ***(B,C)*** *Inhibition of Tat A on THP-1 and KATO III cell lysates.*

The opportune control experiments were carried out as reported by the enzymatic kit manufacture's procedure and, in addition, both the assays with PGK1 and THP-1 cell lysates were performed in presence of 1-epi-Tatridin B, a germacranolide Tat A analog. This molecule, which is inactive in many biological tests (Rivero *et al.*, 2003), doesn't alter PGK1 activity at any tested concentration as shown in Figure 4.8 A and B.

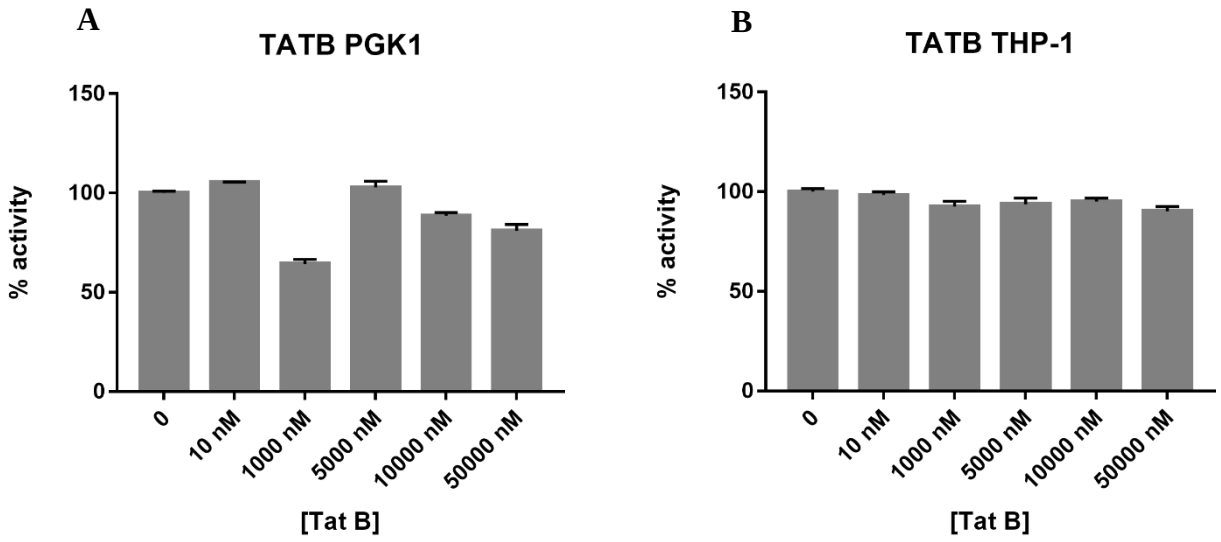

Figure 4.8 ***(A)*** *TatB doesn't reduce PGK1 activity.* ***(B)*** *TatB doesn't even work on THP-1 cell lysate.*

4.5 Tat A cellular activity on gastric carcinoma

To confirm the inhibitory activity of Tat A in a cellular system, the gastric carcinoma cell line KATO III was used thanks to a collaboration with Prof. Alessandra Tosco (University of Salerno, Department of Pharmacy). The cytotoxic activity of the natural compound was measured using an MTT assay both on THP-1 and KATO III and EC_{50} of 38±2 μM and 18±4 μM were obtained on these cellular lines (Figure 4.9).

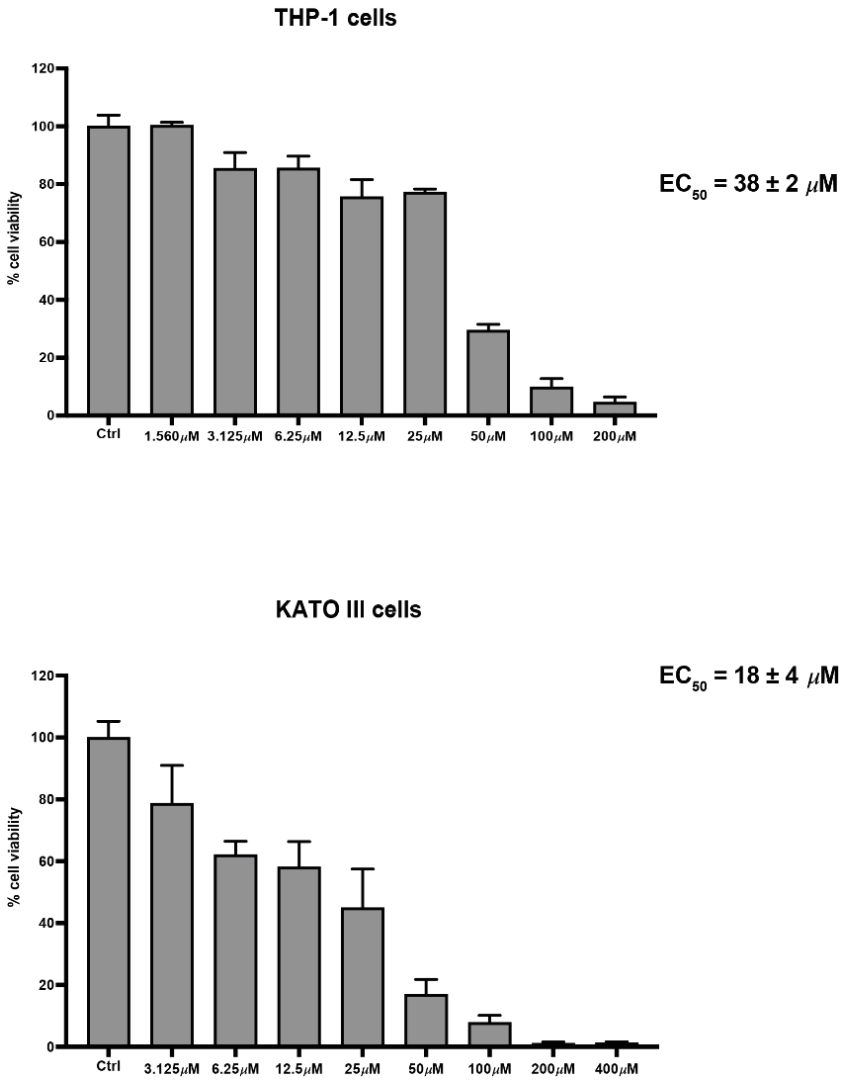

Figure 4.9 *The EC_{50} value of THP-1 and KATO III cells was evaluated by MTT assay. Cell death and corresponding EC_{50} value after incubation with TatA for 72 h. Each data point represents an average of four independent experiments.*

Since PGK1 is described to target CXCR4 and β-catenin in gastric cancer cells (Zieker *et al.*, 2010), promoting peritoneal carcinomatosis, KATO III cells were incubated with 100 µM Tat A for 24 h and CXCR4 and β-catenin expression was measured by

RT-qPCR. Figure 4.10 shows that the natural product administration determines a significant down-regulation of both mRNAs, without altering PGK1 expression.

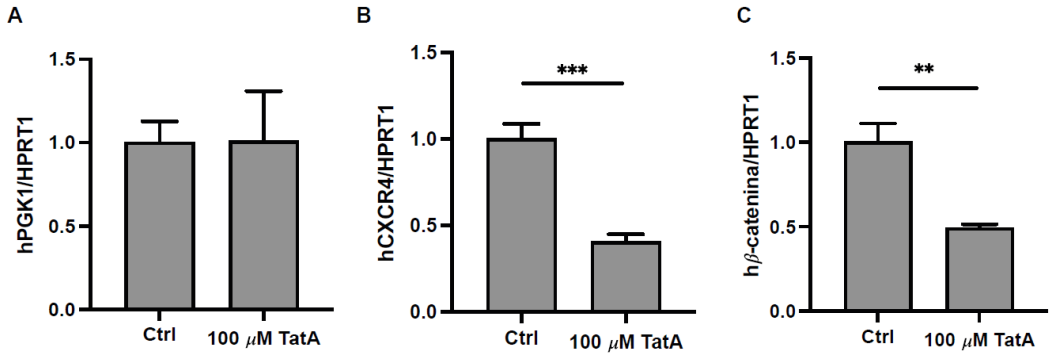

Figure 4.10 *Quantitative Real-Time-PCR (qRT-PCR) analysis of PGK1* ***(A)****, CXCR4* ***(B)*** *and β-catenin* ***(C)*** *in KATO III cells after the 24 h treatment with 100 μM Tat A. HPRT1 was used as a housekeeping gene. Experiments were carried out in triplicate. Data are expressed as mean ± s.d. (t-test; **p-value ≤ 0,01, ***p-value ≤ 0,001).*

Moreover, PGK1 is also described as inducing invasiveness in gastric cancer cells (Zieker *et al.*, 2010) and, for this reason, KATO III cells were incubated with 100 µM Tat A for 24 h, and a transwell invasion assay was performed. As shown in Figure 4.11 A and B, Tat A strongly reduces KATO III invasiveness, suggesting that PGK1 inhibition is effective also in a cellular context.

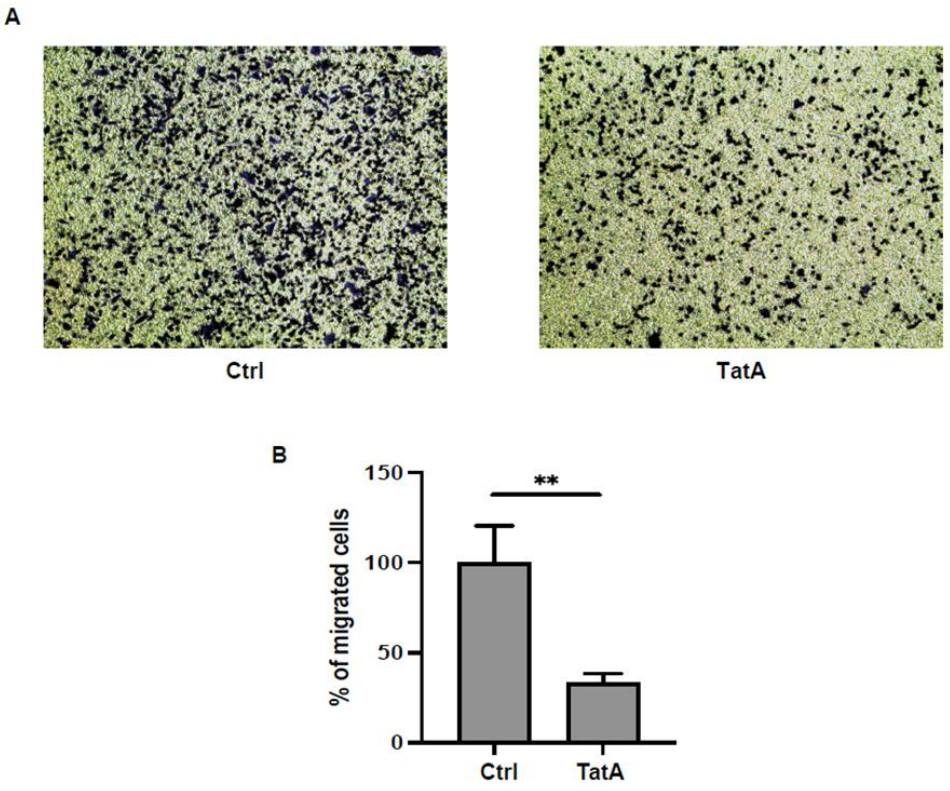

Figure 4.11 (A) *Representative microscopic images of the bottom surface of transwell filters stained with crystal violet (magnification ×10) of KATO III cells treated or not with 100 µM Tat A for 24 h.* ***(B)*** *Quantification of invasive cells. The data are shown as the mean number of cells per 8 visual fields (magnification ×10) of 3 replicate wells ± SD (t-test; **p-value ≤ 0,01).*

CHAPTER 4

PART 2

Discussion

4.6 Conclusive remarks

The scientific interest on sesquiterpene lactones (SLs) has emerged due to their vast biological activity beneficial for human health. They can inhibit numerous transcription factors responsible for downstream effects such as the release of several pro-inflammatory mediators, including cytokines (IL-1β, TNF-α, IL-6, IL-8, etc.) and enzymes (iNOS, COX-2, kinases, proteases, etc.). Besides these effects at the level of gene expression, SLs can also directly affect the release or activity of these mediators. Tat A is a sesquiterpene lactone isolated from for the first time from the aerial parts of *Anthemis melanolepis* (Saroglou *et al.*, 2010). It showed an *in vitro* cytotoxic activity against a panel of human tumor cell lines. In particular, Tat A resulted cytotoxic on the myeloid leukemia cell lines HL-60 and U937 (Rivero *et al.*, 2003).With the aim of deepen Tat A anti-cancer mechanism of action, a combination of drug affinity responsive target stability (DARTS) and targeted limited proteolysis assisted by multiple reaction monitoring mass spec (t-LIP-MRM) has been applied on a human leukemia monocytic cell line (THP-1), chosen as a model system.

Firstly, DARTS workflow has been exploited and the Tat A interactors have been identified. Among the putative identified targets, Phosphoglycerate kinase 1 (PGK1) has been selected as the main and most reliable Tat A partner since it was better protected from proteolysis in all DARTS replicates. The direct interaction between the protein and the small molecule was then unequivocally determined by Western blotting analysis, submitting all DARTS samples to an anti-PGK1 antibody reaction. To further explore Tat A interaction profile with PGK1 target, our optimized t-LiP Multiple Reaction Monitoring (MRM) strategy has been applied.

Interestingly, the peptide 193-199 can be considered symptomatic of Tat A interaction and protection. This peptide covers a large part of the central helix (aa from 187 to 201) which is fundamental for PGK1 activity allowing the two domains of the enzyme to approach each other during the catalytic cycle.

Consecutively, molecular docking experiments have been performed aiming to explore the binding between Tat A and PGK1. In collaboration with Dott. Mozzicafreddo from University of Camerino, molecular docking simulations have been performed: the results demonstrated that Tat A is able to form non-covalent interactions with Tyr75 and Asp374 (H-bonds), and with Arg65 and Lys215 (Salt Bridges). In particular, this site is placed in proximity of the 3-phosphoglyceric acid (3PG) binding site, most likely, hindering its access.

Spurred by these results, an *in vitro* activity assay has been planned by exploiting the glycogenolytic PGK1 activity. As reported, Tat A modulates in a negative mode the activity of PGK1.

PGK1 is an essential enzyme that catalyzes adenosine 5′ -triphosphate (ATP) production in aerobic glycolysis. PGK1 performs a variety of physiologically related biochemical or biophysical functions. PGK1 is both a cell metabolic enzyme and a

protein kinase and it phosphorylates different protein substrates. In addition to the regulation of cell metabolism, PGK1 is involved in multiple biological activities, including angiogenesis, mediated autophagy starting, binding of plasminogen, DNA replication and repair, proliferation and metastasis of tumor cells, cell invasion and is also associated with resistance to chemotherapy and prognosis of cancer patients.

Thus, prompeted by our results, we moved to investigate Tat A involmnet in gastric cancers from a biological point of view, since it was reported that the overexpression of PGK1 increases the invasiveness of gastric cancer in vitro (Zieker *et al.*, 2010) and that targeting PGK-1 in a gastric cancer cell can modulate the expression of the chemokine receptor CXCR4 and the Wnt pathway member β-catenin, which were known to be involved in cancer progression. Indeed, chemokines and their receptors play important roles in migration and activation of leukocytes, angiogenesis and tumor growth. In particular, CXCR4, a seven-transmembrane G-protein-coupled chemokine receptor promotes the progression and spreading of a number of malignant diseases including prostate, non–small-cell lung, pancreatic, breast and gastric cancer. β-catenin, a 92-kDa protein, plays a central role in cadherin-based cell adhesion processes, as a downstream effector in the Wnt-signaling pathway and it is also a potential downstream target of PGK1. In gastric cancer, increased expression of β-catenin is associated with enhanced proliferation, invasiveness, metastasis, angiogenesis and drug resistance.

As shown in results, Tat A works very well on KATO III cells downregulating mRNA levels of the chemokine receptor 4 (CXCR4) and β-catenin and inhibiting the invasiveness of living KATO III cells as a direct consequence of Phosphoglycerate Kinase 1 antagonism. Thus, Tat A can be considered as a novel and very promising natural antagonist of PGK1 endowed with anti-cancer activity on gastric tumour cells,

opening the way to explore more in the deep the class of bioactive sesquiterpenoid germacranolides.

CHAPTER 4

PART 3

Materials and Methods

4.7 Identification of Tatridin A cellular targets

4.7.1 Cell Culture

KATO III cells (gastric carcinoma, derived from a metastatic site, poorly differentiated) and THP-1 cells (human monocytic cell line derived from an acute monocytic leukemia patient) were obtained from the American Type Culture Collection (ATCC, Manassas, VA, USA). Cells were maintained in RPMI 1640 (Euroclone, #ECM2001L, Italy), supplemented respectively with 20% (v/v) fetal bovine serum (FBS, Euroclone, #ECS0180D, South America, origin EU approved) for KATO III cells and 10% for THP-1 cells, Penicillin- Streptomycin solution (100 U/ml penicillin and 100 μg/ml streptomycin) (Euroclone, #ECB3001D, Italy) and were grown at 37°C with 5% CO_2 in a humidified incubator.

4.7.2 Tatridin A Cellular Targets by DARTS

THP-1 cells were lysed in M-PER^{TM} (Mammalian Protein Extraction Reagent, Thermo Scientific) supplied with a protease inhibitor cocktail (final concentration 1x,

Sigma Aldrich). The lysate was centrifuged at 10.000 g for 10 min at 4°C and the Bradford assay was used to determinate the protein concentration of the obtained supernatant. Then, DARTS experiments were conducted as reported: different amounts (1 μM, 10 μM and 100 μM) of Tat A were incubated with 300 μg of THP-1 cell lysate for 1 hour at room temperature. Then, the samples were submitted to limited proteolysis, for 30 minutes at 25°C, at a ratio of 1:1500 w/w of subtilisin (Sigma Aldrich) in respect of proteins amount. Two samples of cell lysates were treated with dimethyl sulfoxide (DMSO) and one of them with subtilisin, as control experiments. Then, the protease was quenched by adding PMSF (phenylmethylsulfonyl fluoride, Sigma-Aldrich, 1 mM final concentration) to each sample. Then, all samples were boiled in Laemmli buffer (60 mM Tris-HCl pH 6.8, 2% SDS, 0.001% bromophenol blue, 1'% glycerol, 2% β-mercaptoethanol) and 20 μg were loaded on a 4%–12% Bis-Tris Criterion™ XT Precast Gel (Bio-Rad Laboratories S.r.l.) which was then stained with a Coomassie solution and submitted to a densitometric analysis through ImageJ. This experiment was repeated in triplicate. Protein bands were excised from the gels and submitted to an *in situ* tryptic digestion protocol (Shevchenko *et al.*, 2006). Briefly, gel slices were reduced with DTT (1,4-dithiothreitol), alkylated with IAA (iodoacetamide), washed and rehydrated on ice for 1 h in a 12 ng/μl trypsin solution. Then, the enzyme excess was removed and replaced with ammonium bicarbonate (AmBic, 50 mM, pH 8.5), allowing protein digestion to proceed overnight at 37 °C. Subsequently, supernatants were collected and peptides were extracted from each gel slice, shrinking them in 100% ACN (acetonitrile). Peptides mixtures were dried under vacuum and dissolved in formic acid (FA, 10%) for the LC-MSMS analysis. Then, 1μl of each sample was injected into a nano-UPLC system (ThermoFisher Scientific, Bremen) separating peptides on an EASY-Spray PepMAPTM RSLC C18 column

(3µm, 100Å, 75 µm x 50 cm, ThermoFisher Scientific, Bremen) at a flow rate of 0.3 ml/min. MS data were acquired on Q-Exactive Classic mass spectrometer (Thermo Scientific), provided with a nano-electrospray (nanoESI) source. Subsequently, database searches were carried out on Proteome Discoverer, employing the SwissProt database and the following parameters: maximum of two missed cleavages, trypsin digestion, carbamidomethyl (C) as fixed modification; oxidization (M), protein N-terminal acetylation as variable modifications; MSPepSearch was used to perform a spectral library search with a mass tolerance of 10 ppm for MS1 and 0.02 Da for MS2.

4.7.3 Validation of DARTS results via immunoblotting

The samples were then submitted to Western blotting analysis. First, 7 µL of each sample were loaded on an 12% SDS-PAGE and transferred onto a nitrocellulose membrane; then, they were incubated for 1 h in a blocking solution (5% milk) and left for 16 h at 4°C with monoclonal antibodies against PGK1 and PGK2 (1:1000). Then, rabbit peroxidase-conjugated secondary antibody (1:1500) was added, and the signal was detected using an enhanced chemiluminescent substrate and Amersham Imager 680 digital imaging system. Finally, an antibody against glyceraldehyde 3-phosphate dehydrogenase (GAPDH) (1:2500) in 5% milk has been tested as a loading normalizer.

4.7.4 t-LiP-MRM analysis

An *in-silico* search for investigating PGK1 tryptic peptides using the bio-informatics tool Peptide Atlas has been optimized to write appropriate MRM methods,

setting the best MRM transitions of the theoretical PGK1 fully tryptic peptides to map the protein sequences.

THP-1 cells were incubated with DMSO or Tat A for 1 h at room temperature. The samples were then submitted to limited proteolysis with 1:1500 (w/w) ratio of subtilisin in respect to protein amount, leaving an aliquot of the DMSO treated one undigested to be kept as a positive control. Subtilisin was then quenched with PMSF (1 mM final concentration) and the mixtures shifted to denaturing conditions adding urea (4 M final concentration) to perform in-solution digestion and desalting, as previously reported. The samples were then injected into the LC-MRM-MS system and analyzed through the optimized MRM method. Each protein tryptic peptide peak area was then measured using the Analyst Software from AB Sciex.

4.7.5 Molecular docking PGK1

To structurally analysis the binding between Tat A and PGK1, we performed a molecular docking using the three-dimensional structures of the binding partners obtained from the PubChem database (Kim *et al.*, 2021) with the CID number of 14466152, and the Protein Data Bank (Berman *et al.*, 2000) with the pdbID of 2wzb (Cliff *et al.*, 2010), respectively, and processed as previously reported (Del Gaudio *et al.*, 2018). The molecular docking procedure was carried out on the SwissDock web server (Grosdidier *et al.*, 2011) considering a docking zone including the entire protein as default. The energetically best complex was analyzed using the Protein Ligand Interaction Profiler (PLIP) web service (Adasme *et al.*, 2021) and rendered by PyMol software (The PyMOL Molecular Graphics System, Version 2.0, Schrödinger, LLC., Cambridge, MA, USA).

4.8 Tatridin A Pampa Assay

Donor solution (50 μM) was prepared by diluting 5 mM Tat A stock solutions using phosphate saline buffer (PBS, pH 7.4). The filter membrane was coated with 5 μL of specific lipid solution prepared as a 1% w/v phosphatidylcholine solution in n-dodecane. Donor solution (150 μL) was added to each well of the filter plate. To each well of the acceptor plate, 300 μL of solution (5% DMSO in PBS) were added. Donor and Acceptor plates were assembled to obtain a sandwich and incubated for 24 h at room temperature under gentle shaking. Then, the sandwich plates were separated and 250 μL of the solution from the acceptor plate and 100 μL of the solution from the donor one was transferred to a new multi-well plate and the absorbance was measured by UV spectroscopy using a Multiscan GO microplate spectrophotometer (Thermo Scientific) at 250−500 nm (5 nm steps). The permeability value Log Pe has been determined. The membranes' integrity was checked using propanolol and furosemide as control molecules.

4.9 PGK1 Activity Assay

The same experiment has been performed both with human recombinant PGK1 (#268-11354, Raybiotech) and using a THP-1 and KATO III cell lysates as a source of PGK1. More in the deep, cell lines have been lysed in M-PER^{TM} (Mammalian Protein Extraction Reagent) supplied with a protease inhibitor cocktail (final concentration 1x). The obtained proteome (14.000 g; 4°C; 15’ in Eppendorf Centrifuge 5424-R) has been quantified by Bradford spectrophotometric assay.

PGK1 at final concentration of 4 nM or THP-1 and KATO III cell lysates (1 µL of 1mg/ml) with and without Tat A (2µL of the following concentrations: 10nM, 1000nM, 5000nM, 10000nM and 50000nM) has been diluted in PGK Assay buffer (47 µL) and in a reaction mix (50µL for each well), containing PGK Assay Buffer, PGK Developer, ATP, NADH (50mM) and PGK substrate. All the samples have been shacked for 30' onto a 96 multiwell plate (final volume of 100ul/well). The experiment was performed in duplicate. The absorbance of the produced NADPH has been monitored in a kinetic mode for 60' using the MultiskanGO spectrophotometer by Thermo Scientific (37°C, orbital shaking: medium intensity, 10'' on/10'' off; λ = 340nm; 1 scan/5'). The same experiments were performed using Tat B in the identical settings.

4.10 Cell Viability Assay

KATO III cells were plated in 96-well plates at a cell density of $1*10^4$ cells/well. After 24 h cells were incubated for 72 h in the presence of Tat A (from 3.125 to 400 µM). The number of viable cells was quantified by the MTT [3-(4,5-dimethylthiazol-2-yl)-2,5-diphenyl tetrazolium bromide] assay. Absorption at 550 nm for each well was assessed using Multiskan GO (Thermo Scientific). Half-maximal inhibitory concentration (IC_{50}) values were calculated using GraphPad Prism 8. Experiments were performed in technical triplicates.

4.11 Quantitative Real-Time-PCR (qRT-PCR)

KATO III cells were seeded in 6 well plates at a cell density of $5*10^5$ cells/well. After 24 h cells were incubated for 24 h in the presence of 100 µM Tat A. Total RNA was extracted using TRIzol reagent (Invitrogen, #15596018, New Zealand) following the manufacturer's instructions, and 1 µg of each RNA was retrotranscribed by M-MLV Reverse Transcriptase (GeneSpin S.r.l, #STS-MRT, Italy). The Real-time PCR was performed using the QuantStudio™ 5 instrument (ThermoFisher). Suitable dilutions of cDNA were used for each gene in a 12 µL reaction using Luna Universal qPCR Master Mix (New Englands BioLabs, #M3003, USA). The primer sequences are reported in Supplementary Table 1. Results from 3 independent experiments in technical duplicates were analyzed using the Delta-Delta CT method and HPRT1 as a reference gene.

4.12 Trans-well Invasion Assay

KATO III invasiveness was analyzed using Trans-well Cell Culture (12 mm diameter, 8.0-µm pore size; Corning Incorporated; USA). The membranes of the upper chambers were coated with Collagen, Type I solution from rat tail (Sigma Aldrich, USA) and placed in wells containing medium supplemented with 10% FBS. Cells were seeded at a number of 1 x 10^5/insert into the upper chambers in serum-free medium. Treatment with 100 µM Tat A was carried out in the upper chamber. After 24 h of incubation at 37°C in 5% CO_2 - 95% air-humidified atmosphere, filters were fixed with 4% p-formaldehyde for 10 minutes and then with 100% methanol for 20 min. Cells on the lower surface of the filter were stained with a 0.5% crystal violet solution.

Cells migrated to the lower surface were counted in twelve random fields using EVOS light microscope (10X) (Life Technologies Corporation).

CHAPTER 5

Conclusions and final remarks

Most of the therapeutically employed natural products and synthetic compounds act on protein targets, physically and functionally interconnected in cellular pathways. Therefore, the identification of *small molecules* target proteins is pivotal to understand their mechanism of action for the development of molecular probes and/or potential drugs. Functional proteomics is a mass spectrometry-based discipline, focused on the analysis of the interactome of *small molecules* and their target discovery. Functional proteomics has become an invaluable tool in target identification of *small molecules* since *Fishing for Partners* strategy, also named as affinity purification mass spectrometry coupled approach (AP-MS), successfully disclosed a multitude of natural compounds interacting proteins in the past 15 years. Unfortunately, this strategy is not universally applicable, being limited by the need of a covalent modification of the molecule probe that should contain at least one reactive chemical group and, most importantly, the molecule modification should not influence its original bioactivity.

Thus, an alternative functional proteomics platform, based on a combination of untargeted Drug Affinity Responsive Target Stability (DARTS) with targeted Limited Proteolysis coupled to Multiple Reaction Monitoring (t-LiP-MRM), has been exploited during my PhD project to disclose and characterize the interacting proteins of bioactive compounds.

During the first year of the PhD project, the interactome of Artemetin (Art) and its more permeable analogue 8-prenyl-Artemetin (8-p-Art) have been investigated. The interactomes of these *small molecules* in HeLa cells proteome have been examined unveiling the Filamin A and Filamin B, as their principal cellular interactors. Both these isoforms are crucial role in the organization of the cytoskeleton interacting with F-actin. After validation by immunoblotting, the interaction has been deepened by a targeted Limited Proteolysis approach coupled with Multiple Reaction Monitoring mass spectrometry (t-LiP-MRM).

Filamins are actin-binding proteins, which participate in the formation of the cytoskeleton, anchor a variety of proteins in the cytoskeleton and regulate cell adhesion, migration, proliferation, apoptosis. Thus, the biological effect of Art and its prenylated form has been studied in detail, revealing an impact on cytoskeleton disassembly and on F-actin filaments disorganization mediated by filamins dissociation. Since F-actin and filamin disorders are critical elements for different fundamental cellular functions, including cell migration, this phenomenon has been investigated in HeLa cells treated or not with both compounds of interest, revealing that Art and 8-p-Art are potent inhibitors of cellular migration.

In conclusion, since the downregulation of cell adhesion and migration in the tumor microenvironment is a crucial step to block tumor metastasis occurrence and development, the discovery of the Art and its analogue 8-p-Art interactome by our functional proteomic platform and the insights on the interaction between the *small molecules* with filamins paves the way for consideration of these compounds as leads in the treatment of cancer.

During the second year of the PhD project, the interactome of a benzodiazepine called 1g, has been investigated, evaluating the ability of the synthetic compound to interfere with the activity and the protein expression of the brain glycogen phosphorylase (PYGB) on U87MG cell line in parallel with the capability of the compound to inhibit the cell growth. DARTS experiments disclosed PYGB as the best protected at each 1 g tested concentration, as also detected by immunoblotting. Moreover, thanks to limited proteolysis and molecular docking analysis, it has been revealed that 1g interacts well inside the AMP recognition hole, establishing favorable contacts with the amino acids into the AMP binding site. Furthermore, an *in vitro* activity assay has been planned by exploiting the effect of 1g on glycogenolytic activity of the enzyme. The results have been suggested that 1g modulates in a negative mode the activity of PYGB.

Glycogen metabolism plays an important role in the cancer progression. In particular, PYGB has been reported to implicated both in tumor progression of gastric cancer through the modulation of Wnt/β-catenin pathway (Xia *et al.*, 2020).

The inhibition of PYGB activity and protein expression by 1g measured in the biochemical assays is well related to a reduction of U87MG cell proliferation due to a decrease of cancer cell fuel.

In conclusion, our research highlights PYGB as a potential therapeutic target in Glioblastoma Multiforme proposing 1g as a lead compound for developing a new class of simplified analogs active as anticancer drugs for glioblastoma, keeping unchanged its ability to cross the blood–brain barrier.

During the third year of the PhD project, DARTS workflow has been exploited to identify the Tatridin A (Tat A) interactors. Among the putative ones, Phosphoglycerate

kinase 1 (PGK1) has been selected as the main and most reliable Tat A partner. To further explore Tat A interaction profile with PGK1 target, our optimized t-LiP Multiple Reaction Monitoring (MRM) strategy has been applied.

Consecutively, molecular docking experiments have been performed aiming to explore the binding between Tat A and PGK1. In collaboration with Dott. Mozzicafreddo from University of Camerino, molecular docking simulations have been finalized: the results demonstrated that Tat A interacts in proximity of the 3-phosphoglyceric acid (3PG) binding site, most likely, hindering its access. Spurred by these results, an *in vitro* activity assay has been planned by exploiting the glycogenolytic PGK1 activity. As reported, Tat A modulates in a negative mode the activity of PGK1.

Thus, prompeted by our results, we moved to investigate Tat A involmnet in gastric cancers from a biological point of view, since it was reported that the overexpression of PGK1 increases the invasiveness of gastric cancer in vitro (Zieker *et al.*, 2010) and that targeting PGK-1 in a gastric cancer cell can modulate the expression of the chemokine receptor CXCR4 and the Wnt pathway member β-catenin, which were known to be involved in cancer progression.

As shown in results, Tat A works very well on KATO III cells downregulating mRNA levels of the chemokine receptor 4 (CXCR4) and β-catenin and inhibiting the invasiveness of living KATO III cells as a direct consequence of Phosphoglycerate Kinase 1 antagonism. Thus, Tat A can be considered as a novel and very promising natural antagonist of PGK1 endowed with anti-cancer activity on gastric tumour cells, opening the way to explore more in the deep the class of bioactive sesquiterpenoid germacranolides.

In conclusion, a label-free functional proteomics platform coupling DARTS and t-LiP-MRM, avoiding any chemical modification of the compound to be studied, has been successfully developed along the three years of my PhD.

DARTS demonstrated to be a fast and straightforward approach for the interactome characterization of virtually any bioactive molecule, regardless of its chemical features. DARTS workflow is indeed fast and in one day multiple experiments can be performed in parallel. Nevertheless, to disclose as thoroughly as possible a molecule target, it is necessary to analyze several experimental conditions, in which increasing amounts of the bioactive compounds need to be incubated with a cell lysate. Thus, a long time of mass spectrometric analysis might often been required. Apart from this drawback, DARTS suffers from the necessity of visualizing, through the low dynamic range SDS-PAGE technique, the proteins sheltered by proteolysis in presence of a given molecule: low abundant proteins and proteins whose molecular weight is lesser than 30 kDa, co-migrating with the peptides generated during the limited proteolysis step, are difficult to visualize and identify.

T-LiP-MRM proved to be a powerful technique to pinpoint protein regions involved in the interaction with a molecule, either identifying putative binding sites or regions distally influenced by the interaction. As for DARTS, t-LiP-MRM workflow is fast, requiring only two days for the samples preparation and less than one day for the preliminary computational analysis. Nevertheless, complementary approaches are needed to give additional validation. When it comes to its shortcoming, the abundance of the protein to be analyzed could be an issue and enrichment or pre-fractionation steps could be necessary, requiring longer experimental times and potentially leading to sample loss. Furthermore, if no validated MRM assay is deposited onto data repositories, alternative prediction strategies must be employed, relying on particular

targeted proteomics programs or on an in house build-up and validation of proper assays on synthetic peptides. This last eventuality would, of course, increase the time and the costs associated with such an experiment.

Thus, relying on the analyzed molecules, DARTS coupling with t-LiP-MRM successfully provided a fast, straightforward and unexpansive label-free platform for the characterization of bioactive compounds interactomic profile.

Bibliography

Adasme, M.F. *et al.* (2021) 'PLIP 2021: expanding the scope of the protein-ligand interaction profiler to DNA and RNA', *Nucleic acids research*, 49(W1), pp. W530–W534. doi:10.1093/NAR/GKAB294.

De Almeida, L.M.S. *et al.* (2016) 'Flavonoids and Sesquiterpene Lactones from Artemisia absinthium and Tanacetum parthenium against Schistosoma mansoni Worms', *Evidence-based complementary and alternative medicine : eCAM*, 2016. doi:10.1155/2016/9521349.

Altemus, M.A. *et al.* (2019) 'Breast cancers utilize hypoxic glycogen stores via PYGB, the brain isoform of glycogen phosphorylase, to promote metastatic phenotypes', *PloS one*, 14(9). doi:10.1371/JOURNAL.PONE.0220973.

Atanasov, A.G. *et al.* (2021) 'Natural products in drug discovery: advances and opportunities', *Nature reviews. Drug discovery*, 20(3), pp. 200–216. doi:10.1038/S41573-020-00114-Z.

Bantscheff, M. and Drewes, G. (2012) 'Chemoproteomic approaches to drug target identification and drug profiling', *Bioorganic & Medicinal Chemistry*, 20(6), pp. 1973–1978. doi:10.1016/J.BMC.2011.11.003.

Belvedere, R. *et al.* (2017) 'The Pharmaceutical Device Prisma ® Skin Promotes in

Vitro Angiogenesis through Endothelial to Mesenchymal Transition during Skin Wound Healing', *International journal of molecular sciences*, 18(8). doi:10.3390/IJMS18081614.

Belvedere, R. *et al.* (2018) 'miR-196a Is Able to Restore the Aggressive Phenotype of Annexin A1 Knock-Out in Pancreatic Cancer Cells by CRISPR/Cas9 Genome Editing', *International journal of molecular sciences*, 19(7). doi:10.3390/IJMS19071967.

Berman, H.M. *et al.* (2000) 'The Protein Data Bank', *Nucleic acids research*, 28(1), pp. 235–242. doi:10.1093/NAR/28.1.235.

Capolupo, A. *et al.* (2017) 'Determination of Gymnemic Acid I as a Protein Biosynthesis Inhibitor Using Chemical Proteomics', *Journal of natural products*, 80(4), pp. 909–915. doi:10.1021/ACS.JNATPROD.6B00793.

Choudhari, A.S. *et al.* (2020) 'Phytochemicals in Cancer Treatment: From Preclinical Studies to Clinical Practice', *Frontiers in pharmacology*, 10. doi:10.3389/FPHAR.2019.01614.

Cliff, M.J. *et al.* (2010) 'Transition state analogue structures of human phosphoglycerate kinase establish the importance of charge balance in catalysis', *Journal of the American Chemical Society*, 132(18), pp. 6507–6516. doi:10.1021/JA100974T.

Crerar, M.M. *et al.* (1995) ‘Chimeric muscle and brain glycogen phosphorylases define protein domains governing isozyme-specific responses to allosteric activation’, *The Journal of biological chemistry*, 270(23), pp. 13748–13756. doi:10.1074/JBC.270.23.13748.

Deutsch, E.W., Lam, H. and Aebersold, R. (2008) ‘PeptideAtlas: a resource for target selection for emerging targeted proteomics workflows’, *EMBO reports*, 9(5), pp. 429–434. doi:10.1038/EMBOR.2008.56.

Dias, D.A., Urban, S. and Roessner, U. (2012) ‘A historical overview of natural products in drug discovery’, *Metabolites*, 2(2), pp. 303–336. doi:10.3390/METABO2020303.

Drewry, D.H. and Macarron, R. (2010) ‘Enhancements of screening collections to address areas of unmet medical need: an industry perspective’, *Current opinion in chemical biology*, 14(3), pp. 289–298. doi:10.1016/J.CBPA.2010.03.024.

Feng, Y. *et al.* (2014) ‘Global analysis of protein structural changes in complex proteomes’, *Nature biotechnology*, 32(10), pp. 1036–1044. doi:10.1038/NBT.2999.

Franco, P. *et al.* (2020) ‘Supercritical impregnation of mesoglycan into calcium alginate aerogel for wound healing’, *The Journal of Supercritical Fluids*, 157, p. 104711. doi:10.1016/J.SUPFLU.2019.104711.

Freter, K.R. (1988) ‘Drug discovery--today and tomorrow: the role of medicinal

chemistry', *Pharmaceutical research*, 5(7), pp. 397–400. doi:10.1023/A:1015924014805.

Del Gaudio, F. *et al.* (2018) 'Chemoproteomic fishing identifies arzanol as a positive modulator of brain glycogen phosphorylase', *Chemical communications (Cambridge, England)*, 54(91), pp. 12863–12866. doi:10.1039/C8CC07692H.

Gemelli, C. *et al.* (2014) 'Cytotoxic effect of hemin in colonic epithelial cell line: involvement of 18 kDa translocator protein (TSPO)', *Life sciences*, 107(1–2), pp. 14–20. doi:10.1016/J.LFS.2014.04.026.

Grasso, S. *et al.* (1999) 'Synthesis and anticonvulsant activity of novel and potent 2,3-benzodiazepine AMPA/kainate receptor antagonists', *Journal of medicinal chemistry*, 42(21), pp. 4414–4421. doi:10.1021/JM991086D.

Griffin, C.E. *et al.* (2013) 'Benzodiazepine pharmacology and central nervous system-mediated effects', *The Ochsner journal*, 13(2), pp. 214–223. Available at: https://pubmed.ncbi.nlm.nih.gov/23789008/ (Accessed: 20 December 2022).

Grosdidier, A., Zoete, V. and Michielin, O. (2011) 'SwissDock, a protein-small molecule docking web service based on EADock DSS', *Nucleic acids research*, 39(Web Server issue). doi:10.1093/NAR/GKR366.

Grossini, E. *et al.* (2015) 'Effects of Artemetin on Nitric Oxide Release and Protection against Peroxidative Injuries in Porcine Coronary Artery Endothelial

Cells', *Phytotherapy research : PTR*, 29(9), pp. 1339–1348. doi:10.1002/PTR.5386.

Harvey, A.L., Edrada-Ebel, R. and Quinn, R.J. (2015) 'The re-emergence of natural products for drug discovery in the genomics era', *Nature reviews. Drug discovery*, 14(2), pp. 111–129. doi:10.1038/NRD4510.

Heck, A.J.R. (2008) 'Native mass spectrometry: a bridge between interactomics and structural biology', *Nature methods*, 5(11), pp. 927–933. doi:10.1038/NMETH.1265.

Henzler-Wildman, K. and Kern, D. (2007) 'Dynamic personalities of proteins', *Nature*, 450(7172), pp. 964–972. doi:10.1038/NATURE06522.

Hwang, H.Y. *et al.* (2020) 'Profiling the Protein Targets of Unmodified Bio-Active Molecules with Drug Affinity Responsive Target Stability and Liquid Chromatography/Tandem Mass Spectrometry', *Proteomics*, 20(9). doi:10.1002/PMIC.201900325.

Iyer, L.K. *et al.* (2019) 'Pulse Proteolysis: An Orthogonal Tool for Protein Formulation Screening', *Journal of pharmaceutical sciences*, 108(2), pp. 842–850. doi:10.1016/J.XPHS.2018.09.018.

Jacinto, E. *et al.* (2006) 'SIN1/MIP1 maintains rictor-mTOR complex integrity and regulates Akt phosphorylation and substrate specificity', *Cell*, 127(1), pp. 125–137. doi:10.1016/J.CELL.2006.08.033.

Jafari, R. *et al.* (2014) ‘The cellular thermal shift assay for evaluating drug target interactions in cells’, *Nature protocols*, 9(9), pp. 2100–2122. doi:10.1038/NPROT.2014.138.

Kienitz, R. *et al.* (2022) ‘Benzodiazepines in the Management of Seizures and Status Epilepticus: A Review of Routes of Delivery, Pharmacokinetics, Efficacy, and Tolerability’, *CNS drugs*, 36(9), pp. 951–975. doi:10.1007/S40263-022-00940-2.

Kim, S. *et al.* (2021) ‘PubChem in 2021: new data content and improved web interfaces’, *Nucleic acids research*, 49(D1), pp. D1388–D1395. doi:10.1093/NAR/GKAA971.

Kim, Y.A., Kim, H. and Seo, Y. (2013) ‘Antiproliferative effect of flavonoids from the halophyte Vitex rotundifolia on human cancer cells’, *Natural Product Communications*, 8(10), pp. 1405–1408. doi:10.1177/1934578x1300801016.

Koenig, T. *et al.* (2008) ‘Robust prediction of the MASCOT score for an improved quality assessment in mass spectrometric proteomics’, *Journal of proteome research*, 7(9), pp. 3708–3717. doi:10.1021/PR700859X.

Lee, Dahae *et al.* (2018) ‘Protective Effect of Artemisia argyi and Its Flavonoid Constituents against Contrast-Induced Cytotoxicity by Iodixanol in LLC-PK1 Cells’, *International journal of molecular sciences*, 19(5). doi:10.3390/IJMS19051387.

Li, Q. and Kang, C. (2020) ‘Mechanisms of Action for Small Molecules Revealed by

Structural Biology in Drug Discovery', *International journal of molecular sciences*, 21(15), pp. 1–18. doi:10.3390/IJMS21155262.

Li, W.X. *et al.* (2005) 'Flavonoids from Vitex trifolia L. inhibit cell cycle progression at G2/M phase and induce apoptosis in mammalian cancer cells', *Journal of Asian natural products research*, 7(4), pp. 615–626. doi:10.1080/10286020310001625085.

Lombardino, J.G. and Lowe, J.A. (2004) 'The role of the medicinal chemist in drug discovery--then and now', *Nature reviews. Drug discovery*, 3(10), pp. 853–862. doi:10.1038/NRD1523.

Lomenick, B. *et al.* (2009) 'Target identification using drug affinity responsive target stability (DARTS)', *Proceedings of the National Academy of Sciences of the United States of America*, 106(51), pp. 21984–21989. doi:10.1073/PNAS.0910040106.

Lomenick, B. *et al.* (2011) 'Target identification using drug affinity responsive target stability (DARTS)', *Current protocols in chemical biology*, 3(4), pp. 163–180. doi:10.1002/9780470559277.CH110180.

Lomenick, B., Olsen, R.W. and Huang, J. (2011) 'Identification of direct protein targets of small molecules', *ACS chemical biology*, 6(1), pp. 34–46. doi:10.1021/CB100294V.

Manfredini, R. *et al.* (1997) 'Antisense inhibition of c-fes proto-oncogene blocks

PMA-induced macrophage differentiation in HL60 and in FDC-P1/MAC-11 cells', *Blood*, 89(1), pp. 135–145. doi:10.1182/blood.v89.1.135.135_135_145.

Margarucci, L. *et al.* (2010) 'Chemical proteomics discloses petrosapongiolide M, an antiinflammatory marine sesterterpene, as a proteasome inhibitor', *Angewandte Chemie (International ed. in English)*, 49(23), pp. 3960–3963. doi:10.1002/ANIE.200907153.

Martim, J.K.P., Maranho, L.T. and Costa-Casagrande, T.A. (2021) 'Review: Role of the chemical compounds present in the essential oil and in the extract of Cordia verbenacea DC as an anti-inflammatory, antimicrobial and healing product', *Journal of ethnopharmacology*, 265. doi:10.1016/J.JEP.2020.113300.

Martins, A. *et al.* (2014) 'In vitro antitumoral activity of compounds isolated from Artemisia gorgonum Webb', *Phytotherapy research : PTR*, 28(9), pp. 1329–1334. doi:10.1002/PTR.5133.

Mateus, A. *et al.* (2020) 'Thermal proteome profiling for interrogating protein interactions', *Molecular systems biology*, 16(3). doi:10.15252/MSB.20199232.

Mathieu, C. *et al.* (2016) 'Insights into Brain Glycogen Metabolism: THE STRUCTURE OF HUMAN BRAIN GLYCOGEN PHOSPHORYLASE', *The Journal of biological chemistry*, 291(35), pp. 18072–18083. doi:10.1074/JBC.M116.738898.

Mathieu, C., Dupret, J.M. and Rodrigues Lima, F. (2017) ‘The structure of brain glycogen phosphorylase-from allosteric regulation mechanisms to clinical perspectives’, *The FEBS journal*, 284(4), pp. 546–554. doi:10.1111/FEBS.13937.

Matos, M.S., Anastácio, J.D. and Dos Santos, C.N. (2021) ‘Sesquiterpene Lactones: Promising Natural Compounds to Fight Inflammation’, *Pharmaceutics*, 13(7). doi:10.3390/PHARMACEUTICS13070991.

Moradian, A. *et al.* (2014) ‘The top-down, middle-down, and bottom-up mass spectrometry approaches for characterization of histone variants and their post-translational modifications’, *Proteomics*, 14(4–5), pp. 489–497. doi:10.1002/PMIC.201300256.

Morretta, E., Belvedere, R., *et al.* (2021) ‘Novel insights on the molecular mechanism of action of the anti-angiogenic pyrazolyl-urea GeGe-3 by functional proteomics’, *Bioorganic chemistry*, 115. doi:10.1016/J.BIOORG.2021.105168.

Morretta, E., Sidibè, A., *et al.* (2021) ‘Synthesis, functional proteomics and biological evaluation of new 5-pyrazolyl ureas as potential anti-angiogenic compounds’, *European journal of medicinal chemistry*, 226. doi:10.1016/J.EJMECH.2021.113872.

Nodwell, M.B. and Sieber, S.A. (2012) ‘ABPP methodology: introduction and overview’, *Topics in current chemistry*, 324, pp. 1–41. doi:10.1007/128_2011_302.

Nomura, D.K., Dix, M.M. and Cravatt, B.F. (2010) ‘Activity-based protein profiling for biochemical pathway discovery in cancer’, *Nature reviews. Cancer*, 10(9), pp. 630–638. doi:10.1038/NRC2901.

Novelli, A. *et al.* (1988) ‘Glutamate becomes neurotoxic via the N-methyl-D-aspartate receptor when intracellular energy levels are reduced’, *Brain research*, 451(1–2), pp. 205–212. doi:10.1016/0006-8993(88)90765-2.

Olsen, R.W. *et al.* (1984) ‘Biochemical properties of the GABA/barbiturate/benzodiazepine receptor-chloride ion channel complex’, *Advances in experimental medicine and biology*, 175, pp. 205–219. doi:10.1007/978-1-4684-4805-4_17.

Orsburn, B.C. (2021) ‘Proteome Discoverer-A Community Enhanced Data Processing Suite for Protein Informatics’, *Proteomes*, 9(1). doi:10.3390/PROTEOMES9010015.

Ortet, R. *et al.* (2011) ‘Furfuran lignans and a flavone from Artemisia gorgonum Webb and their in vitro activity against Plasmodium falciparum’, *Journal of ethnopharmacology*, 138(2), pp. 637–640. doi:10.1016/J.JEP.2011.09.039.

Parenti, S. *et al.* (2016) ‘A novel 2,3-benzodiazepine-4-one derivative AMPA antagonist inhibits G2/M transition and induces apoptosis in human leukemia Jurkat T cell line’, *Life sciences*, 152, pp. 117–125. doi:10.1016/J.LFS.2016.03.051.

Picotti, P. *et al.* (2009) ‘Full dynamic range proteome analysis of S. cerevisiae by targeted proteomics’, *Cell*, 138(4), pp. 795–806. doi:10.1016/J.CELL.2009.05.051.

Plastino, J. and Blanchoin, L. (2018) ‘Dynamic stability of the actin ecosystem’, *Journal of cell science*, 132(4). doi:10.1242/JCS.219832.

Raida, M. (2011) ‘Drug target deconvolution by chemical proteomics’, *Current opinion in chemical biology*, 15(4), pp. 570–575. doi:10.1016/J.CBPA.2011.06.016.

Rivero, A. *et al.* (2003) ‘Potent induction of apoptosis by germacranolide sesquiterpene lactones on human myeloid leukemia cells’, *European Journal of Pharmacology*, 482(1–3), pp. 77–84. doi:10.1016/j.ejphar.2003.09.058.

Rix, U. and Superti-Furga, G. (2009) ‘Target profiling of small molecules by chemical proteomics’, *Nature chemical biology*, 5(9), pp. 616–624. doi:10.1038/NCHEMBIO.216.

Rosa, A. *et al.* (2020) ‘The dietary flavonoid eupatilin attenuates in vitro lipid peroxidation and targets lipid profile in cancer HeLa cells’, *Food & function*, 11(6), pp. 5179–5191. doi:10.1039/D0FO00777C.

Rosa, A. *et al.* (2022) ‘Effect of the natural polymethoxylated flavone artemetin on lipid oxidation and its impact on cancer cell viability and lipids’, *Fitoterapia*, 156. doi:10.1016/J.FITOTE.2021.105102.

Roth, B.L., Sheffer, D.J. and Kroeze, W.K. (2004) ‘Magic shotguns versus magic bullets: selectively non-selective drugs for mood disorders and schizophrenia’, *Nature reviews. Drug discovery*, 3(4), pp. 353–359. doi:10.1038/NRD1346.

Le Roux, A. *et al.* (2020) ‘Structure-Permeability Relationship of Semipeptidic Macrocycles-Understanding and Optimizing Passive Permeability and Efflux Ratio’, *Journal of medicinal chemistry*, 63(13), pp. 6774–6783. doi:10.1021/ACS.JMEDCHEM.0C00013.

Sadaghiani, A.M., Verhelst, S.H. and Bogyo, M. (2007) ‘Tagging and detection strategies for activity-based proteomics’, *Current opinion in chemical biology*, 11(1), pp. 20–28. doi:10.1016/J.CBPA.2006.11.030.

Salamone, S. *et al.* (2021) ‘Effects of quercetin and artemetin prenylation on bioavailability and bioactivity’, *Chemistry and physics of lipids*, 240. doi:10.1016/J.CHEMPHYSLIP.2021.105137.

Sarbassov, D.D. *et al.* (2005) ‘Phosphorylation and regulation of Akt/PKB by the rictor-mTOR complex’, *Science (New York, N.Y.)*, 307(5712), pp. 1098–1101. doi:10.1126/SCIENCE.1106148.

Saroglou, V. *et al.* (2010) ‘Sesquiterpene lactones from Anthemis melanolepis and their antibacterial and cytotoxic activities. Prediction of their pharmacokinetic profile’, *Journal of natural products*, 73(2), pp. 242–246. doi:10.1021/NP9004129.

Saxena, C. (2016) ‘Identification of protein binding partners of small molecules using label-free methods’, *Expert opinion on drug discovery*, 11(10), pp. 1017–1025. doi:10.1080/17460441.2016.1227316.

Schaks, M., Giannone, G. and Rottner, K. (2019) ‘Actin dynamics in cell migration’, *Essays in biochemistry*, 63(5), pp. 483–495. doi:10.1042/EBC20190015.

Schopper, S. *et al.* (2017) ‘Measuring protein structural changes on a proteome-wide scale using limited proteolysis-coupled mass spectrometry’, *Nature protocols*, 12(11), pp. 2391–2410. doi:10.1038/NPROT.2017.100.

Sertie, J.A.A. *et al.* (1990) ‘Anti-inflammatory activity and sub-acute toxicity of artemetin’, *Planta medica*, 56(1), pp. 36–40. doi:10.1055/S-2006-960879.

Sertié, J.A.A. *et al.* (1991) ‘Pharmacological assay of Cordia verbenacea. III: Oral and topical antiinflammatory activity and gastrotoxicity of a crude leaf extract’, *Journal of ethnopharmacology*, 31(2), pp. 239–247. doi:10.1016/0378-8741(91)90008-2.

Shevchenko, A. *et al.* (2006) ‘In-gel digestion for mass spectrometric characterization of proteins and proteomes’, *Nature protocols*, 1(6), pp. 2856–2860. doi:10.1038/NPROT.2006.468.

Shiyama, T. *et al.* (2004) ‘Design and synthesis of novel hydrophilic spacers for the reduction of nonspecific binding proteins on affinity resins’, *Bioorganic and*

Medicinal Chemistry, 12(11), pp. 2831–2841. doi:10.1016/j.bmc.2004.03.052.

Sichaem, J. *et al.* (2021) 'A new labdane-type diterpenoid from the leaves of Vitex negundo L', *Natural product research*, 35(14), pp. 2329–2334. doi:10.1080/14786419.2019.1672687.

Sinha, S. *et al.* (2015) 'Assessment of microtubule depolymerization property of flavonoids isolated from Tanacetum gracile in breast cancer cells by biochemical and molecular docking approach', *Chemico-biological interactions*, 239, pp. 1–11. doi:10.1016/J.CBI.2015.06.034.

Soudijn, W. (1991) 'The role of medicinal chemistry in drug research', *Pharmaceutisch Weekblad Scientific Edition*, 13(4), pp. 161–166. doi:10.1007/BF01957740.

De Souza, P. *et al.* (2011) 'Hypotensive mechanism of the extracts and artemetin isolated from Achillea millefolium L. (Asteraceae) in rats', *Phytomedicine : international journal of phytotherapy and phytopharmacology*, 18(10), pp. 819–825. doi:10.1016/J.PHYMED.2011.02.005.

Stierand, K., Maaß, P.C. and Rarey, M. (2006) 'Molecular complexes at a glance: automated generation of two-dimensional complex diagrams', *Bioinformatics (Oxford, England)*, 22(14), pp. 1710–1716. doi:10.1093/BIOINFORMATICS/BTL150.

Strickland, E.C. *et al.* (2013) 'Thermodynamic analysis of protein-ligand binding

interactions in complex biological mixtures using the stability of proteins from rates of oxidation', *Nature protocols*, 8(1), pp. 148–161. doi:10.1038/NPROT.2012.146.

Sutherland-Smith, A.J. (2011) 'Filamin structure, function and mechanics: are altered filamin-mediated force responses associated with human disease?', *Biophysical reviews*, 3(1), pp. 15–23. doi:10.1007/S12551-011-0042-Y.

Wee, H.N. *et al.* (2020) 'Effects of Vitex trifolia L. leaf extracts and phytoconstituents on cytokine production in human U937 macrophages', *BMC complementary medicine and therapies*, 20(1). doi:10.1186/S12906-020-02884-W.

West, G.M. *et al.* (2010) 'Quantitative proteomics approach for identifying protein-drug interactions in complex mixtures using protein stability measurements', *Proceedings of the National Academy of Sciences of the United States of America*, 107(20), pp. 9078–9082. doi:10.1073/PNAS.1000148107.

Wilkins, M.R. *et al.* (1996) 'Progress with proteome projects: why all proteins expressed by a genome should be identified and how to do it', *Biotechnology & genetic engineering reviews*, 13(1), pp. 19–50. doi:10.1080/02648725.1996.10647923.

Wordeman, L. and Vicente, J.J. (2021) 'Microtubule Targeting Agents in Disease: Classic Drugs, Novel Roles', *Cancers*, 13(22). doi:10.3390/CANCERS13225650.

Wright, M.H. and Sieber, S.A. (2016) 'Chemical proteomics approaches for

identifying the cellular targets of natural products', *Natural product reports*, 33(5), pp. 681–708. doi:10.1039/C6NP00001K.

Xia, B., Zhang, K. and Liu, C. (2020) 'PYGB Promoted Tumor Progression by Regulating Wnt/β-Catenin Pathway in Gastric Cancer', *Technology in cancer research & treatment*, 19. doi:10.1177/1533033820926592.

Xu, Q. *et al.* (2017) 'Filamin B: The next hotspot in skeletal research?', *Journal of genetics and genomics = Yi chuan xue bao*, 44(7), pp. 335–342. doi:10.1016/J.JGG.2017.04.007.

Yue, J., Huhn, S. and Shen, Z. (2013) 'Complex roles of filamin-A mediated cytoskeleton network in cancer progression', *Cell & bioscience*, 3(1). doi:10.1186/2045-3701-3-7.

Zhan, Y. *et al.* (2021) 'Glycogen phosphorylase B promotes cell proliferation and migration through PI3K/AKT pathway in non-small cell lung cancer', *Experimental lung research*, 47(3), pp. 111–120. doi:10.1080/01902148.2020.1864065.

Zhou, J. *et al.* (2021) 'The function and pathogenic mechanism of filamin A', *Gene*, 784. doi:10.1016/J.GENE.2021.145575.

Zieker, D. *et al.* (2010) 'Phosphoglycerate kinase 1 a promoting enzyme for peritoneal dissemination in gastric cancer', *International journal of cancer*, 126(6), pp. 1513–1520. doi:10.1002/IJC.24835.